The affinity and dynamic range of sandwich assays with pre-assembled, linked binders are largely insensitive to changes in linker length and rigidity

Ilias Hurley
Program in Biological and Biomedical Engineering
McGill University
Montreal, Canada

August 2021

A thesis submitted to McGill University in partial fulfillment of the requirements of the degree of
Master of Engineering

Table of Contents

Tables of Figures

Table of Tables

Abstract

There is a need to tune an assay's dynamic range to measure analytes with large concentration ranges of interest in human health and disease. Colocalized bead assays, wherein a matched pair of sandwich affinity binders is pre-assembled to a micron-sized bead via flexible linkers, could offer robust and sensitive analyte measurement for medical research. To modify the apparent affinity and dynamic range of colocalized bead assays, we drew inspiration from multi-domain proteins, which achieve high apparent affinity by having two or more binding domains connected by disordered linker domains. The length and flexibility of the linker determine its conformational entropy, influencing the apparent affinity enhancement by modulating the entropic cost of multivalent binding. This phenomenon has previously been harnessed to develop simple sandwich assays with an adjustable apparent affinity.

In this thesis we explored the factors influencing the apparent affinity of a colocalized bead assay, in particular the role of linker length and flexibility. We evaluated the effect of modifying linker stiffness and reagent stochasticity on colocalized bead assays. Next, we reduced the assay to a liquid-phase model and investigated the role of linker length in the absence of bead surface effects. Finally, we compared our results to existing models for apparent affinity enhancement of simple sandwich assays with flexible linkers.

The results indicate that the apparent affinity of the colocalized bead assay was insensitive to modification of the linker stiffness or the reagent distribution. In the absence of the bead, we found that when the distance between binding sites is around ~5 nm the apparent affinity is only slightly sensitive to linker length. Greater sensitivity is achieved when the distance between binding sites is decreased. Finally, we determined that current models for apparent affinity enhancement are not accurate for simple sandwich assays.

These conclusions suggest that if an adjustable dynamic range is desired, affinity binders should be chosen that interact with epitopes in proximity. Future models for affinity enhancement of simple sandwich assays should use more complex models to define the dynamics of the flexible linker. Models for colocalized bead assays should account for the affinity binder size and flexibility and the density and stochasticity of reagents on the surface, in addition to linker length and flexibility.

Résumé

Il y a besoin de régler la plage dynamique des essais biologiques afin de mesurer les antigènes avec de larges plages de concentration pertinentes pour la santé humaine. Les essais colocalisés sur microsphères, où une paire de ligands d'affinité sandwich est pré-assemblée à une particule à l'échelle du micron, pourraient offrir une analyse d'antigène robuste et sensible pour la recherche médicale. Dans le but de modifier l'affinité apparente et la plage dynamique des essais colocalisés sur microsphères, nous nous sommes inspirés de protéines multi-domaines, qui réalisent une affinité forte en associant deux ou plus domaines de liaison par les connecteurs intrinsèquement désordonnés. La longueur et la flexibilité du connecteur déterminent son entropie conformationnelle. Elles influencent l'affinité apparente en modulant le coût entropique la liaison multivalente. Ce phénomène a été exploité pour développer des essais sandwich simples avec une affinité apparente ajustable.

Dans cette thèse nous avons exploré les éléments qui influencent l'affinité apparente des essais colocalisés sur microsphères, surtout le rôle de la longueur et la flexibilité du connecteur. Nous avons évalué l'effet de la modification de la rigidité du connecteur et de la stochasticité des réactifs sur les essais colocalisés sur microsphères. Ensuite, nous avons réduit l'essai à un modèle en phase liquide et étudié le rôle de la longueur du connecteur en l'absence d'effets de surface des microsphères. Finalement, nous avons comparé nos résultats aux modèles actuels pour la modification de l'affinité apparente des essais sandwich colocalisés simples avec connecteurs flexibles.

Les résultats indiquent que l'affinité apparente des essais colocalisés sur microsphères était insensible à la modification de la rigidité du connecteur ou de la distribution des réactifs. En l'absence de la microsphère, nous avons constaté que lorsque la distance entre les sites de liaison est d'environ 5 nm, l'affinité apparente n'est que légèrement sensible à la longueur du connecteur. Une plus grande sensibilité est obtenue lorsque la distance entre les sites de liaison est diminuée. Enfin, nous avons déterminé que les modèles actuels de l'affinité apparente ne sont pas précis pour les essais sandwich colocalisés simples.

Ces conclusions suggèrent que si une plage dynamique ajustable est souhaitée, les ligands d'affinité doivent être choisis qui interagissent avec les épitopes à proximité sur l'antigène. En

outre, les futurs modèles de l'affinité des essais sandwich colocalisés simples devraient utiliser des modèles plus complexes pour définir la dynamique du connecteur flexible. Les modèles pour les essais de sandwich colocalisés sur des microsphères doivent tenir compte de la taille et flexibilité du ligand d'affinité et de la densité et stochasticité des réactifs à la surface, en plus de la longueur et flexibilité du connecteur.

Acknowledgements

First and foremost, I would like to thank my primary supervisor, Prof. David Juncker, for his guidance and feedback throughout my project and my time in his lab. Without his enduring support and encouragement, this work would not have been possible. I would also like to thank my co-supervisor, Prof. Maureen McKeague, for her invaluable guidance. Despite joining my committee almost two years into my degree, she contributed enormously to make this research a success.

Secondly, I would like to thank Dr. Andy Ng for his suggestions, feedback, and overall willingness to answer my questions; Dr. Milad Dagher, for providing the foundation on which this work was built; Dr. Ryan Walsh, for sharing his expertise on reaction kinetics and binding dynamics; Rosalie Martel and Philippe DeCorwin-Martin, for providing mentorship throughout my degree; and Brittany Roberts, Dr. Lucile Alexandre, Molly Shen, and all the other Juncker Lab for supporting me, challenging me, and offering me their friendship. I would also like to thank the members of the CLAMP-nplex team: Dr. Milad Dagher, Dr. Jeffrey Munzar, Dr. Jinglin Kong, Arya Tavakoli, and Woojong Rho, for their patience and guidance during the early phases of this project.

I wish to acknowledge the financial support of the Biomedical Engineering Department through the Recruitment Award and FRQNT through the Master's Research Scholarship. I would also like to acknowledge NSERC and CQDM, which funded part of the research in this thesis.

Finally, I would like to deeply thank the friends and family that helped me complete this thesis despite the unprecedented circumstances. Nikola, Viv, Evie, Célia, and Alex, for giving me a wonderful space to come home to (or stay in) every day; Mom and Dad, for always lending an ear when I needed it; Chris, Laura, Jen, Pete, Bob, Taylor, Dave S, Dave K, Raven, Brady, Brittany, Jay, Dov, and Alex, for helping me escape every week. Lastly, I would like to thank Vinko for helping me find adventure everywhere, and for his endless patience and support, especially during the long preparation of this thesis.

1. Project Description

1.1 Motivation

The clinically relevant concentration range of a human biomarker can span more than six orders of magnitude. Meanwhile, the typical interval of concentrations where an assay provides meaningful information, known as the dynamic range, is about two orders of magnitude[1]. As such, there is a need to modify an assay's dynamic range.

Colocalized assays, consisting of a matched pair of sandwich affinity binders assembled via flexible linkers, have emerged as a powerful detection method, as they are robust to cross-reactivity[2–5]. The motivation for this work is the exploration of methods to modify the dynamic range of colocalized assays, in particular those that do not require modification of the sample or the affinity binders. The identified techniques could be applied to existing colocalized assays to expand the addressable analyte concentration range without loss of precision.

1.2 Project Goals

This project had three main goals: (i) Explore the parameters determining apparent affinity in pre-assembled colocalized bead assays, (ii) assess the effect of linker length and rigidity on apparent affinity in isolation from the bead, and (iii) compare the results to published models for intrinsically disordered linkers.

1.3 Contribution of Authors

For the present thesis, Ilias Hurley performed almost all the experimental work and data analysis. Protocols for the fabrication and use of the CLAMP were developed by Dr. Milad Dagher. Fabrication of CLAMP beads in section 3.5.1 was performed by Dr. Jinglin Kong, Arya Tavakoli, and Woojong Rho, with post-fabrication modifications performed by Ilias Hurley. The procedure and algorithm for analysis of colocalized bead assays were adapted from work by Dr. Jinglin Kong. The analysis of liquid-phase colocalized assays using the quadratic binding equation was adapted from work by Dr. Ryan Walsh. Literature for Figure 2 was collected in part by Dr. Ryan Walsh. The thesis and accompanying figures were prepared by Ilias Hurley, with revision help from Prof. David Juncker, Prof. Maureen McKeague, and Dr. Andy Ng.

2. Introduction

2.1 Preface: Clinical Range of Circulating Blood Proteins

More than 10,000 biological analytes are found in human blood, occurring at concentrations spanning more than nine orders of magnitude[6]. These include albumin and IgG antibodies, in the g/L range, as well as cytokines and interleukins, which occur at concentrations of <1 ng/L (Figure 1)[7]. Within the myriad of proteins, genetic material, and chemical molecules present in blood, there are some that can act as indicators of health or disease, which are referred to as biomarkers. The detection and quantification of biomarkers can be critical for diagnosis, selection of appropriate treatment, and monitoring disease response.

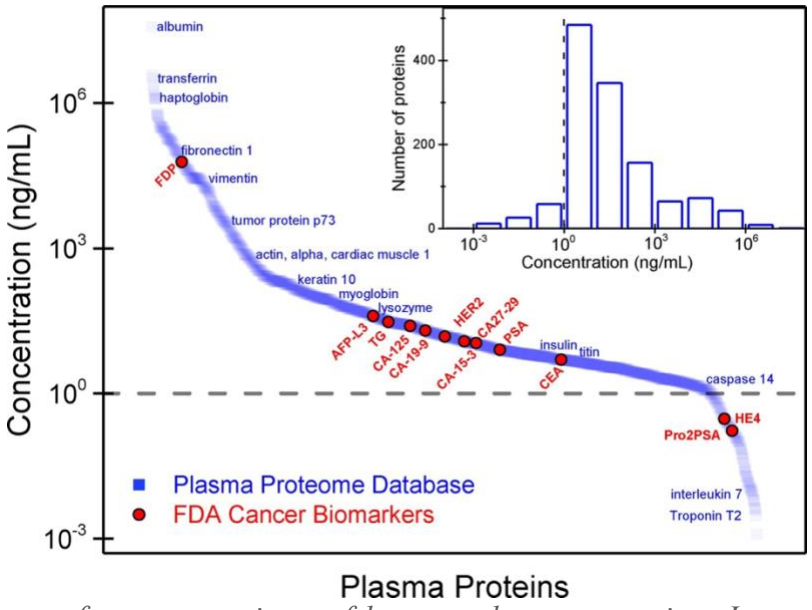

Figure 1: Range of concentrations of human plasma proteins. Inset: histogram of human plasma protein concentrations. Reproduced from Kosaka, Calleja, and Tamayo[6].

Inflammatory cytokines and acute-phase proteins have been recognized as biomarkers for a wide range of pathological conditions[8]. For many proteins, the difference in concentration between the healthy and disease conditions is quite small. However, some targets have clinically relevant ranges of two, four, or more than six orders of magnitude (Figure 2)[8]. For instance, the average level of interleukin-6 (IL-6), a key component of the adaptive immune system[8], in the blood of healthy individuals is ~1 pg/mL[9,10]. But for some individuals, this healthy baseline can be as low as 0.01 pg/mL[9,10]. Meanwhile, the diagnostic threshold of circulating IL-6 for distinguishing soft

tissue sarcomas from benign tumours was proposed to be 6.6 pg/mL. The prognostic threshold for survival of sarcoma patients was proposed at 26.7 pg/mL[11]. The cut-off of circulating IL-6 levels for identifying patients at risk of complications from sepsis was determined to be 500 pg/mL[12]. Therefore, the relevant range of IL-6 concentrations in blood is almost five orders of magnitude. By comparison, binding assays typically have a quantifiable range of about two orders of magnitude. This range is commonly known as the dynamic range and will be defined at length in the next section. High-resolution sensors and ultra-low-background methods have allowed some assays to attain greater dynamic ranges[1], but these have not yet achieved widespread applicability.

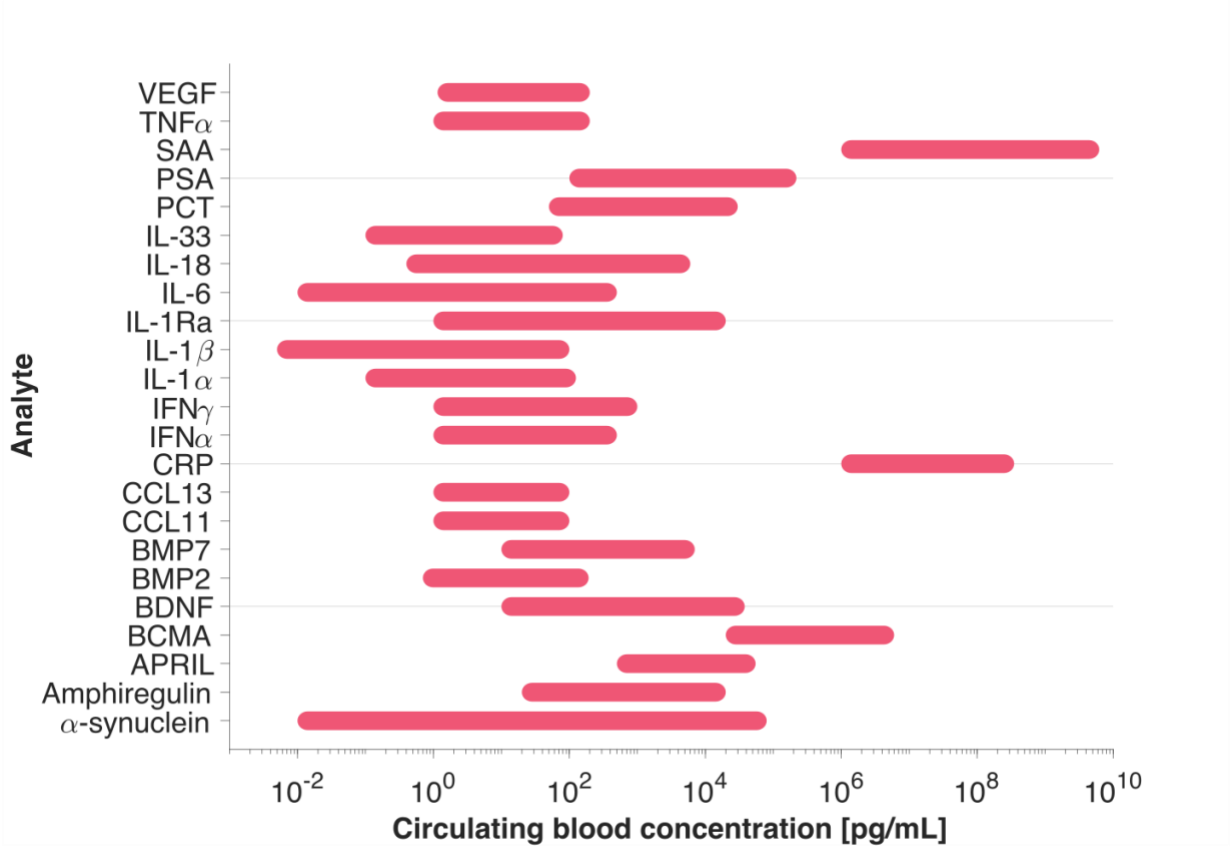

Figure 2: Protein biomarkers with clinical ranges greater than two orders of magnitude. Solid grey lines are a guide to the eye. Abbreviations and sources: α-synuclein[13], amphiregulin[14], a proliferation-inducing ligand (APRIL)[15], B-cell maturation antigen (BCMA)[16], brain-derived neurotrophic factor (BDNF)[17], bone morphogenic protein 2 (BMP2)[18], BMP7[19], C-C motif chemokine ligand 11 and 13 (CCL11,13)[20], C-reactive protein (CRP)[21,22], interferon-α and -γ (IFN-α,-γ)[23], interleukin-1$^{\alpha}$ (IL-1$^{\alpha}$)[24], IL-1β[9,24,25], IL-1 receptor antagonist (IL-1Ra[21,24]), IL-6[9–12], IL-18[9,26,27], IL-33[24], procalcitonin (PCT)[21], prostate-specific antigen (PSA)[28], serum

amyloid A (SAA)[22,29]*, tumour necrosis factor-α (TNF-α)*[21,23]*, vascular endothelial growth factor (VEGF)*[9].

Conventionally, if an assay's dynamic range does not align with its analyte's clinical range, then one of two approaches may be taken. Either multiple assays are run in parallel using serial dilutions of the sample, or affinity binders with different affinities are combined in a single assay[30]. In both cases, additional costs are incurred due to the consumption of additional reagents or the acquisition of new ones. Therefore, there is a need to modify an assay's dynamic range without using serial dilutions or multiple affinity binders.

The need to directly tune an assay's dynamic range is further exemplified by the case of tests that can quantify multiple proteins simultaneously, referred to as multiplexed assays. Such assays offer more information from the same volume of sample, which can increase patient comfort as well as expand the number of targets that can be analyzed without substantially increasing cost[31,32]. Multiplexed assays are particularly desirable in the pharmaceutical industry, where they can be used to eliminate candidate drugs that would cause undesirable side effects earlier in the discovery pathway[33], and in the growing field of personalized medicine, where they can allow sampling of a broad spectrum of indicators to direct or monitor treatment[34,35]. However, dilution is not an option if one assay's dynamic range is not aligned with its clinical range. The required dilution for one analyte may result in the concentration of another being out of quantifiable range. To expand the capacity of multiplexed assays it is necessary to adjust the dynamic range for the detection of a single analyte.

2.2 Assays

The term assay is used in chemistry, metallurgy, pharmacology, and microbiology to refer to procedures that assess a variety of parameters of interest. Within this work we will use the term assay as a shorthand for a molecular biological assay. A biological assay is an analytic procedure that allows the qualitative or quantitative measurement of the presence, concentration, purity, or biological activity of an analyte. We will primarily discuss assays that measure the concentration of a target molecule in a liquid sample, such as blood or urine.

An assay relies upon one or more affinity binders, which react with or bind to the analyte and can transmit a detectable signal through a transducer[36]. In this section we will review different

choices of assay reaction phase, affinity binder, and assay format. We will briefly define methods of signal transduction but will not cover these at length. Finally, we will discuss cross-reactivity-free assay formats, including colocalized assays.

2.2.1 Assay Characteristics

There are several terms that describe the assay binding reactions and response: association and dissociation rate constants, equilibrium constants, Hill slope, dynamic range, limit of detection, and limit of quantification. In this section we will define these terms and discuss their underlying assumptions.

Consider a simple biomolecular system: a probe, P, binds to its target, T, forming the complex PT. Most biomolecular systems are reversible, so the opposite is also true: a complex PT dissociates into independent molecules P and T.

$$P + T \rightleftharpoons PT \tag{1}$$

The rate at which the forward reaction occurs is governed by the *association rate constant*, denoted k_a, k_{on} or sometimes k_+. The association rate constant accounts for the diffusivity of the constituent molecules and the geometric alignment of the binding sites[37]. The association of P and T is a second-order reaction, and its rate can be written as

$$Association\ rate = k_a[P][T] \tag{2}$$

Where k_a has units of $M^{-1}s^{-1}$. The dissociation reaction, having only one reactant, is a first-order reaction. The *dissociation rate constant* (k_d, k_-, or k_{off}) has units of s^{-1} and represents the probability that the complex will spontaneously break apart[38,39].

$$Dissociation\ rate = k_d[PT] \tag{3}$$

The rate constants can be determined through kinetic experiments, which require repeated measurement of a reaction as it approaches equilibrium.

The system at equilibrium is defined by a different set of constants. The *association equilibrium constant*, K_A or K_{eq}, is equal to the ratio of the forward and reverse rate constants or the ratio of products to reactants.

$$K_A = \frac{k_a}{k_d} = \frac{[PT]}{[P][T]} \tag{4}$$

The association equilibrium constant has units of M^{-1}, litres-per-mol. The *dissociation equilibrium constant*, K_D, is its inverse and has more familiar units of M. Either equilibrium constant may be quoted as the affinity of the probe for its target. In this thesis we will use the term affinity to refer to the dissociation constant – the lower the K_D value (ex. nM vs. μM), the more its equilibrium state is shifted towards the products.

Equilibrium binding curves may be generated by fixing the concentration of one reactant while varying the other, allowing the reaction to reach equilibrium, then measuring the concentration of the product or one of the reactants. For one-site binding the form of this curve is a smooth hyperbolic saturation, commonly fitted with a form of the Hill-Langmuir equation derived as follows[40,41].

The total concentration of probes is conserved:

$$[P]_{free} + [PT] = [P]_{total}$$

$$\text{but } [PT] = K_A[P]_{free}[T]_{free}$$

$$[P]_{free} + K_A[P]_{free}[T]_{free} = [P]_{total}$$

$$1 + K_A[T]_{free} = \frac{[P]_{total}}{[P]_{free}} = \frac{[P]_{total}[T]_{free}K_A}{[PT]}$$

$$[PT] = \frac{K_A[T]_{free}[P]_{total}}{1 + K_A[T]_{free}}$$

$$or\ [PT] = \frac{[T]_{free}[P]_{total}}{[T]_{free} + K_D} \tag{5}$$

Typically, the probe concentration is held constant while the target concentration is varied. The formation of complex PT transmits a signal through a transduction pathway, such as fluorescence or electron permittivity.

The binding reaction of one probe with multiple targets is written as follows:

$$P + nT \rightleftharpoons PT_n \tag{6}$$

The total concentration of probes is conserved:

$$[P]_{free} + [PT_n] = [P]_{total}$$

$$\text{and } [PT_n] = K_A[P]_{total}[T]_{free}{}^n$$

$$[P]_{free} + K_A[P]_{free}[T]_{free}{}^n = [P]_{total}$$

$$1 + K_A[T]_{free}{}^n = \frac{[P]_{total}}{[P]_{free}} = \frac{[P]_{total}[T]_{free}{}^n K_A}{[PT_n]}$$

$$[PT_n] = \frac{[T]_{free}{}^n[P]_{total}}{[T]_{free}{}^n + K_D} = \frac{[T]_{free}{}^n[P]_{total}}{[T]_{free}{}^n + K_{0.5}{}^n} \tag{7}$$

Where $K_{0.5}$ is the inflection point of the binding curve and n is the *Hill coefficient*. For one-site binding the value of n is unity and the inflection point equals the K_D. The Hill coefficient was originally defined as being equal to the number of target molecules each probe can bind, but empiric testing demonstrated a more complex meaning[41]. In fact, the Hill coefficient represents the combined effect of the number of binding sites and the cooperativity between them[41,42].

A curve displaying [PT] as a function of [T], with [P] held constant, is shown in Figure 3A. In biomolecular assays the curve is more commonly plotted on log-log or semi-log axes (Figure 3B), where the curve has a familiar 'S' shape. The slope of the curve at the midpoint corresponds to the Hill coefficient.

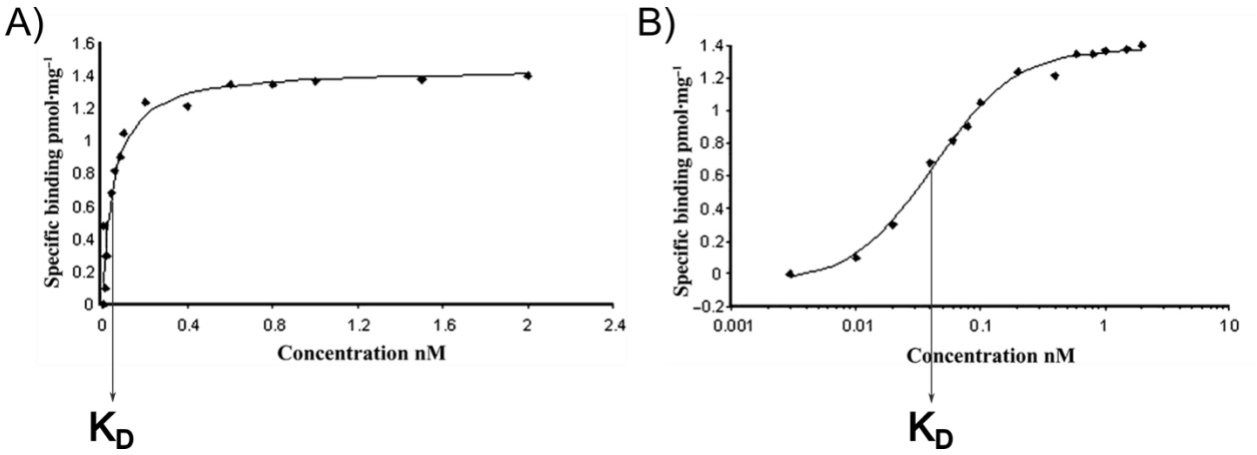

Figure 3: Representative saturation binding curves for single-site binding displayed on A) linear axes and B) linear y scale, logarithmic x scale. Adapted from Hulme and Trevethick[40]

Considering equations 5 and 7, when $[T]_{free} = K_D$ or $K_{0.5}$ then half of P will have been converted to the complex PT. Thus, the probe's affinity can be directly from the binding curve. Use of these equations relies on the assumptions that the reaction is at equilibrium, that all the binding sites of a single receptor are simultaneously occupied[41] (in the formation of PT_2 the concentration of PT_1 is negligible), and the free concentration of T is always essentially equal to the total concentration of T added[38,40,41,43]. This final assumption requires that the concentration of P is much lower than the K_D value, ideally at most $[P] = 0.1\ K_D$. In this case the K_D value calculated using the Hill-Langmuir equation with $[T]_{total}$ exceeds the actual K_D by at most 5%[40]. Especially for high affinity probes, this condition is difficult to achieve in practice as it may require operating below the detection limit of most detection systems.

As an alternative, one can account for the depletion of free target by the probe according to the following derivation:

$$[P]_{free} = [P]_{total} - [PT], \qquad [T]_{free} = [T]_{total} - [PT]$$

$$K_D = \frac{[P]_{free}[T]_{free}}{[PT]} = \frac{([P]_{total} - [PT])([T]_{total} - [PT])}{[PT]}$$

$$[PT]^2 - ([T]_{total} + [P]_{total} + K_D)[PT] + [T]_{total}[P]_{total} = 0$$

Applying the quadratic formula,

$$[PT] = \frac{([P]_{total} + [T]_{total} + K_D) - \sqrt{([P]_{total} + [T]_{total} + K_D)^2 - 4[P]_{total}[T]_{total}}}{2} \quad (8)$$

Equation 8, known as the *quadratic binding equation*, is considered appropriate to use when the probe concentration is on the order of K_D or up to 10-fold greater[43]. Some cases of its accurate use have been documented for [P]=100*K_D [43], but this requires data with minimal noise. In general, as the probe concentration increases the relative contribution of K_D decreases, therefore decreasing the precision with which the dissociation constant can be determined.

In addition to determining equilibrium constants, the binding curve can also be used to quantify an unknown concentration of a target molecule. For instance, the amount of a cancer-associated protein may be measured in a blood sample. In this case a series of known quantities of the target are added to buffer or a matrix representative of the test sample. The resulting binding curve is called a *calibration curve.* The signal measured from the unknown sample is compared to this standard, and the apparent target concentration in the sample is interpolated[44].

When visualized with a logarithmic *x* axis (Figure 3B), a portion of the binding curve between the upper and lower asymptotes appears linear and is often referred to as the "linear region". Of course, it is not actually linear, and attempts to fit the log-transformed data with a linear curve are discouraged because they can hide important information[38] or introduce bias[45]. The so-called linear region represents the interval of analyte concentrations where the assay can provide quantitative information, otherwise known as the detection or *dynamic range*.

The dynamic range can be defined either mechanistically or statistically, with both definitions being equally common in the literature. From a mechanistic standpoint, the binding curve is determined by fitting the data with the Hill-Langmuir equation[46]. The dynamic range is then considered to be between the concentrations that provide 10% to 90% of the signal saturation level[47,48]. It is worth noting that this is not identical to the original definition by Hill, which predicts receptor occupancy rather than signal transduction[41]. On the other hand, the dynamic range is often defined in terms of statistical values, such as standard deviation or relative error. For instance, the dynamic range may be defined as extending from the lower *limit of detection* (LLOD) or *limit of quantification* (LLOQ) to the upper. The LLOD is the smallest signal that can

be distinguished from the background, but not necessarily quantified. Alternatively, the LLOQ is the lowest concentration at which a signal can be detected and reliably quantified, according to some accepted limit. These values may be defined in terms the standard deviation: for example, the LLOD is often expressed as being the concentration at which the signal is equal to the background signal plus three times the standard deviation of the background signal measurement[32,49]. It then follows that the ULOD would then be the concentration that provides a signal equal to the saturation level minus three times the standard deviation (Figure 4A). Different multipliers for the SD, such as 2, 4, or even 10 have also been used[50]. The limits are also expressed in terms of the signal-to-noise ratio (S/N): for example, the LLOQ may be defined as the first point at which the S/N is greater than 10[49,51]. Finally, the limits may be defined as the concentrations for which the relative bias[51,52] or CV[50] is less than some determined limit (Figure 4B). This method of defining the dynamic range is considered most preferable for pharmaceutical or clinical use[52], as it demonstrates that an assay meets accuracy requirements over its entire working range. For instance, the FDA Bioanalytical Method Validation[53] specifies that the bias "should be ±20% of the nominal (theoretical) concentrations, except at LLOQ and ULOQ where the calibrator should be ±25% of the nominal concentrations…", while the total relative error "should be ±30%, except at LLOQ, ULOQ ±40%."

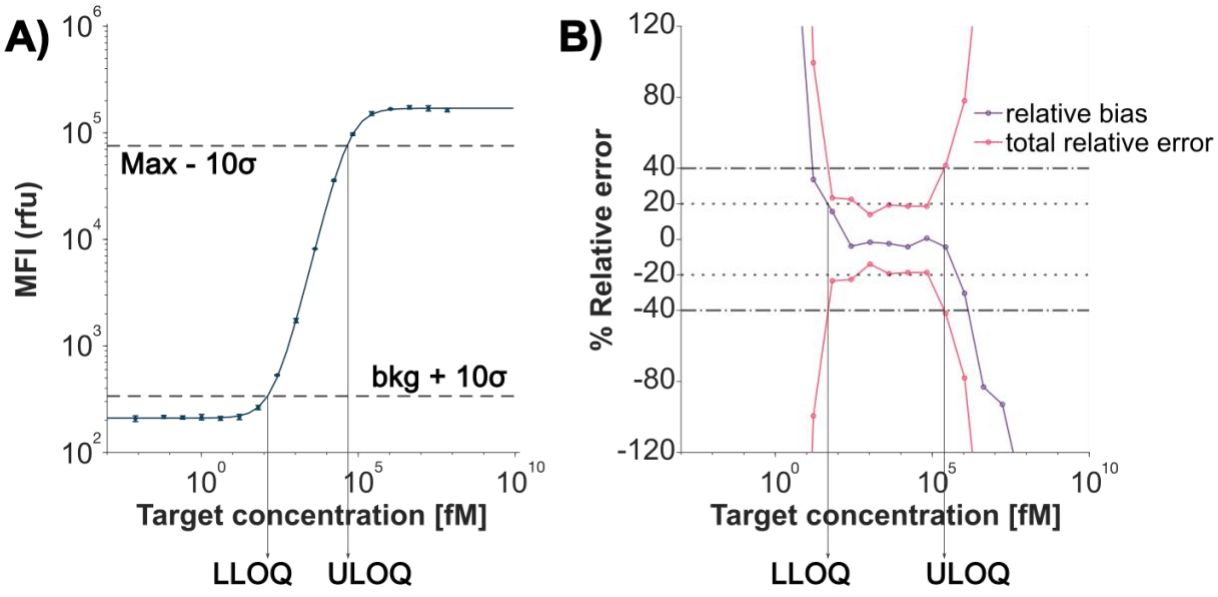

Figure 4: Definitions of the limits of quantification based on A) standard deviation, B) relative error. The dashed lines in A) indicate the background signal plus 10 standard deviations of the background (LLOQ) and the saturation signal minus 10

standard deviations of the saturation. The dotted and dot-dashed lines in B) are the acceptance limits of ±20% relative bias and ±40% total relative error, respectively. The dynamic range would then be the interval of concentrations between the two limits. LLOQ: lower limit of quantification, ULOQ: upper limit of quantification

2.2.2 Assay Reaction Phase: Liquid and Solid Phases

Molecular assays can broadly be classified depending on whether the binding reaction takes place in solution (liquid-phase assay, Figure 5A) or at the interface between solid and liquid (solid-phase assay, Figure 5B). The earliest immunoassays, developed in the 1960s, were liquid-phase assays, where antibodies were labelled with radioisotopes[54]. In the following decades the field of molecular assays moved away from the liquid-phase toward solid-phase assays for simplicity, higher sensitivity, reduction of cost, and adaptability to point of care[55,56]. However, there are some applications where the former is most appropriate.

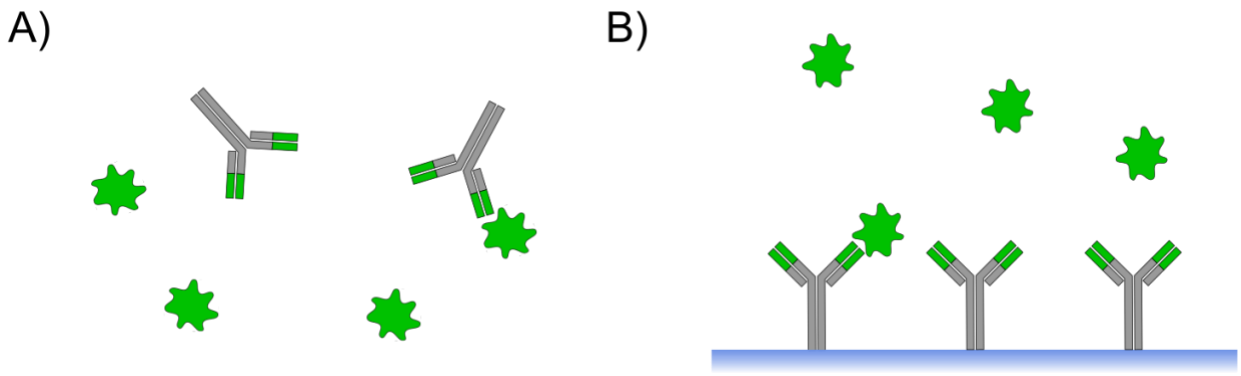

Figure 5: Simplified representations of a A) liquid-phase assay, where binding occurs in solution. B) solid-phase assay, where binding occurs at the interface between the solution and a solid substrate, such as a glass slide or polystyrene bead.

Liquid-Phase Assays

Liquid-phase assays can be further sub-divided into homogeneous and heterogeneous, or separation, sub-types. In homogeneous assays the bound and free labelled reagent (antigen or affinity binder) are not isolated from each other. Instead, the measured signal is modulated by the formation of the bound complex. For instance, interaction of the affinity binder and target may bring together a radioisotope or fluorescent label and its appropriate quencher, or an enzyme and activator[54,55]. These assays are considered fast and simple, as there is no need for washing or separation. However, in practice it is difficult to achieve 100% modulation of the signal, so homogeneous assays are best used when low detection limits are not required[55].

In the case of heterogeneous assays, the bound and free reagent are separated, and one or both are quantified. Examples of separation steps include adsorption of free reagent to a substrate (ex. charcoal), precipitation of bound complexes, or techniques such as chromatography or gel filtration that separate molecules by size or charge[54–56]. Methods wherein bound complexes are pulled down to a solid substrate (ex. a well-plate coated with secondary antibodies) are used widely, as the substrate can be washed to remove the unbound, labeled reagents which contribute to the background noise[55]. However, in practice it is difficult to achieve total separation of the free and bound reagents, contributing to assay bias and imprecision[56]. Another disadvantage of heterogeneous liquid-phase assays is that separation steps often increase the time and labour required for the assay and involve the use of specialized equipment (centrifuge, gels, columns, or manual washing)[55,56]. These disadvantages have led to a transition toward solid-phase assays, which are described below. However, solution-phase and solid-phase assays using the same reagents have been found to have divergent results[57,58]. For example, del Rosario Stumpo and colleagues[58] observed that solution-phase assays for anti-insulin antibodies tended to isolate rare, high-affinity antibodies while solid-phase assays were enriched for more abundant, low-affinity antibodies. They proposed that in solid-phase assays, where the local insulin density at the surface is very high, antibodies with fast off-rates can rebind to another antigen in proximity. Whereas in solution, the concentration of insulin is lower and thus the antibody affinity is the dominating factor[58].

Despite the disadvantages listed here, in some cases it is more appropriate to use a liquid-phase assay than solid-phase. Adsorption or linkage of reagents to a substrate often causes changes in binding characteristics or total loss of function due to molecule denaturation or steric hindrance of epitopes[55–57]. Further, homogeneous liquid-phase assays can be designed for point-of-care use with naked-eye readout or smartphone[59,60].

Solid-Phase Assays

In solid-phase assays, at least one reagent is attached to attached to a solid surface such as a well-plate, glass slide, polymer membrane, metal, or paper. The target and affinity binder then interact at the interface between the solid and adjacent media. Some of the most widely used assays fall into this category, such as DNA microarrays and ELISA plates. A surface blocking agent, such as bovine albumin or casein, is almost always necessary to prevent the free reagents from

binding non-specifically to the surface, which can lead to a high background signal[61]. An advantage of using a solid substrate is that it allows washing, which can remove non-specifically bound reagents while leaving the specific complexes intact, reducing background signal generation. However, the electrostatic charge of the surface and reagents (in particular, DNA is negatively charged at neutral pH), the size and diffusivity of the free reagent (analyte, affinity binder), and the density of the surface-bound reagent can all influence the reaction dynamics. For example, in DNA microarrays when the surface-bound capture probes are too tightly packed, steric hindrance can result in hybridization efficiencies <10% [62]. In addition, the negatively charged backbone of DNA is repulsed the layer of DNA on the surface, and in some cases the charge of the surface itself (gold surfaces), leading to a reduction in hybridization reaction dynamics[62]. These effects result in solid-phase DNA hybridization being thermodynamically disfavoured compared to the same sequences hybridizing in bulk solution[63–65].

However, the primary factor controlling the reaction is mass transfer limitation[66]. For high-affinity probes or large, diffusion-limited targets, a depleted layer forms near the surface. The fluid directly next to the surface experiences little movement, even with the use of shaking or mixing. Assays may require hours to reach equilibrium due to limited diffusion[66]. When the effective concentration of probes exceeds the true affinity of the probe for its target (as measured without depletion), the bulk solution will become depleted of target molecules. In this *ligand-depletion regime*, the dynamic range is dependent on the density of probes on the surface and the sample volume, and the detection limit is higher than theoretically achievable. The sensor's specificity is also diminished, as the difference in the probe's affinity to its target vs. analogous molecules has less effect on binding[67]. Some assays intentionally operate in this regime in order to shift equilibrium towards the bound state[68,69]; however, this requires that extra care is taken while performing the assay. Deviations in the volume or probe density will shift the binding response and can lead to incorrect calculation of the target concentration in a sample[67].

Micro- and Nanoparticle-Based Assays

A subset of surface assays is those that use micro- or nano-scale particles as the assay substrate. These particles may be fabricated from polymers, hydrogels, gold, or other materials. Particle-based assays are easier and less expensive to multiplex than microwell or plate-based assays[31,70,71]. Each bead is a self-contained assay, thus providing statistical rigour without

massive parallelization[31,72,73]. More significantly, the beads are equivalent and experience uniform assay conditions due to mixing. This limited bias contrasts with microarrays and well-plate assays, which experience spatial bias that can substantially distort results[74,75]. Modeling[76] and experimental analysis[77] of bead assays indicates that they achieve higher reaction rates than plate assays, approaching the performance of liquid-phase assays[70,77]. The particles' small size also allows them to be easily isolated from the supernatant using magnets (for ferro-magnetic cores), vacuum filtration, or pelleting via centrifugation. This facilitates stringent washing and can be automated.

An advantage of particle assays is the ability to measure using flow cytometry, wherein particles are isolated in a flow stream and passed through a series of lasers. Due to the narrow stream and the optical setup, very little background signal is generated from free fluorescent labels in solution[78]. This has permitted development of assays without any washing steps, reducing time and labour demands[70,77]. Further, cytometry can measure thousands to tens-of-thousands of particles per second[78]. The cytometer can differentiate between microparticles targeting different analyte molecule via detection of fluorescent barcodes or small variations in size that lead to varied scattering of visible light[71].

2.2.3 Affinity Binders

Assays typically rely on the ability of an affinity binder to recognize and bind to some portion of the target molecule. Antibodies are the most commonly used affinity binder for protein and small molecule targets[79]. Deoxyribonucleic acid (DNA) and ribonucleic acid (RNA) probes are typically used when the target is a nucleic acid[65]. Synthetic nucleic acid probes, known as aptamers, have also been developed for some protein and small molecule targets[79].

Antibodies

Assays which recognize analytes through reaction with one or more antibodies are called immunoassays. Antibodies are specialized proteins secreted by the immune system to identify foreign antigens. Several different classes of antibodies exist. We will focus on immunoglobin G (IgG) antibodies, as most antibodies used in immunoassays are of this class. IgG antibodies are roughly Y shaped, consisting of 2 identical antigen-recognizing (Fab) domains and one constant (Fc) domain (Figure 6A). Only the tip of the antigen-recognizing domain is involved in binding,

through a site known as the hyper-variable region. Six different peptide loops are combined to form this binding site, which allows the immune system to generate a tremendous diversity of antibody specificities from a relatively small pool of genes[80]. The binding site may be a small pocket or a broad surface, depending on the shape of the antigen. The portion of the antigen recognized is called an *epitope*. The antibody does not recognize its epitope through a single event, but rather through the combination of several non-covalent interactions. At the recognition surface, peptide chains participate in van der Waals interactions, hydrophobic interactions, hydrogen bonds, and electrostatic interactions between charged side chains. Although a small number of amino acids contribute most of the binding energy, overall surface complementarity also plays a role in reducing off-target binding. The absence of a single binding element between an antibody and a close analogue of its antigen decreases the avidity, and may prevent any detectable binding between the two molecules[80]. The affinity of an antibody can be enhanced through selective mutation of the binding elements, which will be discussed later in section 2.3.2.

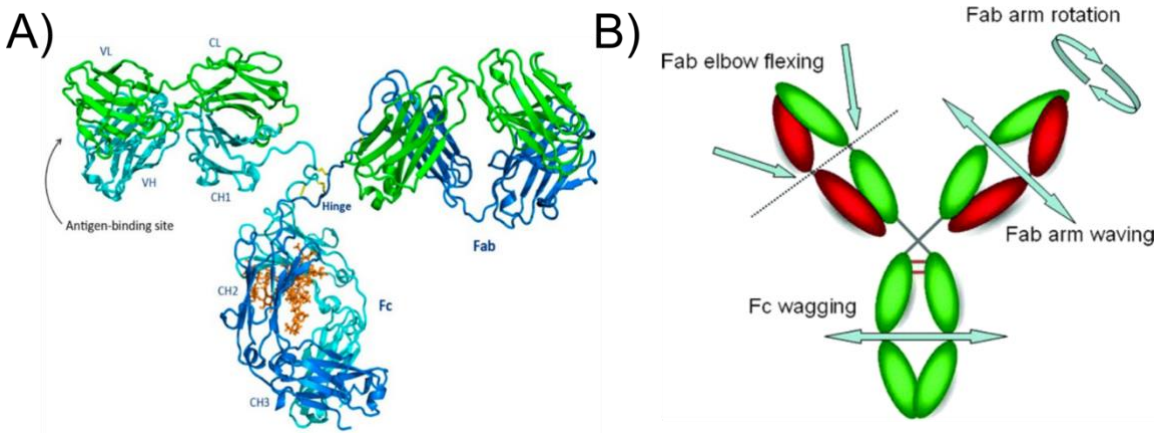

Figure 6: Two representations of an IgG antibody. A) Ribbon diagram, demonstrating the sub-domains making up the 2 Fab components and the Fc component. Note the single ribbon representing the hinge domain as well as the linkage connecting the VL and CL and the VH and CH1 sub-domain. Reproduced from Chiu et al.[81] B) Simplified schematic with planes and axes of motion indicated. Each ellipse represents a compact peptide sub-domain. Reproduced from Hopkins[82].

An antibody is not a single rigid body but rather is composed of multiple loosely connected parts. The three components – two Fab domains and an Fc domain – are joined at the center by the hinge domain (Figure 6A)[81,83–85]. The hinge domain permits the Fab components to move independently and adopt inter-Fab angles from 0 to up to 180°, depending on the antibody species[83,86]. In addition to the substantial motion permitted by the hinge domain, there is also

flexibility within the three primary components of the antibody[82,83]. Each component is composed of multiple rigid sub-domains, connected by a relatively unstructured linkage. This semi-flexible linkage permits rotation akin to a ball-and-socket joint (Figure 6B)[83].

Nucleic Acids

Nucleic acids are biomolecules that are well-known for providing the genetic code of all living things (and some non-living things as well, like viruses). Nucleic acids are polymers of nucleotides: molecules containing a sugar, a phosphate group, and a base. The sugar of one nucleotide bonds with the phosphate of the next, forming the sugar-phosphate backbone. The base can be one of five structures: adenine, cytosine, guanine, and either thymine or uracil in DNA or RNA, respectively. The bases of one polynucleotide strand pair with those of another by forming hydrogen bonds with their specific complement, in a process called hybridization. In regular Watson-Crick base pairing, cytosine pairs with guanine through three hydrogen bonds, and adenine pairs with thymine or uracil through two hydrogen bonds. Other pairing arrangements exist, though they are not as stable as these standard pairings. The stability of the duplex, and by extension the affinity of one strand for the other, depends on the identity of each base pair and the overall sequence[87]. We will primarily discuss DNA affinity, as the molecule is better characterized than RNA due to its higher stability. DNA hybridization is considered to be one of the most specific molecular binding events ever reported[88]. DNA affinity and mechanical properties will be discussed further in sections 2.3.2 and 2.4.

Aptamers

Aptamers are single-stranded DNA or RNA molecules that, through secondary or tertiary structures, form a shape that can bind target molecules with moderate affinity. Aptamers were first speculated after the discovery of ribozymes, folded RNA structures that catalyze reactions like protein enzymes[89]. Aptamers are developed synthetically through an evolution process known as SELEX (Systematic Evolution of Ligands by EXponential enrichment)[89], though naturally-occurring aptamer-like molecules known as riboswitches have been identified[90]. Most aptamers are relatively unstructured in solution, and fold into their binding position upon interaction with their target[91]. As nucleic acids lack the diversity of functional groups available in amino acids[91,92], the binding of aptamers to their targets is primarily through hydrogen

bonding[91]. A common motif is pseudo-base-pairing between a single base and polar groups on the ligand, stabilized by a planar surface formed by a non-Watson-Crick base pair or triplet such as a Hoogsteen G-G pair[91]. Alternatively, hydrophobic regions of the ligand may interact with the major groove of the duplex, which bulges to form a binding pocket. A single-stranded loop then folds over the ligand, securing it in place. This binding motif highlights how an aptamer discriminates against molecules similar to its intended target; the addition of a single methyl group, such as from theophylline to caffeine, causes steric hindrance and prevents the analogue fitting in the binding pocket[91]. Though in general aptamers have lower affinity than antibodies, high affinity (K_D ~ pM) have been synthesized. The integration of modified bases can further enhance aptamer affinity[92], and will be later discussed in section 2.3.2.

2.2.4 Basic Assay Formats

Numerous assay formulations have been developed over the last several decades that are optimized for sensitivity, speed, throughput, ease-of-use, or one of many other parameters. However, they generally have two core steps: target recognition and signal transduction. The target recognition reaction can be classified into several basic types. Here we will review competitive assays and non-competitive single-binder and sandwich assays. Assays are also classified based on their method of signal transduction. In direct assays the labelling molecule (fluorophore, enzyme, biotin, etc.) is conjugated to the interacting affinity binder, whereas in indirect assays the label is conjugated to a secondary binding molecule. For example, if a target is recognized by an antibody raised in mouse cells, a fluorophore-labelled rabbit anti-mouse antibody may be used for indirect detection. Finally, "label-free" assays detect the binding of probes or targets through changes in refractive index, mass, or electron permittivity[93]. For the remainder of this section, we will focus on the target recognition step, regardless of whether the assay is direct, indirect, or label-free.

Competitive Assays

Competitive assays depend on competition between the analyte and a known quantity of its analogue for a limited number of affinity binders (Figure 7A, B). Quantification of the analyte is often indirect, as it is easier to detect the analogue in some competitive techniques[61,94]. Competitive assays can be solid or liquid phase, or a hybrid of the two involving a pull-down

step. Competitive binding assays are commonly used for detection of small molecules, where steric hindrance from multiple binders would be a concern, or when only one affinity binder for the analyte exists[94].

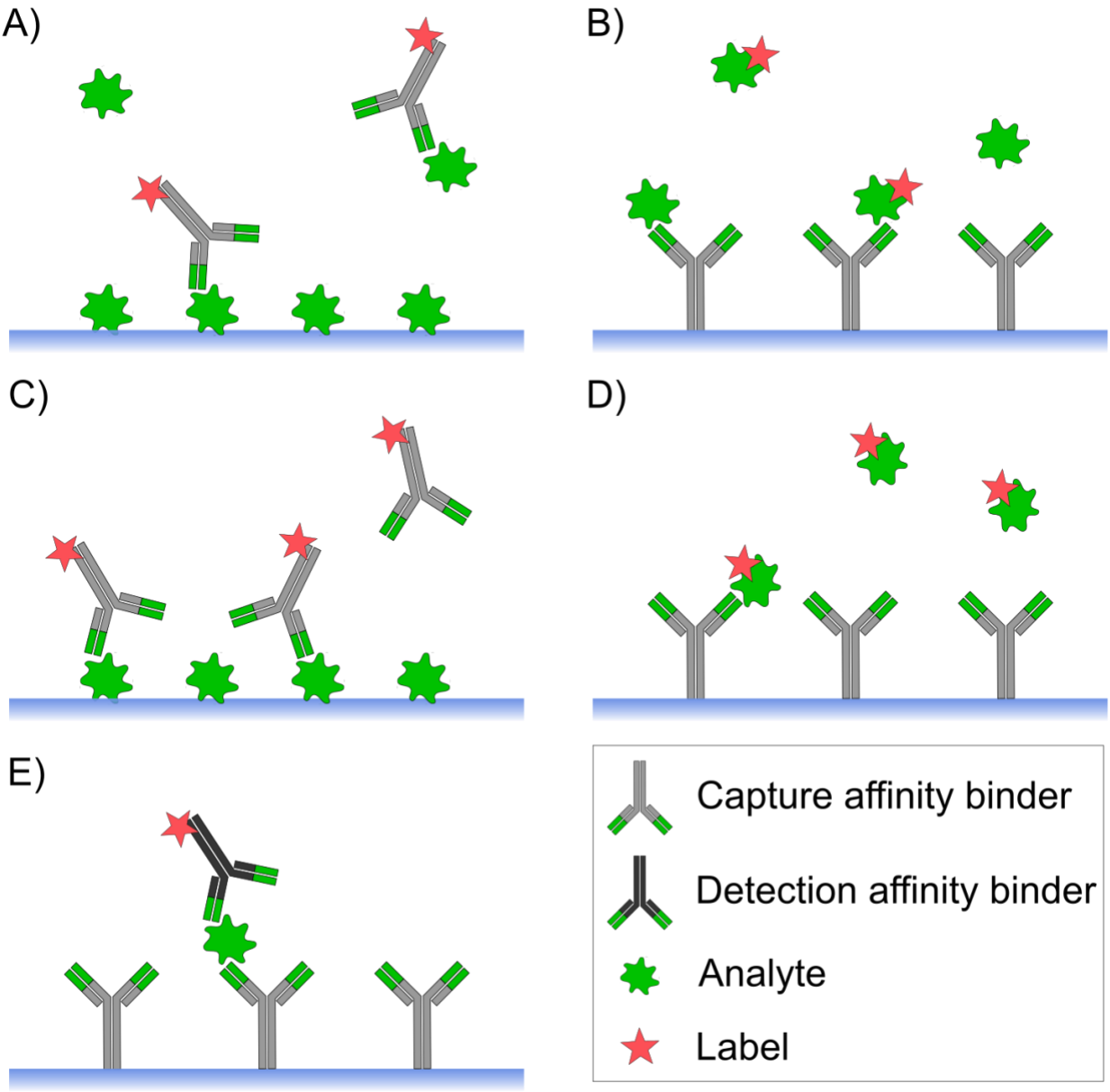

Figure 7: Simplified representations of solid-phase formats of (A and B) competitive assays, (C and D) non-competitive single-binder assays, and (E) sandwich assays. Whereas antibodies are shown here, they are representative of any affinity binder. Similarly, although the assays are shown using direct labelling (the star symbol represents biotin, a fluorophore, etc.), they could also be performed using indirect or label-free methods. A) The sample is mixed with affinity binders and incubated with a surface coated with an analogue of the analyte. The analyte in the sample competes with the surface molecules for binding sites. After

incubation, the portion of affinity binders that have interacted with the analogue or the solution analyte is quantified. B) The sample is mixed with a labeled analogue of the analyte and incubated with a surface coated with affinity binders. The labeled and unlabeled analyte compete for binding sites. After incubation, the amount of labeled analyte bound to the surface is quantified and used to determine the amount of analyte that was in the sample. C) The sample is adsorbed to the surface, and then incubated with affinity binders. The number of affinity binders that interact with the surface is directly proportional to the quantity of analyte in the sample. D) The sample is incubated with a surface coated with affinity binders. The number of analytes that interact with the surface is measured, and correlates directly to the quantity of analyte in the sample. E) The sample is incubated with a surface coated with capture affinity binders. At the same time, or after washing, detection affinity binders are added which bind to a different epitope on the analyte molecule. The number of detection affinity binders that interact correlates directly to the quantity of analyte in the sample.

Non-competitive Assays

By comparison, non-competitive assays use an excess of the affinity binder to bind all the available analyte. The quantity of probe-target complexes formed is proportional to the total amount of the analyte in the sample; for this reason, they are sometimes called immunometric assays[54–56,95]. Non-competitive assays are more sensitive than competitive assays using the same affinity binders, based on mathematical modelling (Figure 8). This is because non-competitive assays directly measure the probe sites bound to an analyte, while competitive assays effectively measure the probe sites that are not bound to an analyte[95,96]. More simply, the use of excess affinity binders ensures that even trace amounts of the analyte can be bound and detected. However, the excess binders also increase the signal produced from non-specific binding events, thus requiring stringent assay controls[55].

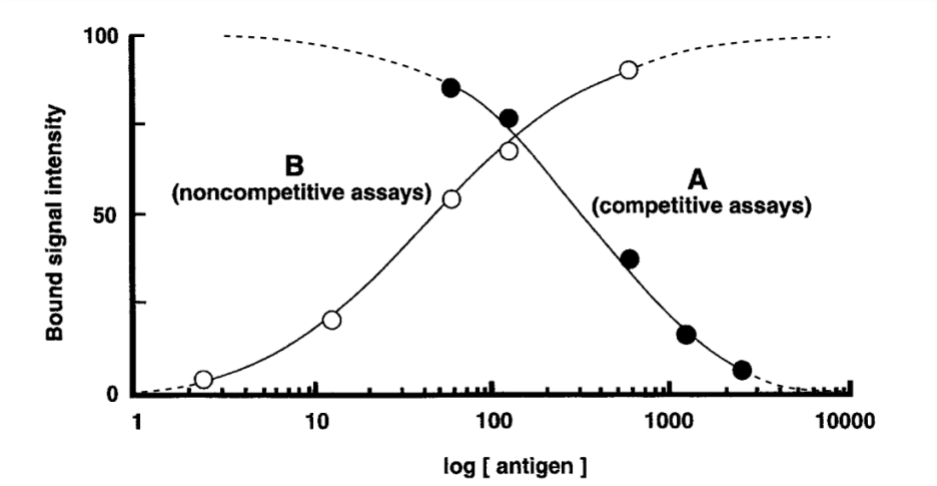

Figure 8: Typical binding curves for a A) competitive assay (filled circles) and B) non-competitive assay (unfilled circles) using the same affinity binders. The solid lines indicate the dynamic range (from 10 to 90% signal) while the dashed lines indicate the total detectable range. Adapted from Kobayashi and Goto[95]

Non-competitive assays can be further differentiated based on whether they detect one or two binding sites on the same analyte. Single binder assays, having only one target recognition reaction in their detection step, are commonly used for measuring small molecules (Figure 7C, D). Like competitive assays, reagent-excess single-binder assays can be performed with either the analyte or affinity binder adsorbed to a solid phase, or the reaction can occur entirely in the liquid phase[61,94].

Sandwich assays make use of two affinity binders that recognize different epitopes of the same analyte (Figure 7E). They are primarily used for detection of macromolecules, where multiple high-affinity epitopes may be available and steric hindrance between binders is less of a concern[95]. Typically, the first binder, often called the *capture* molecule, is bound to a solid substrate. Following incubation with the sample, the second *detection* binder is added and binds to the target molecule, thereby "sandwiching" it between the two binders[94]. Liquid phase and hybrid sandwich assays have also been developed, examples of which will be discussed in section 2.2.6. Sandwich assays have a higher specificity than single binder assays due to the increased stringency of requiring two recognition reactions[95]. They are commonly used for rare targets in complex samples or samples containing similar molecules that must be differentiated[61]. They have the obvious disadvantage of requiring two affinity binders that recognize non-overlapping epitopes, the identification of which can be time-consuming and expensive[97].

Fortunately, sandwich antibody pairs for common biological targets are sold as sets by many suppliers.

2.2.5 Cross-reactivity and Non-specific Binding

All assays depend on the transduction of a signal, whether it is a change in colour, electrophoretic mobility, or optical permittivity. However, in practice it is difficult to determine whether a measured signal is the result of a true binding event or experimental noise. There are a plethora of potential sources of noise[98], but we will focus on non-specific binding and cross-reactivity. We define non-specific binding as interactions of an analyte or affinity binder through regions other than its binding sites[99]. For instance, a labeled plasma protein adsorbs to a surface, producing a signal when no target is present (Figure 9A, left). Alternatively, hydrophobic groups in the protein interact with those in a surface-bound antibody (Figure 9A, middle). In contrast, in cross-reactivity most or all the affinity binder's target-recognition sites interact specifically with an unintended epitope[99]. For instance, a surface-bound capture antibody binds to a molecule with structural similarity to the target it was raised against (Figure 9B, middle). Sandwich assays were developed to mitigate sources of noise-derived signal by requiring two binding events to generate detectable signal (Figure 9C). The likelihood of two cross-reactive or non-specific binding events occurring is very low, making sandwich assays against a single target (singleplex) more robust to noise-derived signal[93].

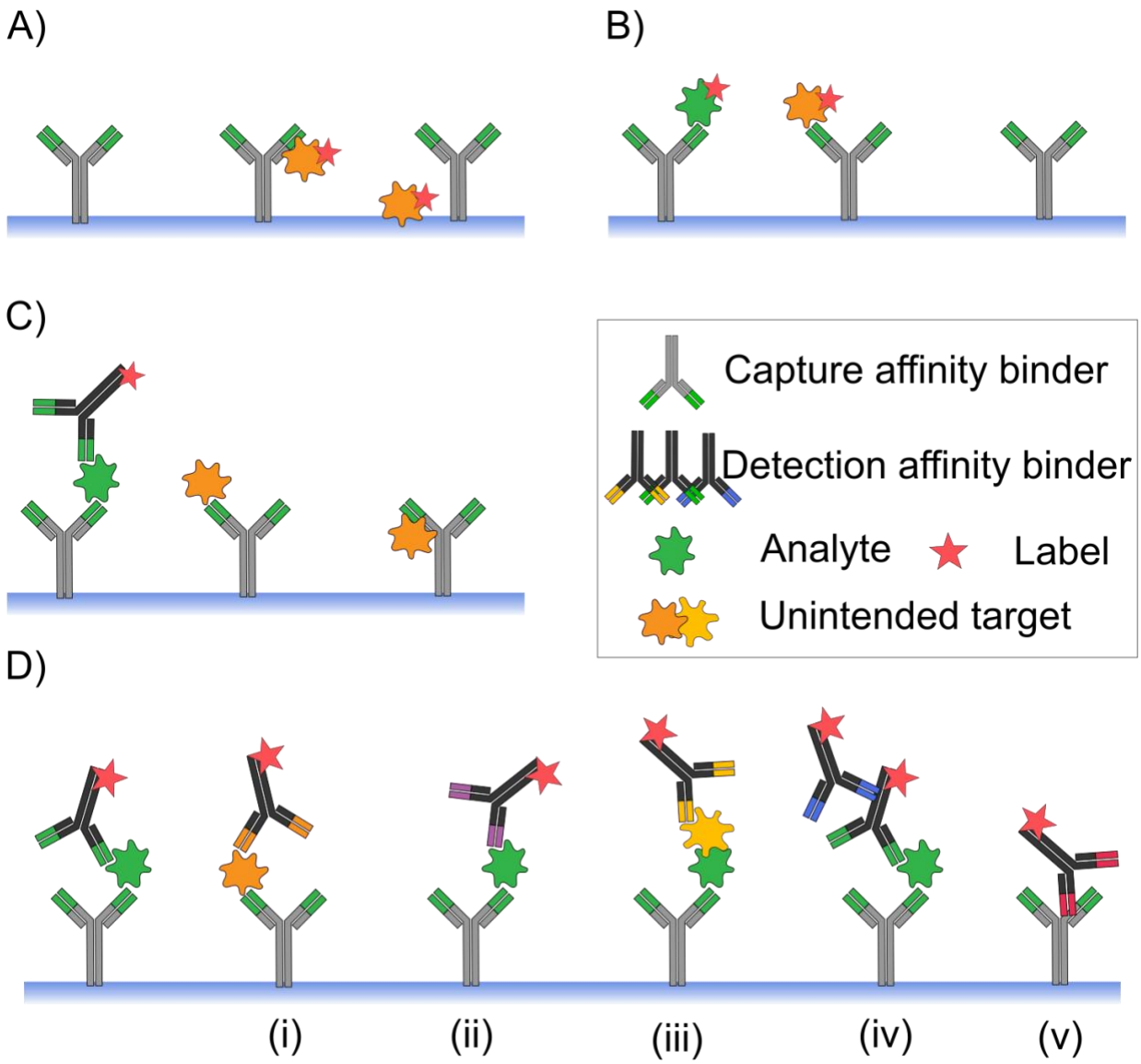

Figure 9: Cross-reactivity and non-specific binding in different assays formats. Whereas antibodies are shown here, they are representative of any affinity binder. Similarly, although the assays are shown using direct labelling, the same cross-reactive and non-specific binding pathways generate incorrect signals from indirect or label-free assays. A) In a single-binder assay, (middle) non-specific binding of a labeled plasma protein to a capture affinity binder or (right) to the surface leads to a noise-derived signal. B) (left) a capture affinity binder interacts specifically with its true target. (middle) Cross-reactive binding of a capture affinity binder to a protein with structural similarity to its intended target leads to a false-positive signal. These mechanisms are commonly referred to as sample-driven cross-reactivity. C) In a sandwich assay, two binding events are required to generate a signal. In a single-plex assay, the likelihood of two cross-reactive or non-specific binding events occurring is very low. Sandwich assays are therefore robust to sample-driven cross-reactivity. D) In a conventional multiplex sandwich assay the substrate is incubated with the sample, followed by application of pooled detection

affinity binders. The mixing of reagents provides an opportunity for reagent-driven cross-reactivity between (i) a capture affinity binder and an unintended target, (ii) a detection affinity binder and an unintended target, (iii) two different analytes, (iv) two different detection affinity binders, and (v) a detection affinity binder and a capture affinity binder. (left) intended sandwich complex.

Cross-reactivity presents a significant obstacle when multiple analytes are to be measured in a single sandwich assay (multiplexing). Conventionally, multiplexed sandwich assays are performed by isolating different capture affinity binders in spots on a microarray or microparticles. The substrate is incubated with a sample, followed by application of the pooled detection affinity binders for all targets. This provides an opportunity for interaction of each analyte or detection affinity binder with all other analytes, detection affinity binders, and capture affinity binders (Figure 9D)[93]. The number of possible cross-reaction scenarios increases quadratically with the number of analytes, N, according to 4N(N-1), such that a multiplexed sandwich assay for 5 targets has 80 possible cross-reactive combinations[100].While commercially available affinity binder pairs are tested to confirm they do not react with each other, testing of affinity binders between pairs is not commonly performed.

2.2.6 Cross-reactivity-free Multiplex Sandwich Assays

The assays reviewed in this section are designed with more stringent reaction or transduction requirements, such that only specific binding by both affinity binders leads to a measurable signal. They achieve this limitation of cross-reactivity-driven signal through compartmentalization, co-assembly by linkage of affinity pairs, or proximity-dependent signal transduction, as described below.

Compartmentalization

Assays in this category reduce cross-reactivity by isolating the affinity binders against one target from those against other targets. Therefore, the detection affinity binders only encounter their complementary capture affinity binders. Cross-reactivity between affinity binders and unintended targets can still occur, but two off-target binding events would be necessary to produce a signal. Two examples of this technique will be discussed: the antibody colocalization microarray and the aqueous two-phase system ELISA.

Antibody Colocalization Microarray (ACM)

The antibody colocalization microarray (ACM) reduces cross-reactivity signal by sequentially printing capture antibodies and their corresponding detection antibodies in discrete spots on a substrate. As in a typical microarray assay, droplets of capture antibodies are dispensed onto a reactive glass slide using a microarray printer. The slides are washed, blocked, incubated with the sample, then washed again. Unlike conventional microarray assays, the slides are then returned to the microarray printer and aligned in their previous position using spring-loaded clips. Droplets of detection antibody are dispensed at the same location as their respective capture antibody, forming a liquid compartment where sandwich binding occurs. The volume of the droplet must remain constant during incubation to allow the system to reach equilibrium. This is achieved either by maintaining the printer chamber at elevated humidity[100] or by including glycerol or other additives in the printing buffer[101]. After incubation with the detection antibodies the slides are washed, incubated with labelled streptavidin, washed, and then detected via fluorescence scanning[100]. The full protocol is represented graphically in Figure 10A. To assess the reduction in cross-reactivity, the authors performed assays with all possible combinations of reagents. This analysis demonstrated considerable cross-reactivity-derived signal, especially from antibody pairs with relatively low affinity for their target. A subsequent assay demonstrated that the addition of these cross-reacting reagents reduced the accuracy of a conventional multiplex sandwich assay. Meanwhile, the ACM signal was robust to the inclusion of these reagents[100]. The use of automated pin-spotting facilitates scaling to higher plex levels without increasing labour needs, albeit with long print times. However, the multi-spotting procedure requires accurate re-alignment after removing and replacing the slides. The developers of this platform achieved an accuracy of <20 μm using mechanical alignment aids[100]. A microarray printer with optical recognition capabilities would also be an option. Finally, the use of very small volumes of liquid as the reaction compartments makes the system sensitive to evaporation, as any loss will drive the system out of equilibrium and result in inaccuracy.

To address some of the disadvantages of the ACM, the snap chip platform was developed. In this platform, the capture and detection antibodies are printed on two separate slides (assay and transfer slide respectively) in a mirrored pattern. The assay slide is blocked, incubated with the sample, then washed. Next, the assay and transfer slide are clamped into a custom apparatus and pressed together, such that the detection antibodies are transferred to the capture spots. A

mechanical alignment method is used during printing, such that visual alignment is not required when the slides are placed in the snap apparatus. When 300 µm capture spots and 700 µm detection spots were used, the average centre-to-centre distance was measured to be 147 µm[102]. A subsequent design, where both antibodies are dispensed on transfer slides in nanolitre-scale droplets and snapped onto the assay slide, had an average misalignment of 16 µm[103]. It was also found that the slides could be dried, stored at -20°C for 1 month, and later rehydrated with no loss of signal. This storage method was proposed as a means of decoupling the slide preparation, which requires specialized equipment, from the assay execution[102].

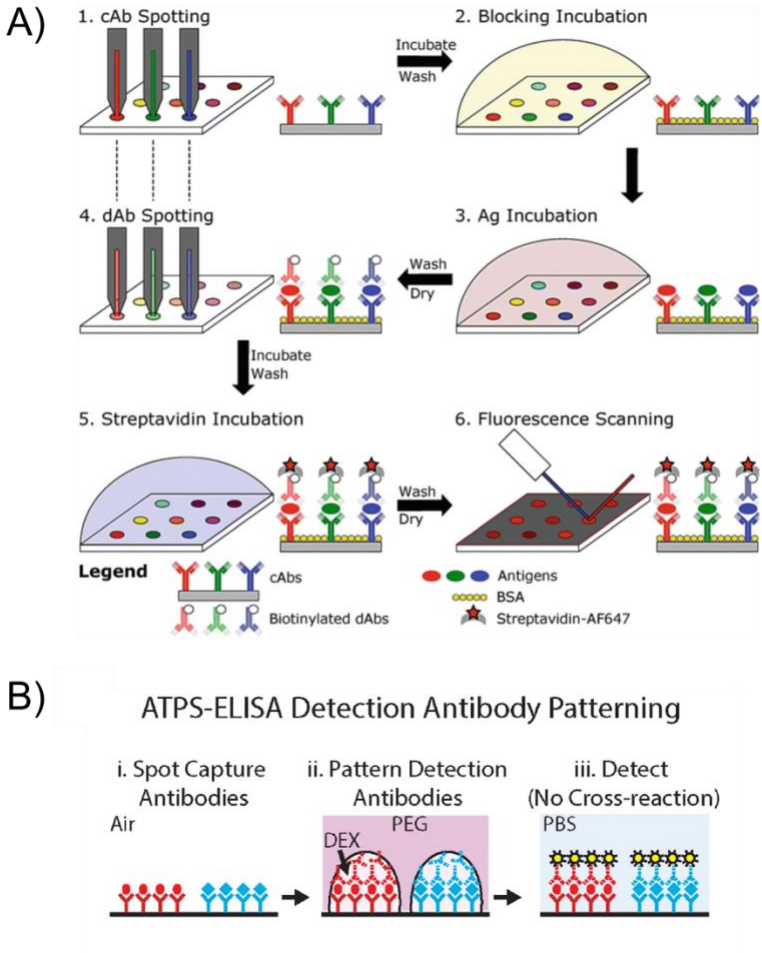

Figure 10: Two assay techniques using compartmentalization. A) Antibody colocalization microarray: (1) capture antibodies are spotted on a functionalized slide, (2) after washing the surface is blocked, then (3) incubated with the sample. (4) the slide is returned to the printer and biotinylated detection antibodies are dispensed in the same location, forming a liquid compartment. (5) after washing the surface is incubated with fluorophore-conjugated streptavidin, then (6) the slide is imaged. Reproduced from Laforte et al.[35] B) Aqueous two-phase system: (i) capture

antibodies are spotted in a well, then incubated with the sample. (ii) the well is filled with PEG, then droplets of dextran containing detection antibodies are dispensed. The dextran droplet forms a reaction compartment. (iii) the wells are washed, incubated with the label, and imaged. Adapted from Frampton et al.[104]

Aqueous Two-phase System (ATPS)

Like the ACM, the aqueous two-phase system ELISA (ATPS-ELISA) prevents antibody cross-reactivity by spatially segregating the capture and detection antibodies within aqueous droplets. The different capture antibodies are spotted within a polystyrene well in a non-overlapping pattern. The entire well is washed, incubated with the sample, and washed again. The well is then filled with a polyethylene glycol (PEG) solution, and droplets of a dextran solution containing detection antibodies are dispensed into the well. The dextran and PEG solutions are immiscible, and the denser dextran sinks to the well surface. Embossed features in the well are used to guide droplet placement, such that each detection antibody is dispensed on top of its corresponding capture antibody. After incubation, the wells are washed and then an enzyme and substrate are added as in a conventional ELISA[104]. The technique is represented graphically in Figure 10B. The protocol was subsequently modified to include mixing the sample into the PEG phase[105], pre-drying the dextran, capture and detection antibodies on the surface[106], and mixing the enzyme into the PEG phase[107]. These changes reduced the assay steps performed by an end-user and the overall time required for the assay. The formulations of the PEG and dextran phases were extensively tested to determine the ideal mixture for rehydration[106], and to facilitate analyte and enzyme diffusion into the reaction compartments while limiting detection antibodies diffusing out (50% retention after 1 hour)[107]. The advantage of this method is that it permits multiplexing in segregated volumes without the need for humidity control to prevent evaporation during incubation. However, the detection antibodies are not completely retained in the reaction compartments. The loss of antibodies to diffusion would prevent the compartments reaching a stable equilibrium, making the results susceptible to variations in incubation time. It may also limit miniaturization of the assay, as smaller droplets would have a higher surface-to-volume and possibly greater diffusion loss. When evaluating the platform's susceptibility to cross-reactivity, the authors only tested the intentional mixing of a goat detection antibody with an anti-goat capture antibody. Therefore, it is unclear if the platform could differentiate close analogues where both antibodies have a moderate affinity, but specific interaction with the unintended

target. The reduced-wash assays could be especially prone to produce erroneous signals from this type of cross-reactivity.

Pre-assembly and Linkage of Affinity Binder Pairs

Assays in this category pre-assemble the capture and detection affinity binders to each other or a solid substrate via flexible or semi-flexible connectors. This connection increases the effective concentration of the second binder once the first binds a target, promoting the formation on-target sandwich complexes. The overall off rate is also decreased, as the target molecule must unbind from both affinity binders to entirely unbind from the probe. This phenomenon of apparent affinity enhancement will be discussed further in section 2.3.3. Two notable assays using co-assembly will be described below: the nanoswitch-linked immunosorbent assay and the colocalization-by-linkage assay on microparticles.

Nanoswitch-linked Immunosorbent Assay

The nanoswitch-linked immunosorbent assay (NLISA) consists of two sandwich antibodies attached to different locations on a kilobase-scale double-stranded DNA scaffold (Figure 11A,i)[5]. When both antibodies bind to a single target molecule, the probe adopts a looped form. The looped structure forms a distinct band from the linear structure when visualized with gel electrophoresis, solely due to their different topology (Figure 11A,ii)[108]. The authors proposed that the electric forces generated by the electrophoresis procedure drive the system out of equilibrium and prevent the rebinding of any probes that open during the process. Therefore, on-target binding is enriched compared to off-target interactions, which may be shorter-lived. To assess the reduction in cross-reactivity, a standard ELISA and NLISA were prepared using the same antibody pair against luteinizing hormone (LH). Each assay was performed using LH and a similar molecule, chorionic gonadotropin (CG). The NLISA demonstrated no detectable binding to CG, while the ELISA produced a weak signal (0.5% relative to on-target binding)[5]. Nanoswitch probes were also developed using single-stranded DNA as the affinity binder to detect nucleic acid targets. For two 12-nt binding strands, a single nucleotide mismatch led to a 40% reduction in signal. Reduction of the binding sites to 10-nt resulted in no signal from a single nucleotide mismatch. The authors performed a 6-plex assay targeting both protein and nucleic acids and demonstrated no cross-reactivity (Figure 11B)[109]. The advantage of this method is it very simply incorporates a stringent requirement for signal transduction – specific

binding by both affinity binders is necessary to maintain the looped structure. Further, colocalization of the affinity binders enhances the assay's sensitivity, achieving a reduction of LOD compared to a commercial ELISA[5]. However, the requirement for long-lived on-target binding events prevents the use of affinity binders with high off-rates. In addition, the use of gel electrophoresis as a readout method, although inexpensive and accessible, limits the barcoding space to the number of distinct bands that can be visualized in a single gel lane.

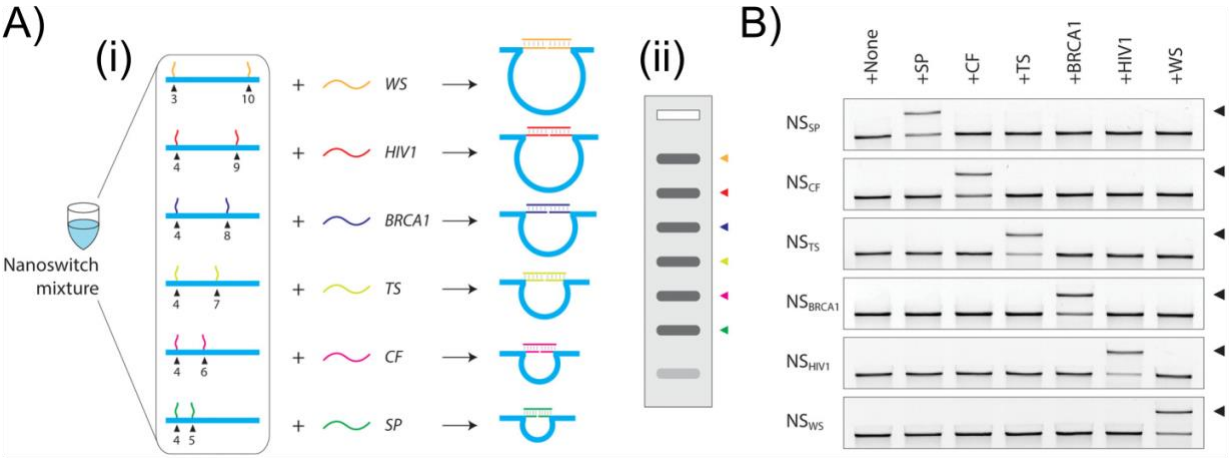

Figure 11: Multiplexed NLISA. A) nanoswitches with different loop sizes can be formed using the same linker (i), producing distinct bands in gel electrophoresis readout (ii). B) nanoswitches produce a detectable signal only in the presence of their intended target. Adapted from Chandrasekaran et al.[109]

Colocalization-by-linkage Assay on Microparticles

The colocalization-by-linkage assay on microparticles (CLAMP), developed by the Juncker lab, consists of matched pairs of antibodies associated to micron-sized beads. Each bead has antibodies against a single target, such that the sandwich binding reaction is compartmentalized[110]. The capture antibody is attached directly to the bead surface, while the detection antibody is tethered close to the bead surface through a flexible hook oligo (Figure 12A). After incubation with the sample, the CLAMP probes are mixed with a fluorescently labelled strand called the displacer oligo. This oligo invades the duplex linking the hook oligo to the surface via toehold-mediated strand displacement (Figure 12B, iv, inset). If the detection antibody has not bound to a target, then it is lost to the bulk solution, where it is unlikely to interact with another CLAMP bead. A stringent wash removes any antibodies which may have bound non-specifically. However, if the detection antibody has formed a sandwich complex with a surface-bound capture antibody then it is held by this interaction when the hook oligo is

released. The displacer oligo is also localized, and acts as a label for the sandwich complex (Figure 12B, v). The displacer oligo's dual role ensures that the background signal remains low – only hook oligos that are properly released can contribute to the assay signal. The assay signal is quantified by flow cytometry, with each bead contributing an independent measurement[110]. The platform's ability to reduce cross-reactivity was evaluated by performing a 6-plex assay using the same targets and antibodies for the CLAMP and a conventional bead-based sandwich assay. The antibodies and antigens selected had been shown to exhibit cross-reactivity and non-specific binding in a previous multiplexed sandwich assay[111]. The conventional bead-based sandwich assay had numerous false-positive signals owing to reagent cross-reactivity. Meanwhile, the CLAMP had one instance of cross-reactivity, which was identified as being due to a detection antibody with low specific affinity[111]. An advantage of the CLAMP system compared to other cross-reactivity-free assays in this section is that the bead-based system facilitates automated washing and cytometry measurement. Scaling up to higher plex levels only requires the addition of a new barcode[2].

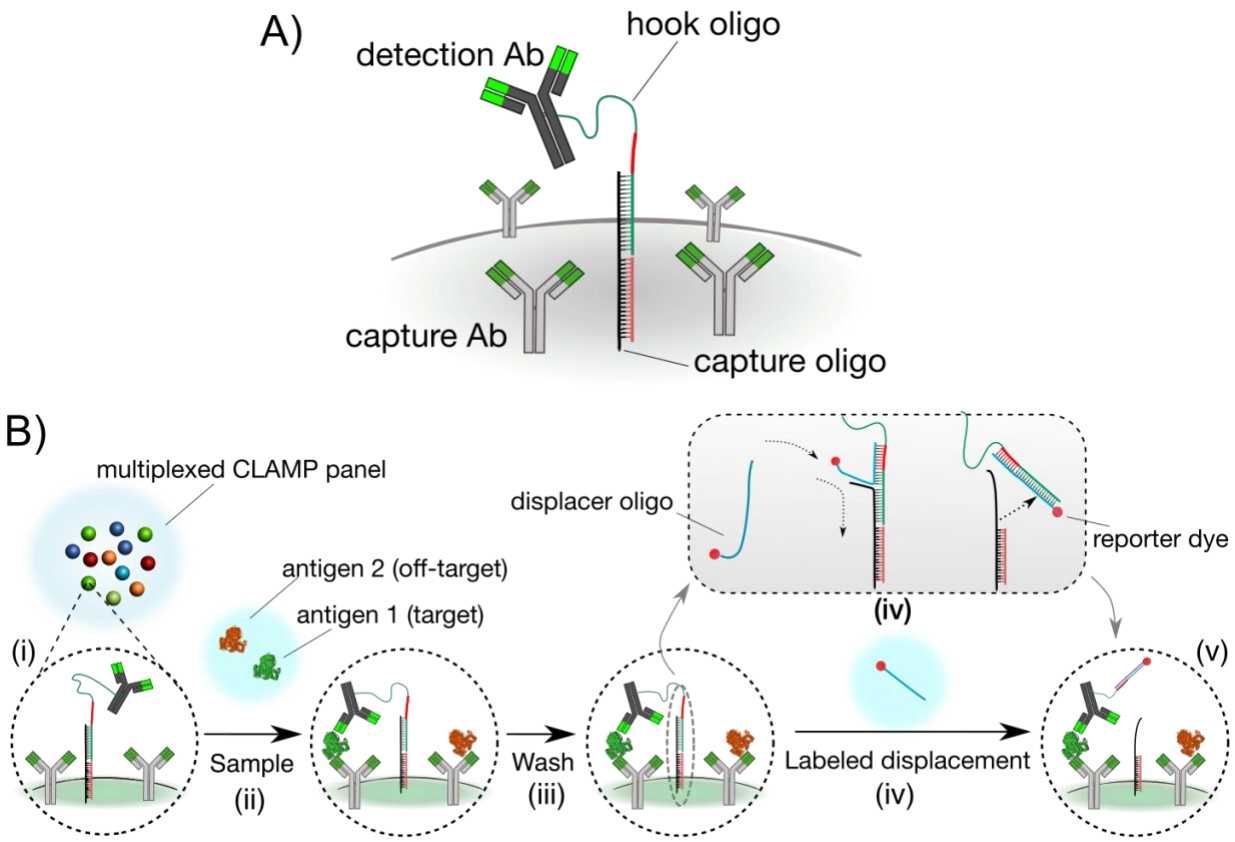

Figure 12: CLAMP bead surface and assay process. A) Each CLAMP bead contains antibodies against a single target. Capture antibodies are conjugated directly to the bead surface, while detection antibodies are tethered through a flexible hook oligo. B) (i) CLAMP beads against multiple targets are pooled (ii) The beads are blocked, then incubated with a sample. Both antibodies bind to the correct target in a sandwich complex, whereas dual binding to an incorrect target is unlikely. (iii) The beads are washed to reduce non-specifically bound or weakly cross-reacting reagents. (iv) The beads are incubated with a Cy5-labeled displacer oligo. (inset) The displacer oligo invades the duplex securing the hook oligo through toehold-mediated strand displacement. (v) Detection antibodies that have not formed a sandwich are lost to the bulk, while those that have bound to a target are retained by this interaction. The displacer oligo acts as a label for the sandwich complex. Adapted from Dagher[2].

Proximity-dependent Signal Transduction

Unlike the other methods discussed in this section, proximity-dependent techniques do not prevent cross-reactive binding from occurring. Instead, assays in this category add an extra recognition step between the capture and detection affinity binders. Signal transduction only occurs if two matching binders interact with the same target molecule. Two examples will be discussed here: the proximity ligation assay and the proximity extension assay.

Proximity Ligation Assay

In the proximity ligation assay (PLA) the capture and detection affinity binders are each linked to an oligonucleotide. Both affinity binders are added to the sample simultaneously. After incubation, an excess of connector oligos, a ligase, and PCR primers are added. If the two affinity binders have both bound to the same target molecule, then the connector oligo hybridizes to a short sequence on each binder's oligo. The resulting complex is ligated, and then the reaction is transferred to a qPCR instrument for measurement. Very low concentrations (~ pM) of the affinity binders are combined with the sample, and further diluted on addition of the ligation mix, in order to reduce the incidence of target-independent ligation[3,112]. As an alternative to PCR, the ligated DNA can serve as a template for rolling circle amplification (RCA), followed by labelling with fluorescent oligos. Use of RCA provided an improvement in sensitivity and precision[113], and allowed for in-situ tissue imaging via PLA[114]. Cross-reactivity was assessed by spiking one of six targets into plasma, followed by the antibodies for all six. No significant cross-reactivity-derived signal was detected[34]. Later, the signals from a 24-plex assay were compared to those from 4-5 antigen sub-mixes. Some false-positive results were identified, but they were attributed to incomplete purification of some antigen standards[115]. The advantage of the PLA method is that it is performed in a single container and does not require washing, making it very straightforward to automate. Further, PCR amplification allows even rare binding events to be detected. However, the performance of DNA ligases was found to be reduced in complex samples, such as human plasma[4]. More significantly, PLA experiences a hook effect, wherein increasing target concentration beyond the upper limit of the dynamic range results in a reduction of measured signal. This reduction is due to the decreasing probability that each target molecule is bound by two affinity binders. The hook effect is commonly observed in assays where both sandwich binders are added simultaneously. The assay may report erroneous quantification values if used outside its dynamic range, requiring sample titration or prior knowledge of the target's concentration range.

Proximity Extension Assay

To address the weaknesses in PLA, the proximity extension assay (PEA) was developed. Like PLA, in the PEA method the sample is incubated with both sandwich antibodies, which are conjugated to oligo labels. However, in PEA one of the antibody-oligo conjugates is pre-hybridized to a slightly longer oligo (the connector), such that it leaves a short overhang. When

the pair of antibodies bind in proximity, the connector strand hybridizes to the other oligo label. Next, a DNA polymerase is added that extends the connector strand, using the oligo label as a template. The reaction is then transferred to a qPCR instrument, and the extended connector strand is amplified and quantified. An exonuclease added at the same time as the polymerase was found to improve the SNR, which the authors attributed to degradation of non-hybridized oligo labels, preventing their erroneous amplification[4]. In a later iteration of PEA the connector strand was eliminated, and the two oligo labels hybridize to each other if they have matching barcode sequences[116]. The PEA method's robustness to cross-reactivity was evaluated by comparing the results of four targets in a 23-plex assay to their corresponding single-plex assays. The signals were not found to be significantly different, though for some targets the background signal was higher in the multiplex assay[4]. Like PLA, PEA does not require handling and washing. However, the total target that can be bound by the PEA probes is limited by the non-saturating antibody concentration used. Increasing the antibody concentration would make target-independent extension events more common, and therefore increase the background signal[4].

Assays using proximity-dependent signal transduction techniques have broad dynamic ranges of 3-5 orders of magnitude. This is due to the very low background signal achieved by limiting noise-derived signal transduction[113,115]. However, for both PLA and PEA, the use of DNA oligo proximity probes creates an additional pathway for cross-reactivity. Orthogonal probes must be carefully designed to limit false-positive signals generated by unintended oligo interactions[117]. To date, PLA has been demonstrated for up to 24 sequences in parallel[4,117], and PEA has been demonstrated for up to 96 sequences[116].

2.2.7 Other Advanced Assay Formats

Digital Assays

Digital assays divide the sample into a multitude of identical compartments[118]. The volume of each compartment is very small, often on the scale of femtolitres, such that most contain either zero or one target molecule. PCR or ELISA reagents are then added to each compartment, and the portion of partitions that produce positive results is counted directly to determine the quantity of target molecule in the original sample. This method is valuable for the detection of rare targets, as it approaches single-molecule sensitivity. Due to Poisson statistics, as the number of

positive compartments increases so too does the incidence of compartments containing more than one target molecule. Above 10% positivity, direct counting no longer provides an accurate result[118]. Correcting for the incidence of wells with multiple targets, counting can continue up to 50-70% positivity. Beyond this limit the signal deviates from linearity[119,120]. For instance, Rissin and colleagues measured streptavidin-β-galactose (SβG) concentrations with a LLOQ of 350 zM, compared to 15 fM for a contemporary plate reader assay. The upper limit occurred at 3.5 fM, for a total dynamic range of 4 orders of magnitude[119].

2.3 Assay Dynamic Range and Modification Thereof

As discussed in section 2.2.1, the dynamic range is the interval of analyte concentrations for which an assay provides quantitative information. Clinical requirements for assays define the upper and lower limits of the dynamic range in terms of SD, bias, or CV[50–53]. Therefore, the width of the dynamic range is dependent on the assay quality (how much signal variation and background are present?) and the resolution of the detection method (can it reliably discriminate a 0.1% signal change? 0.01%?). For conventional sandwich assays, the dynamic range spans two to three orders of magnitude[1].

When an assay's dynamic range does not overlap with its analyte's clinically relevant range, or when the analyte's relevant range is too wide, the assay's dynamic range must be adjusted. The various methods for modifying the dynamic range can be divided into three basic categories: modification of the sample, modification of the affinity of the binding molecules, and modification of the apparent affinity.

2.3.1 Sample Modification

Methods of modifying the sample include parallel dilution, target depletion, and partitioning the sample.

Parallel Dilution

Most assays begin with a standard dilution of the sample to bring the expected analyte concentration within the dynamic range. The standard dilution is based on the sample matrix and the affinity binders used and is typically determined by the assay developer. In the case that the analyte's relevant range does not align with the assay's dynamic range, multiple dilutions of the

sample may be tested in parallel. Parallel measurement is especially important for assays with a hook effect at low or high concentrations, as operating outside the dynamic range will lead to false measurements[121]. Parallel dilution is by far the simplest method of dynamic range modification and will appear several more times in this section in combination with other techniques. However, repeating an assay in parallel increases the consumption of sample, reagents, and labour. Particularly in multiplex assays, where the correct dilution factor for one target might not be right for another in the same sample, parallel dilution may not be the most efficient method to modify the dynamic range.

Target Depletion

Target depletion methods consist of incubating the sample with an unlabelled affinity binder that competes with the capture or detection binder. This technique has been demonstrated for DNA assays[122,123] as well as immunoassays[124]. For example, Di Kang and colleagues designed an electrochemical DNA assay, in which labelled DNA probes were bound to a gold surface[122]. An identical, unlabelled probe was added in solution, which competed with the signalling probes for the target strand. By increasing the concentration of the depletant strand, the authors were able to shift the ULOD from 100 nM to 10 μM[122]. Alexis Vallée-Bélisle and colleagues designed a similar system, where the target was captured via DNA stem-loop probes in solution[123]. Unlabelled linear probes, with a sequence identical to the loop region, were added to deplete the target. By increasing the depletant concentration the ULOD was shifted from 1 μM to 10 μM[123]. However, in both of these examples the overall dynamic range was not significantly extended, as the use of the depletant narrowed the dynamic range of each assay to approximately 5-fold[122,123]. This might be because the binding curves of the depletant and signalling probe had considerable overlap. Perhaps if the depletant had a much higher affinity for the target then the dynamic range of each assay would not be narrowed.

Heidi Hyytiä and colleagues designed a nanoparticle-based immunoassay whose dynamic range could be modified using the depletion method[124]. The authors used an established nanoparticle sandwich assay method, wherein one half of an antibody sandwich pair is conjugated to the nanoparticles while the other is biotinylated and immobilized on a streptavidin surface. The nanoparticles were pre-incubated with the sample, then the whole mixture was transferred to the antibody-coated wells. After incubation and washing, the immobilized nanoparticles were

measured as an indication of the target molecule concentration. To extend the dynamic range, free capture and detection antibodies were added to the pre-incubation step. The free antibodies competed with the nanoparticles and surface-bound antibodies for the target molecules, sequestering them and shifting the measured dynamic range towards higher concentrations. By increasing the concentration of depletant antibodies, the total dynamic range was measured at 3 orders of magnitude. The actual extension may have been greater, as some of the binding curves were still in the linear range at the lowest concentration tested[124].

Sample Partitioning

Digital assays, as discussed in section 2.2.7, quantize the sample into a series of partitions that can only report binary signals. Very low limits of detection are achieved by concentrating reactants in very small volumes, such that the activity of a single enzyme can be distinguished from background[119,120]. However, the dynamic range and precision of a digital assay are intrinsically linked, due to the method of counting active partitions. Achieving the dynamic range and precision desired for most biological applications requires massive numbers of compartments – on the order of thousands to millions[125]. This quickly increases the cost and complexity of reagents and liquid handling.

Pawel Debski and colleagues presented a technique to increase the dynamic range of digital assays without sacrificing precision and using orders of magnitude fewer compartments[125]. Rather than an array of identical compartments, the authors proposed an array of compartments whose volumes form a geometric series. They argued that a classic digital assay gathers a large amount of information from a small dynamic range, while for a sequence of compartment volumes the amount of information gathered is constant over a larger range. Not all the compartments provide relevant information in this method; those with a critical concentration furthest from the input will have probabilities close to zero or one. However, an "active stripe" of compartments which have a probability significantly different from zero or one offer more information than the same number of identical compartments. Based on statistical modeling and simulation, Debski et al. estimated that a modified digital assay could measure 4 orders of magnitude and a maximum standard deviation of 10% using 192 compartments. Meanwhile, a classical digital assay would require 2000 compartments to achieve the same dynamic range. The authors identified a weakness in their assay design, that manufacturing minute compartments

with volumes differing by 1% could be expensive and error prone. As an alternative, they determined that using multiple copies of a series compartments with a larger geometric factor would still allow a reduction in total number of compartments, while simplifying manufacturing[125].

Rissin and colleagues proposed a combination of digital and analog (signal intensity) quantification approaches, depending on the portion of active partitions. For arrays with above 10% active partitions, Poisson statistics were used to estimate the average enzymes per partition. Use of this method maintained linearity and precision until about 70% of the partitions were active. At this level, the average fluorescence intensities of the active partitions were measured and used to estimate the number of enzymes. The authors noted that enzymes demonstrate significant heterogeneity in their activity, and thus it was not possible to determine the exact number of enzymes in each partition. The average intensity per enzyme was determined by measuring a calibration array where partitions have at most one enzyme active – averaging the intensity of thousands of partitions reduced the impact of the static heterogeneity. The dynamic range for the detection of SβG was increased from four to six orders of magnitude[120].

2.3.2 Binding Site Modification

Instead of modifying the sample, the affinity binders themselves can also be modified. Two or more binders with different affinities can be used in a parallel assay or combined to obtain a single assay with an extended dynamic range. If different signals are used (i.e., different fluorophores) then sensitivity is maintained across the new range. Alternatively, the same detection signal can be used to obtain a wider dynamic range without requiring more complex optics[30,123,126].

For some common biological targets, there are already multiple binders with a range of affinities to choose from. However, it may be possible to alter an existing binder to systematically tune its affinity to be higher or lower. In this section we will discuss methods to directly modify the affinity of antibodies, nucleic acid probes, and aptamers.

Antibody affinity modification

The binding site of an antibody achieves high affinity through avidity – it contains many smaller binding sites which recognize different parts of the same epitope. Changing one amino acid for another in the binding site will have the effect of disrupting one or more of the binding sub-sites. In some cases, a single amino acid substitution can completely eliminate the antibody's affinity for its target[127]. In other instances, substitution of an amino acid for one with a different side chain can tune the affinity. For example, in 1993 Jim Xiang and colleagues used site-directed mutagenesis to alter a single amino acid in the heavy chain of a chimeric antibody[128]. With the native amino acid, a histidine, the antibody had a measured dissociation constant of 1.7 nM. However, substitution with glutamine or asparagine, amino acids with polar sidechains, decreased the K_D to 0.63 nM. Substitution with isoleucine or other hydrophobic amino acids increased the K_D to 5.0 nM[128]. More recently, critical binding sites have been identified through crystallography or serial substitution and then targeted for random mutagenesis[129,130]. This targeted approach, using structural knowledge, allows for a more systematic method. With a sufficiently large mutation library, this method can achieve affinity improvements of up to 1000-fold[129].

Nucleic acid affinity modification

The binding of nucleic acid strands is functionally different from that of antibodies and their antigens[131]. The latter relies on a precise steric fit between binding domains, and a single mismatched element produces a significant increase in free energy of binding. In contrast, nucleic acids bind through a "zipper" model rather than a "lock and key" model. A single mismatched base pair results in a small but tolerable energetic penalty, and the incorrect probe and target achieve equilibrium at the same rate as the perfect match[131]. Thus, the introduction of one or two isolated mismatches can be used to reduce the affinity of a probe and alter its dynamic range. Mariottini et al. demonstrated a 5-fold affinity shift by introducing a single mismatch to their DNA probe[132]. The combination of these probes could be used to achieve a total dynamic range of 3 orders of magnitude. However, it is important to note that this only applies to linear nucleic probes[133]. For probes that form a hairpin or stem-loop, this secondary structure is more energetically favourable than the duplex with the mismatched target, though

less favourable than pairing with the perfect target. Complete hybridization to the mismatched target will not occur for such a probe[133].

Aptamer affinity modification

Aptamers, as described in section 2.2.3, bind to their targets through secondary and tertiary structures. Aptamers undergo extensive affinity enhancement as part of their development process[134]; however, they are limited by the use of only four nucleic acids[91,92]. SOMAmers (Slow Off-rate Modified Aptamers) were developed which incorporate deoxyuridine bases with modified side chains to expand their chemical diversity. In particular, the addition of side chains with aromatic characters was found to enhance affinity most significantly[135] – this is a motif that appears in some amino acids but is absent in DNA[92]. For example, the affinity of an aptamer against GA733-1 was improved by more than an order of magnitude through SELEX using modified bases. The incorporation of different modified bases can reliably generate aptamers with affinities in the nanomolar to picomolar range. After SELEX, the affinity of an aptamer can be modified by swapping out individual modified bases for each other[135]. If the crystal structure is known, targeted substitution can increase or decrease the apparent affinity by an order of magnitude[136].

2.3.3 Apparent Affinity Modification

An alternative to direct modification of the affinity binder is the modification of their apparent affinity, such that they behave like a binder of higher or lower affinity. Adaptations of this kind can be found readily in nature and have been replicated in vitro. In this section we will discuss competitive binding, dynamic regulation, and entropic modulation.

Competitive Binding

Competitive binding assays, as described previously, are often used when only one antibody for an analyte is available. However, modifying the concentration of the competitor can also be used to shift or extend the dynamic range. For example, Hartmann et al.[7] designed a combined competitive and sandwich assay in order to quantify an expanded concentration range of human IgG antibodies in serum. A competitor human IgG, labelled with Cy3, was added to the sample. Spots of antihuman IgG were printed on a slide and then incubated with the sample. The slide was washed, incubated with Cy5-labelled antihuman antibodies, then imaged. By comparing the

ratio between the two fluorescent signals, the authors were able to determine the concentration of human IgG in the original sample over two orders of magnitude. Next, they tested the effect of varying the competitor IgG concentration between 0-10 mg/L. Increasing the competitor shifted the detection curve towards higher concentrations of the target, while decreasing the competitor concentration shifted the curve to lower target concentrations. The resulting detection curves had a total dynamic range of 5 orders of magnitude. Thus, combining competitive and sandwich assay methods permitted tuning of the detectable range without altering the assay dynamics[7].

Dynamic Regulation

Those accustomed to working with antibodies may assume that all affinity binders have a static form until they are degraded. However, many natural and synthetic affinity binders such as aptamers, molecular beacons, and enzymes exist in a state of dynamic equilibrium where molecules shift spontaneously between a binding-competent and a non-binding state[137]. Researchers have proposed leveraging this property to alter the apparent affinity of the binding reaction. Methods of altering this binding/non-binding state equilibrium often involve changing the length/stability of a stem-loop nucleic acid structure[47,137–141], though aptamer complementary strands have also been used to sequester the affinity binder in a non-binding state[142,143]. Some techniques further incorporate additional molecules that inhibit or facilitate transition from the non-binding to binding-competent state as a replication of allosteric regulation that occurs in biological systems[138,139,141]. Apparent affinity shifts of up to three orders of magnitude have been achieved, albeit often with a loss of signal window, and by extension loss of precision of the calibration curve[47,138,141,142].

For example, Alessandro Porchetta and colleagues[138] modified an aptamer for cocaine to alter its apparent affinity. The aptamer folds into a three-way junction upon interaction with its target, as shown in Figure 13A. By changing the sequence and length of each of the arms the authors were able to change the stability of the aptamer. This resulted in a shift in the binding affinity from 0.5 μM (parent) to 23, 82, and 1390 μM (Figure 13B). However, they were unable to establish a systematic approach to design the modifications, instead relying on “hit-or-miss” methodology[138]. As an alternative, the authors explored allosteric inhibition. Allostery is a control pathway wherein a molecule binds to the receptor at a location other than its target-binding site and either prevents it from reacting with the ligand or facilitates binding. In this

case, the authors added a short DNA strand complementary to a segment of the cocaine aptamer. The inhibiting strand stabilized the aptamer in its open form, which the authors theorized would shift the aptamer population towards the non-binding state (Figure 13C)[138]. The affinity of the inhibiting strand for its allosteric site was modulated by altering the number of bases complementary to the aptamer. By changing the length and concentration of the inhibitor, the authors observed a shift of the apparent binding affinity of the cocaine aptamer from 0.5 µM to 2.9, 19, and 235 µM (Figure 13D)[138].

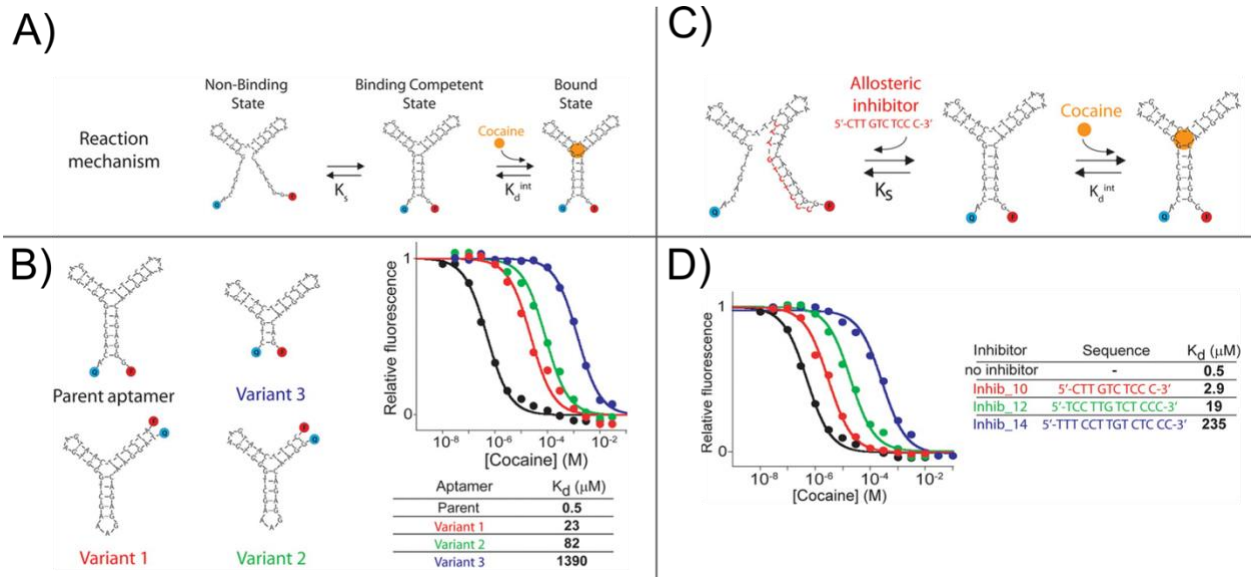

Figure 13: Modification of the apparent affinity of a cocaine aptamer. A) Conformational selection binding mechanism, B) The apparent affinity was modified by altering the stability of the "closed" state, C) Inhibitor binding pathway, D) The apparent affinity was modified by increasing the inhibitor strand length. Only normalized data without error bars are presented, so assessment of the effect on the signal window or variation are not possible. Adapted from Porchetta et al[138].

However, the mechanism for the transition between the non-binding and binding-competent states is not as simple as it seems[143,144]. Based on the names commonly given to the states, one might assume that a molecule in the non-binding state is incapable of specific interaction with the target. By changing the equilibrium between the two states, the portion of affinity binder sequestered in the non-binding state changes, and its effective concentration increases or decreases. Considered from the perspective of a single molecule, the likelihood of binding is affected by a new term: the probability that the molecule is in the binding-competent state when it encounters a target. As a result, the measured on-rate and the apparent affinity decrease

compared to a static molecule (recall that $K_D = k_{off}/k_{on}$). This mechanism is referred to as the *conformational selection* pathway (Figure 14, top)[143,144]. The alternative is the *induced-fit* mechanism (Figure 14, bottom), wherein the target molecule interacts with the affinity binder in its so-called non-binding state and induces it to shift to the binding-competent state and/or stabilizes this conformation[144]. The likelihood of unbinding gains a new term: the probability that the molecule shifts back to the non-binding state if the target unbinds momentarily. As this probability increases, the measured off-rate does as well, thereby decreasing the affinity.

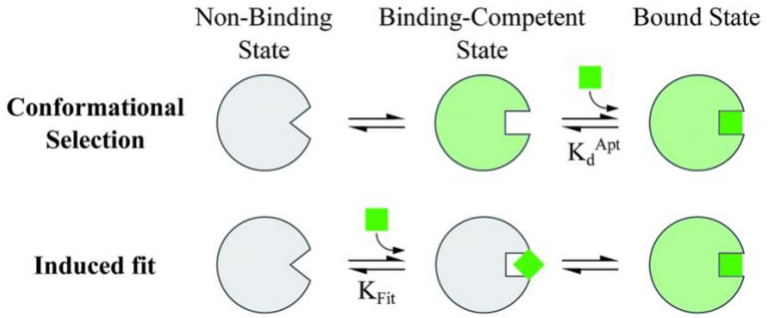

Figure 14: Binding transition mechanisms. (Top) The affinity binder spontaneously shifts from the non-binding to the binding-competent state and then interacts specifically with its target. (Bottom) The target interacts with the affinity binder in its non-binding state and stabilizes its transition to the binding-competent state. Reproduced from Munzar et al.[143]

For most affinity binders, both the induced-fit and the conformational-selection pathways are occurring[144]. Which one dominates depends on the system and the reaction conditions. For example, consider a simple stem-loop molecular beacon that binds a linear target strand (Figure 15A). At low reaction temperatures the stem opening process is the rate-limiting step – the target binds easily to the loop of the molecular beacon, and then must compete with the stem to fully hybridize (Figure 15B, dashed line)[133]. The stem sequence has a relatively small effect on the rate of strand displacement compared to stem length[133,145,146], so in this condition the induced-fit pathway dominates. By comparison, at high temperatures the binding of the target to the molecular beacon is the rate limiting step due to the rapid melting of individual base pairs (Figure 15B, dotted line)[133]. The target will thus preferentially bind to molecular beacons in the open position, where base zippering can occur more quickly. In this case, the conformational-selection pathway dominates.

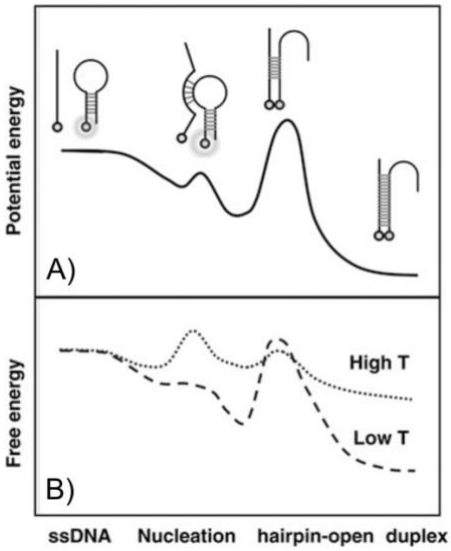

Figure 15: Hybridization mechanisms of a molecular beacon, in terms of A) Potential energy, B) Free energy of the reaction. At high reaction temperatures (dotted line) the binding of the target to the beacon is the rate-limiting step, and the conformational-selection pathway dominates. Meanwhile at low reaction temperatures (dashed line) the opening of the stem-loop structure is the rate-limiting step, and the induced fit pathway dominates. Adapted from Peng and Tan[133].

The dominant transition mechanism has consequences for modification of the apparent affinity. Systems in which conformational selection dominates have been shown to be sensitive to the non-binding/binding-competent equilibrium[144], allowing intuitive apparent affinity tuning. The effect of changing the binding state equilibrium on induced-fit-dominant systems is more difficult to predict. In some cases it has been shown to result in narrowing of the signal window without a significant change in apparent affinity[143]. An assessment of commonly used aptamers found that the cocaine DNA aptamer presented earlier in this section is conformational-selection-dominant. Meanwhile, the cocaine RNA aptamer, RNA and DNA ATP aptamers, and thrombin DNA aptamer are all induced-fit-dominant[143]. Although this list represents a small subset of aptamers used, it suggests that the induced-fit mechanism is widespread. This phenomenon limits the opportunities where altering the non-binding/binding-competent equilibrium can be used to tune the apparent affinity.

However, it is still possible to alter the apparent affinity of an induced-fit-dominant aptamer. Rachel Armstrong and Geoffrey Strouse located an ATP aptamer within a stem-loop structure and demonstrated its binding affinity could be altered[140]. The same aptamer, originally developed

by Huizenga and Szostak[147], was shown to bind two ATP molecules through the induced-fit mechanism when duplexed[143]. Armstrong and Strouse observed that when more of the aptamer sequence was located in the stem, the apparent affinity decreased, with a maximum shift of 3 orders of magnitude. The authors determined that the change in K_D correlated with the free energy of the duplexed aptamer sequence, and not that of the stem[140]. This indicates that the aptamer binds ATP through the induced-fit mechanism, and that the apparent affinity can be tuned by increasing competition between the ATP and the duplexed stem.

Entropic Modulation

The concept of entropy appears in many areas of science and is broadly defined as being a measure of the randomness, or disorder, of a system. In biophysics, several different aspects of entropy are considered – we will focus on *conformation entropy*. Conformational entropy is a measure of the total number of positional states that a molecule can occupy. For instance, a stable globular protein has low conformational entropy, while an unfolded polypeptide has high conformational entropy[148]. Processes that decrease conformational entropy, such as the folding of a polypeptide chain into a globular protein, are often thermodynamically unfavourable. In other words, they are less likely to occur spontaneously.

Protein domains having high conformational entropy, known as intrinsically disordered proteins, are commonly found in natural systems[148]. They are often present in multi-domain proteins, where they act as flexible linkers connecting binding domains[149]. In section 2.3.2 we discussed how antibodies use avidity – the combined affinity of multiple binding sub-sites – to achieve high apparent affinity. Similarly, multi-domain affinity binders produce high-affinity interactions by connecting two or more binding domains that have moderate-strength interactions with the same target via an intrinsically disordered linker. When one binding domain binds to its epitope, the encounter rate between the other domains and their epitopes is increased due to the connection, improving the likelihood that they will also bind. The impact of the linker can be expressed in terms of effective concentration – the concentration of the other binding domain(s) that would produce the same encounter rate in the absence of the linker (Figure 16A)[149–151]. At the same time, the apparent off-rate of the multi-domain binder is decreased: if one domain unbinds it is held in proximity by the linker and may rebind to its epitope before the second domain unbinds[149,151,152]. Recalling that $K_D=k_{off}/k_{on}$, reduction of the off-rate results in an

enhancement of the apparent affinity. The magnitude of the affinity enhancement can be understood in terms of entropy[132,152,153]. The disordered linker has many degrees of freedom, and thus a high conformational entropy. Binding of both domains constrains the linker (Figure 16B), incurring an entropic penalty that decreases the favourability of polyvalent binding. The entropic penalty of binding increases with the linker's length and flexibility, decreasing the apparent affinity (Figure 16C). An affinity binder with a sufficiently long/flexible linker will theoretically never achieve polyvalent binding to the same target molecule[132,152].

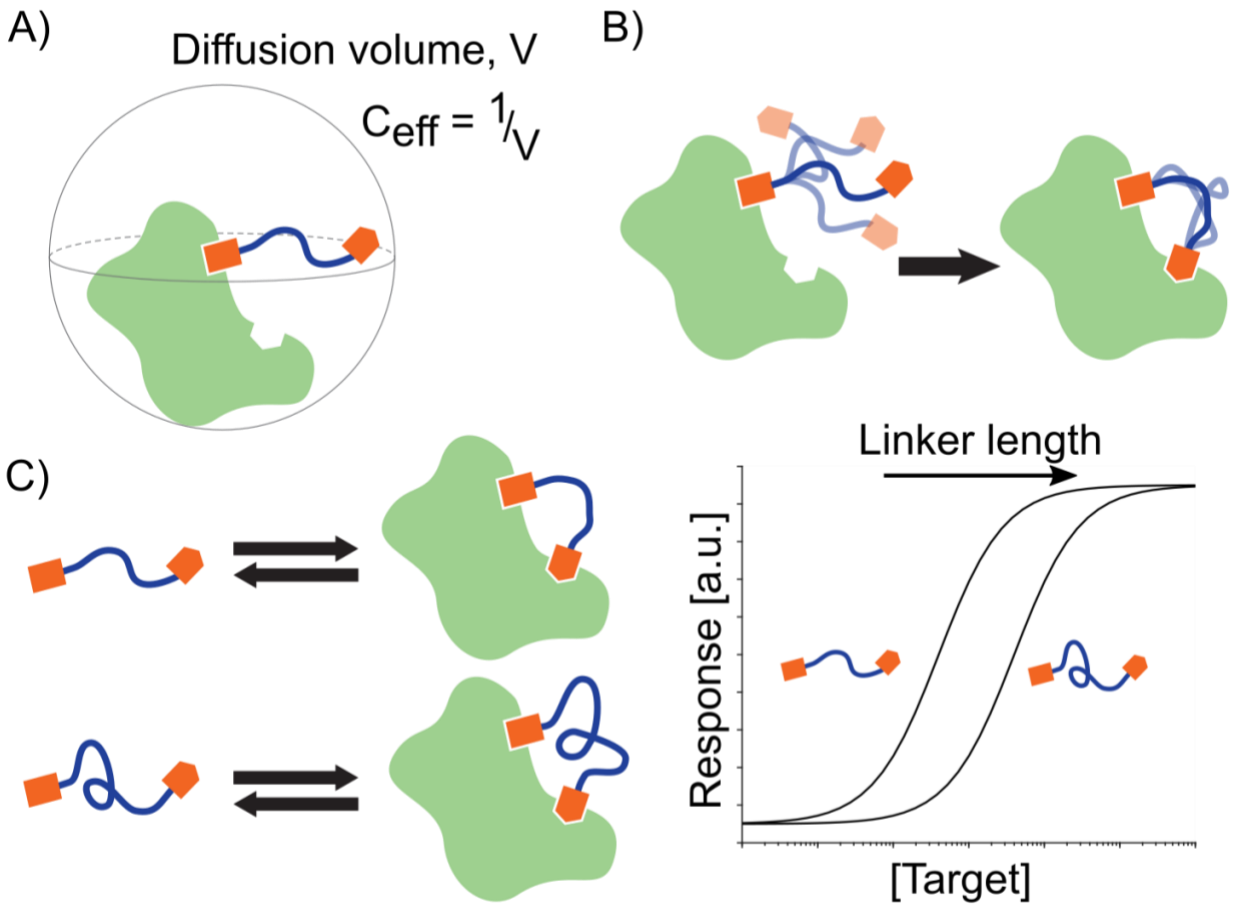

Figure 16: Conceptualization of a bivalent affinity binder with two binding domains (orange) linked via an intrinsically disordered domain (blue) binding to its target (green). A) The linker increases the effective concentration of the unbound domain by limiting its diffusion volume, increasing its apparent affinity. B) Bivalent binding constrains the linker, incurring an entropic cost. C) Increasing the length and flexibility of the linker increases the cost of binding, decreasing the apparent affinity.

Using the principle of avidity, synthetic high-affinity binders against HIV virions[153], protein molecules[149–151,154,155], and DNA targets[132,154] have been developed by connecting affinity

binders with a flexible or semi-flexible linker. However, systematic design of apparent affinity enhancement requires the application of a mechanical model for the flexible linker. The apparent affinity can be calculated as

$$K_{D,apparent} = \frac{K_{D,1} \times K_{D,2}}{C_{eff}} \quad (9)$$

Where $K_{D,1}$ and $K_{D,2}$ are the monovalent affinities of the binding domains, and C_{eff} is a theoretical parameter defining the effective concentration produced by the linker. C_{eff} represents the linker's conformational entropy, expressed in terms of the number of positions the linker can occupy. To derive this expression, the flexible linker is commonly modeled as a freely-jointed chain (Figure 17A)[132,152] or a wormlike chain (Figure 17B)[151,154], though more complex models have also been proposed[149].

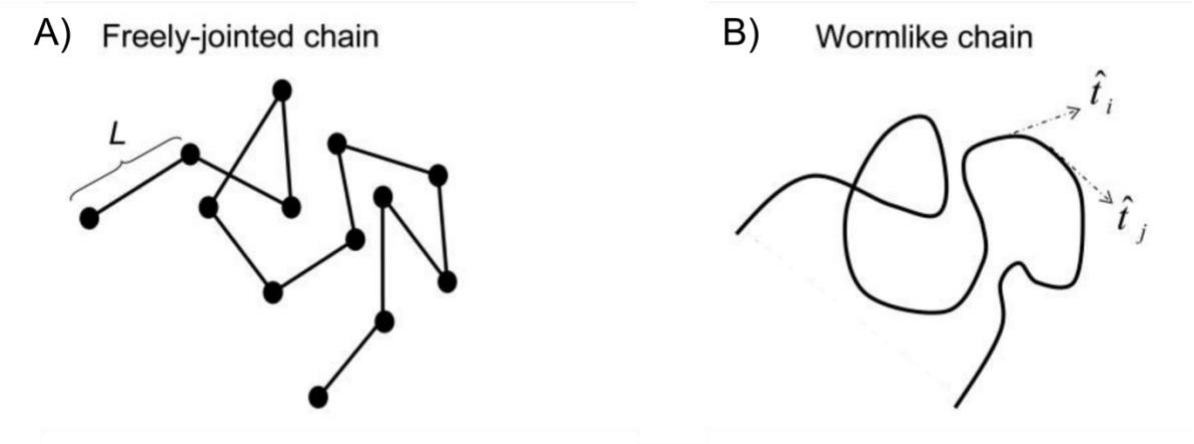

Figure 17: Conceptual representations of simple linker models. A) Freely jointed chain, having rigid links of length L. B) Wormlike chain, having a persistence length of l_p (not shown) defined as the maximum length over which two tangents (t_i, t_j) are correlated. Adapted from Anderson and Granzier[156].

The effective concentration produced by a wormlike chain is defined as the Probability Density Function (PDF) for its end-to-end vector, which is derived from statistical mechanics[157]. The PDF has been expressed as follows[151,158]:

$$p(r) = \left(\frac{3}{4\pi l_p l_c}\right)^{\frac{3}{2}} \exp\left(-\frac{3r^2}{4l_p l_c}\right)\left(1 - \frac{5l_p}{4l_c} + \frac{2r^2}{{l_c}^2} - \frac{33r^4}{80l_p{l_c}^3} - \frac{79{l_p}^2}{160{l_c}^2} - \frac{329r^2 l_p}{120{l_c}^3} + \frac{6799r^4}{1600{l_c}^4} - \frac{3441r^6}{2800l_p{l_c}^5} + \frac{1089r^8}{12800{l_p}^2{l_c}^6}\right) \quad (10)$$

Where r is the end-to-end vector, l_p is the persistence length and l_c is the contour length of the linker. The effective concentration is calculated by evaluating the PDF for the end-to-end vector of the linker to have a distance equal to the distance between the binding sites on the target, d_0. The distribution of $p(r)$ is not uniform, due to the varied conformational entropy of each position. For example, only a single conformation (full extension) allows the linker to adopt $r=l_c$. Huan-Xiang Zhou validated this model by comparing it to published experimental results for bivalent affinity binders and found good agreement[151]. Evaluating the model for a polypeptide linker, Zhou estimated that the value of C_{eff} could vary by more than 4 orders of magnitude (Figure 18). However, the distance between binding sites has a significant impact: the affinity of a system with a very short d_0 cannot be modified more than one order of magnitude, even with a very long linker (Figure 18, $d_0 = 10$Å)[151].

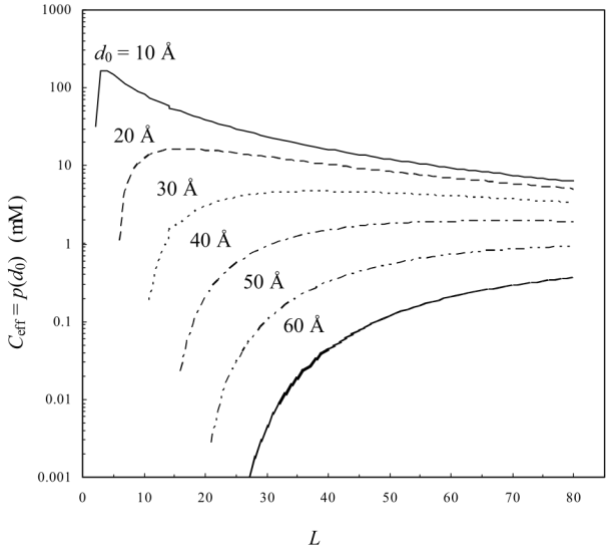

Figure 18: Change in effective concentration based on linker length (L, number of amino acid residues) and binding site separation (d_0). Reproduced from Zhou[151].

The equation for the effective concentration produced by a freely-jointed chain was also derived from statistical mechanics[159]. It is commonly expressed as follows[132,152]:

$$C_{eff}(d) = \frac{p}{N_A\left(L\sqrt{N}\right)^3}\left(\frac{3}{2\pi}\right)^{\frac{3}{2}} e^{-\frac{3d^2}{2\left(L\sqrt{N}\right)^2}} \quad (11)$$

Where L is the length of a chain segment, N is the total number of segments, d is the root-mean-square distance between the linker ends, and p is a volume exclusion factor. The unbound domain of the bivalent affinity binder is assumed to be able to access a sphere with radius equal to its contour length (Figure 16A). However, the linker and the target cannot occupy the same volume, which increases the effective concentration[159]. For instance, if the accessible volume is limited to a hemisphere, then the probability of the linker adopting the remaining conformations is doubled (p=2). Vijay Krishnamurthy and colleagues[152] validated the model for a target (sulfonamide) attached to the surface of a receptor protein (human carbonic anhydrase II) via an ethylene-glycol linker of 0 to 20 monomers. They observed good agreement between their data and the model, albeit using a volume exclusion factor of p=0.12 – much lower than the indicated minimum value of one. Moreover, the authors measured a change in apparent affinity of more than 1.5 orders of magnitude[152]. Davide Mariottini and colleagues subsequently validated the freely-jointed chain model for a system consisting of two single-stranded DNA binding sites connected via a poly(T) linker, and for an ATP aptamer split into two fragments and linked via a poly(T) linker (Figure 19A)[132]. They also found good agreement with the model, using volume exclusion factors of p=0.0016 and 0.19 respectively for their two systems. The lack of consistency between values of p indicates that it is correcting for unknown factors, such as steric hindrance or electrostatic charge. Nonetheless, the authors were able to shift the apparent affinity of the split aptamer more than one order of magnitude by increasing the linker length from 4 to 70 nucleotides (Figure 19B)[132].

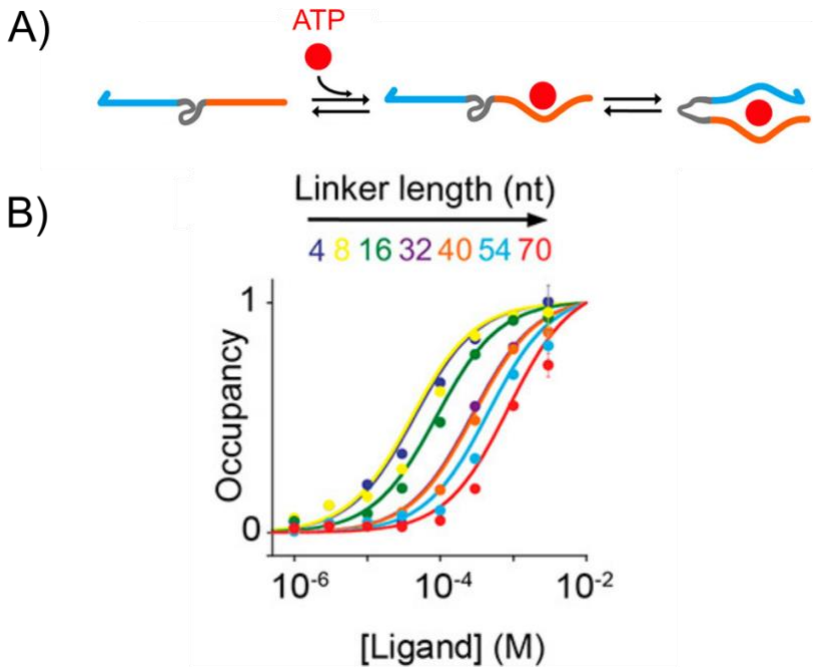

Figure 19: Entropic modulation of the apparent affinity of a split ATP aptamer. A) representation of the split ATP aptamer. B) Binding curves generated using linkers from 4 to 70 nt, demonstrating a shift in apparent affinity Adapted from Mariottini et al.[132]

2.4 DNA as a Nanoscale Scaffold

In sections 2.2 and 2.3 we discussed how, in addition to carrying genetic instructions for all organisms, DNA can be used as an affinity binder. This application takes advantage of single-stranded DNA's highly specific binding to its complementary strand. DNA is also used as a building block in nano-engineering applications due to the ease of custom synthesis and its predictable structure and mechanical properties.

Mechanical Properties

In its single-stranded form, DNA exists as a highly flexible linear molecule. The length per nucleotide of ssDNA has been measured using a number of methods, with results between 0.6-0.7 nm/base[160–162]. The persistence length of ssDNA is dependent on the salt content of the medium, and has been measured to vary from 1.5-3 nm[160–163], with lower values measured at higher salt concentrations. Some authors find that ssDNA is well-described by the worm-like chain polymer model[162], while some argue that the simple chain model is better[132,163], or other models.

When DNA forms a double-stranded molecule its properties change significantly. dsDNA forms a double-helical structure due to hydrophobic and hydrophilic interactions. The coiled dsDNA has a length per nucleotide pair of 0.34 nm. Its persistence length is between 50-80 nm[164,165], depending on salt conditions. dsDNA is well-described by the worm-like chain polymer model[165].

Toehold-mediated Strand Displacement

Toehold-mediated strand displacement is a fundamental tool in DNA engineering. The kinetics of the phenomenon were first characterized by David Zhang[166]. Strand displacement is a reaction wherein a single-stranded oligonucleotide displaces another to form a duplex with a third strand (Figure 20A). In some cases, the third strand may have short single-stranded overhang, also known as a toehold, which the invading strand binds to first and initiates the strand displacement reaction. Through base breathing – spontaneous breakage and reformation of base pairs within the double helix, occurring on a scale 10-100μs[166,167] – the invading strand may gradually displace the existing strand. The branch migration can occur in either direction with equal probability, though the presence of toehold reduces the chance of the invading strand diffusing away. Displacement reaction speed is affected by both the length of the toehold and its sequence. Generally, longer toeholds and those with a higher G/C content achieve higher displacement rates, though this effect saturates at between 5 and 9 nucleotides (Figure 20B)[166].

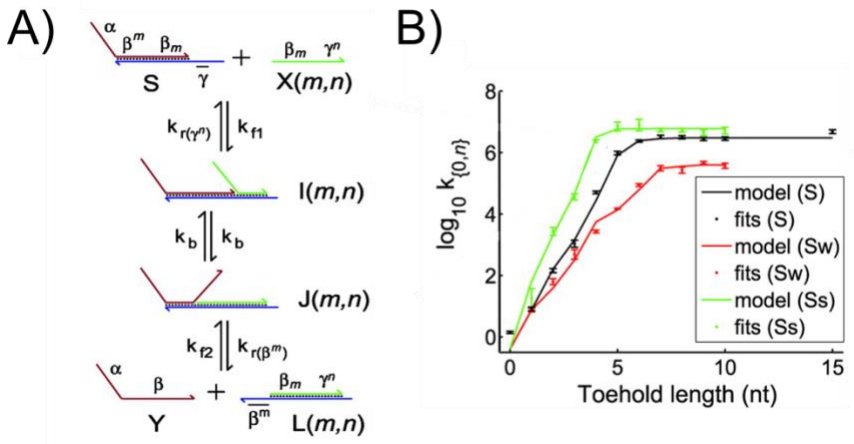

Figure 20: Toehold-mediated strand displacement A) Branch migration mechanism. The invading strand (green) binds to a toehold region on the substrate strand (blue). The invading and incumbent strand (red) then trade places through spontaneous breakage and reformation of base pairs. Once the incumbent strand has completely displaced the incumbent strand, the latter may diffuse away. B) Rate

of displacement reaction vs. toehold length. S represents a toehold with roughly equal A/T and G/C content, while Sw is mostly A/T and Ss is mostly C/G. Adapted from Zhang and Winfree[166].

2.4.1 Molecular Beacons

Molecular beacons are nucleic acid probes that detect the presence of a target strand via hybridization[88]. The probes consist of a single-stranded DNA oligonucleotide that adopts a stem-loop secondary structure in solution. The ends of the probe are labelled with a fluorophore and quencher pair, such that in the closed position fluorescence emission is at a minimum. The loop portion of the probe has a sequence that is designed to be complementary to a target strand. When the probe binds to its target it causes conformational changes that open the stem portion, allowing fluorescence emission (Figure 21)[88].

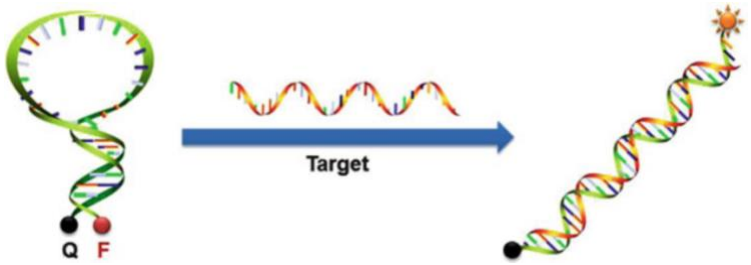

Figure 21: Representation of the basic principle of molecular beacons. A stem-loop probe (left) undergoes a conformation change on binding to its target. This change separates a fluorophore and quencher. Increased fluorescence emission is used as an indicator of binding. However, in practice the stem-loop probe is not stable, and fluorescence can be detected in the absence of binding. Reproduced from Zhu[88]

The unbound probe is not static, but instead fluctuates spontaneously between the open and closed states. Depending on the probe design and assay conditions, the target may either induce the stem-loop structure to melt or bind to the probe only when it fluctuates to the "open" position[133,143]. The stability of the stem portion, and thus the probability that the probe is found in the open configuration, is dictated primarily by the stem sequence[133]. However, the size of the loop also influences the probe stability: increasing loop size results in an increased entropic penalty of binding. This is akin to increasing the activation energy barrier between states.

2.4.2 DNA Origami

DNA origami uses the predictable nature of DNA binding to create shapes from the nano-metre scale to as large as micrometers. These shapes can be used to control surface distribution, or act

as substrates for drug delivery[168]. The origami molecules make use of dsDNA's long persistence length to create rigid trusses. The trusses are then connected in scaffolds, often using triangles as a base unit, to produce structures with high rigidity over large scales.

DNA origami has been used to produce a range of nano-scale shapes, including 2D polygons[169], triangular and cubic prisms[170], tubules of bundled helices reaching micrometer lengths[169], and DNA nano-particles[171]. One of the most commonly used DNA nano-shapes is the tetrahedron, which is preferred for its ease of design and assembly, as well as its mechanical properties[172].

DNA tetrahedrons are typically assembled from four strands of equal length[172,173], though they can also be assembled from a single strand[174] or multiple strands of unequal length[172,175]. Small 4-strand tetrahedrons, with side lengths of 30 bp (10 nm) or less, self-assemble within minutes when the strands mixed in high salt[172,176]. The yield of correctly folded structures, measured via migration in gel electrophoresis, is upwards of 85%[172,176,177]. Conversely, there is evidence that larger, multi-strand tetrahedrons require several hours to reach equilibrium, and achieve yields of only 20-40% [175]. If high purity is required, assembled tetrahedrons can be purified by cutting out the desired band from the electrophoretic gel, grinding it to a powder, soaking it overnight in buffer, then filtering to remove residual gel fragments[178].

When tetrahedrons are assembled from multiple strands the sites where the ends meet produce single-stranded breaks, or "nicks". Due to the circular nature of the strand assembly, the DNA sequences can be designed such that the ends of each strand fall at a vertex or in the middle of an edge. The ends can be ligated, used as linking sites to concatenate multiple tetrahedrons[172], or functionalized with different molecules[177]. Functionalization allows the tetrahedrons to be bound to biosensor surfaces, where they can serve as nano-scale spacers to precisely control the separation between probes[177].

2.5 Summary

In this chapter we have discussed the broad concentration ranges of biological analytes found in human blood, and the need to modify an assay's dynamic range to adequately analyse the targets. We reviewed important assay parameters, including reaction phase, affinity binders, assay formulation, and signal transduction. Next, we investigated methods tuning an assay's dynamic

range by modifying the sample, the affinity binders, or the apparent affinity. Finally, we briefly explored the mechanical properties of DNA and its applications as a nanostructure.

Of the methods of dynamic range modification reviewed, we selected entropic modulation for further investigation. This method has the potential to be used with off-the-shelf affinity binders and without requiring complex sample manipulation. To date, the use of entropic modulation has only been demonstrated for simple sandwich assays with limited clinical applicability. The cross-reactivity-free sandwich assay formats reviewed in this chapter rely on co-assembly (ACM, ATPS), physical linkage (PLA, PEA), or both (NLISA, CLAMP) to limit false-positive signals. We chose the CLAMP as our representative complex assay because it shares many similarities with commonly used commercial assays, and therefore can inform future improvements in many applications. Finally, we used DNA as the linker due to its utility as both a flexible connector and a semi-rigid scaffold.

3. Materials and Methods

3.1 Materials

Secondary antibodies were purchased from ThermoFisher Scientific (Waltham, MA, USA). Capture and detection antibodies against IFNγ, IL-1β, and IL-12 were purchased from R&D Systems (Minneapolis, MN, USA). Antibodies against DIG were purchased from R&D Systems (Minneapolis, MN, USA). Dynabeads M-270 Streptavidin, Dynabeads protein G, Zeba spin desalting columns, dithiothreitol (DTT), sulfosuccinimidyl 4-(N-maleimidomethyl) cyclohexane-1-carboxylate (sulfo-SMCC), all gel electrophoresis materials and buffers, Pierce silver stain kit, cytometry tubes, and all well plates were purchased from ThermoFisher Scientific (Waltham, MA, USA). 10X phosphate buffered saline (PBS), Tween-20, and sodium chloride (NaCl) were purchased from Millipore Sigma (Burlington, MS, USA). Bovine serum albumin (BSA) was purchased from Cedarlane (Burlington, ON, Canada). All DNA oligonucleotides were purchased from IDT (Coralville, IA, USA). Further discussion of oligo purchase specifications and purification can be found in section 3.7. A complete list of oligos used can be found in the appendix (section 7.2).

3.2 CLAMP Fabrication and Assembly

The Colocalization-by-Linkage Assay on Microparticles (CLAMP), previously developed by the Juncker lab[2], was used as a starting point for testing of colocalized bead assays (CBA). The CLAMP probes are assembled from several different components. This section will discuss the fabrication of each component and steps to combine them.

3.2.1 Antibody-oligo Conjugation

Monoclonal antibodies were conjugated to thiol-modified oligonucleotide linkers (“hook” oligos) and then purified. These were subsequently pulled down onto functionalized microparticles via the hook oligo. The protocol for fabricating, purifying, and quantifying the antibody-oligo conjugates is detailed below.

Hook oligos with 5’ thiol modifications were acquired from IDT. These oligos were diluted to 30 μM in reducing buffer (PBS 1X + 0.05% tween-20 + 250 mM dithiothreitol (DTT)) and incubated for 1 hour at 37°C. After reduction, the oligos were buffer exchanged to PBS 1X using

a Zeba desalting column (7K MWCO, ThermoFisher Scientific) to remove the excess DTT. Sulfosuccinimidyl 4-(N-maleimidomethyl) cyclohexane-1-carboxylate (sulfo-SMCC) dissolved in PBS at 9 mM was then added to the reduced oligos at 60-fold molar excess, and the mixture was incubated for 10 minutes at room temperature to activate the oligos. The oligos were then buffer exchanged to PBS 1X using a Zeba desalting column to remove the excess sulfo-SMCC. The activated oligos were distributed to tubes containing 10 µL of 1 mg/mL IgG antibodies, at a final DNA-to-Antibody ratio of 1.4. The conjugation mixtures were incubated for 30 minutes at room temperature, then overnight at 4°C. Following this incubation, the antibody-oligo conjugates were diluted 10-fold and transferred to a new tube. 2 µL of each diluted sample was reserved for evaluation via gel electrophoresis, while the rest was mixed with Protein G-coated beads (Dynabeads™ Protein G, Invitrogen) according to the manufacturer's protocol. The mixture was incubated for 45 minutes at room temperature with end-over-end rotation to isolate the antibodies, conjugated and unconjugated, from the unreacted oligos. The beads were washed 3 times (PBS 1X + 0.1% tween-20) to remove the unreacted oligos. The contents were then transferred to a new tube to avoid eluting oligos adsorbed to the tube surface. The beads were washed once with PBS 1X to reduce foaming, resuspended in 30 µL of elution buffer (50 mM glycine pH 2.7), then incubated for 2 minutes with pipette mixing. The beads were then pelleted and the eluant transferred to new tubes containing 3 µL of neutralizing buffer (2M TBS pH 8). The beads were resuspended in elution buffer and the process was repeated, with the eluant added to the same neutralizing tubes, to ensure complete elution of antibodies. The purified antibodies were stored at 4°C until further use.

Quantification by Gel Electrophoresis

The reserved antibody-oligo conjugate was diluted in LDS sample buffer (NuPAGE, Novex) and incubated on a 70°C heat block for 15 minutes, then cooled to room temperature for 15 minutes. A 3-8% NuPAGE Tris-acetate pre-cast gel (Novex) was prepared according to the manufacturer's protocol using SDS running buffer. The samples were loaded into the gel, and the system was run at 150V for 1 hour. After completion of the electrophoresis, the gels were removed and stained with silver staining (Pierce™ Silver Stain, Thermo Scientific). The intensity of each band was determined using Fiji[179] and used to estimate the ratio of conjugated to unconjugated antibodies. The concentration of monovalent and multivalent-conjugated

antibodies was determined, based on the initial concentration of antibodies added to the conjugation reaction.

Following the results of the gel electrophoresis analysis, the conjugation efficiency was classified as low, medium, or high. The quantity of barcoded beads to be mixed with the conjugated antibodies was empirically adjusted based on this determination.

3.2.2 Microparticle Barcoding

Streptavidin-coated superparamagnetic microparticles served as the substrate for the CLAMP probe. The beads were functionalized with DNA and antibodies using the following procedure.

Biotinylated capture and spacer oligos, and fluorescently labelled barcoding oligos were acquired from IDT. The barcoding oligos contained one of Atto-488, Cy3, Cy5, Cy5.5, or no dye. Each CLAMP species was assigned a spectral barcode made up of a ratio of the four dyes, designed with consideration of the Förster resonance energy transfer[180]. The capture and spacer oligos were each diluted in barcoding buffer (PBS 1X + 0.05% tween-20 + 300 mM NaCl) to 10 μM and mixed with each of the barcoding oligos at 10% excess. These capture- and spacer-dye stocks were then annealed by incubating them on a 70°C heat block for 5 minutes, and then cooling to room temperature for at least 15 minutes. At all times, the dyes were protected from light exposure using foil. The capture and spacer oligo solutions for each dye were then mixed at a ratio of 2:7. Next, 90 pmol of DNA (containing the desired ratio of fluorophores) was mixed with 6.7 pmol of biotinylated antibodies and buffer was added to make 25 μL of barcoding solution. For example, a barcoding mixture might contain 10 pmol of Atto-488 coder and 80 pmol of blank coder. These would be evenly distributed between the capture and spacer oligos.

Meanwhile, ~3.25 million beads (Dynabeads™ M-270 Streptavidin, Invitrogen) (5 μL of bead stock) were washed three times (PBS 1X + 0.1% tween-20) and then resuspended in 25 μL of barcoding buffer. The beads were added to the barcoding mixture, mixed at least 10 times with a pipette, then rotated end-over-end on a rack for 1.5 hours at room temperature. During incubation the beads were protected from light exposure using foil. Following incubation, the beads were washed three times and then resuspended in the washing buffer at a final concentration of 10,000 beads per μL. The beads were stored at 4°C in the dark until further use.

3.2.3 Hook Oligo Pulldown

The barcoded beads were resuspended in 10 µL of PBS 1X + 300 mM NaCl and mixed with 20 µL of purified conjugated antibodies. The number of beads used was determined based on the gel electrophoresis results as noted previously. The contents were mixed at least 10 times with a pipette, then rotated end-over-end on a rack for 1.5 hours at room temperature. During incubation the beads were protected from light exposure using foil. Following incubation, the beads were washed three times (PBS 1X + 0.1% tween-20) and then resuspended in the washing buffer at a final concentration of 10,000 beads per µL. The completed CLAMP beads were stored at 4°C in the dark until further use.

3.3 Colocalized Bead Assay

3.3.1 Blocking

The fully fabricated colocalized bead assay (CBA) probes were retrieved from storage, and the required amount of each type was pooled in a single tube. The buffer was exchanged to the blocking buffer (PBS 1X + 0.05% tween-20 + 150 mM NaCl + 0.5% BSA) and mixed vigorously with a vortex mixer for at least 2 seconds. The beads were then incubated for 1 hour at room temperature, during which they were rotated end-over-end and protected from light.

3.3.2 Assay

Aliquots of the desired target antigens were defrosted, pooled, and serially diluted in assay buffer (PBS 1X + 0.05% tween-20 + 0.5% BSA). The diluted antigens were held on ice until the blocking process was complete.

After blocking, the tubes containing beads were spun on a benchtop microcentrifuge for at least 5 seconds to retrieve droplets stuck to the cap. The buffer was then exchanged to the assay buffer, and the beads were distributed to a 96 well plate (Eppendorf LoBind PCR plate). Approximately 2000 beads in 25 µL of buffer were added to each well, and the bead stock tube was vortexed for one second between each pipetting step. 25 µL of the antigen solution was added to each well, and the contents were pipette mixed at least 10 times. The well plate was then incubated on a covered orbital shaker at 950 rpm for either 3 hours at room temperature or overnight at 4°C. These conditions had previously been shown to produce nearly identical results[181].

Assay Wash and Displacement

After incubation with the sample, the beads were washed 4 times (PBS 1X + 0.1% tween-20) using either a manual pipette or an automated liquid handler. The beads were then resuspended in displacement buffer (PBS 1X + 0.05% tween-20 + 450 mM NaCl). Displacer oligos were diluted in displacement buffer and added to the wells at a final concentration of 10 μM. The contents of the wells were pipette mixed at least 10 times, then incubated on a covered orbital shaker at 950 rpm for 30 hours at room temperature. After incubation, the beads were washed 4 times using either a manual pipette or an automated liquid handler. The plate was covered in adhesive foil and immediately stored on ice for transportation to the flow cytometer.

3.3.3 Cytometry Measurement Protocol

Flow cytometry was performed using a BD LSR Fortessa (BD Biosciences). Unlabelled streptavidin-coated beads and rainbow fluorescent particles were measured at the beginning of each session as a calibration. Gain values were adjusted manually to locate the fluorescence peaks within the machine's linear range ($< 10^5$ rfu). The foil covering the well plate was pierced with a sterile syringe, and a pipette was used to resuspend and then remove the contents of each well. The beads and buffer were transferred to a clean cytometry tube, vortex mixed, and introduced to the sample injection port (SIP). To limit bleaching and complex dissociation, the well plate was kept on ice throughout the measurement process and only one well was transferred to a cytometry tube at a time. Each tube was held on the SIP for 70 seconds or until 500 beads were measured for each bead set. Due to the large number of manual steps, flow cytometry could take several hours for a single assay.

3.4 Colocalized Bead Assay Analysis

The unprocessed cytometry data were visualized in FlowJo (BD Biosciences). The spectral barcodes were decoded manually, and the median fluorescence intensity (MFI) and bead-to-bead coefficient of variation (CV) data of each well were exported for further analysis. The data were imported into Excel (Microsoft Suite) and separated based on target. Wells where less than 100 beads per bead set were collected were excluded, as the results were not considered accurate[72]. The well-to-well CV was calculated and used to detect outliers; conditions with a CV > 20% were flagged and assessed visually. If one replicate differed substantially from the others, and its

removal reduced the CV below 20%, then it was labelled an outlier and removed from analysis. If one replicate could not be identified as an outlier, then all were retained. In the case of multiplexed assays, a replicate labelled as an outlier for one target was removed from analysis of all targets. Review of the fluorescence intensity histograms often indicated that these outlier wells had a bimodal distribution, suggesting the beads had non-uniform exposure during the assay.

The retained data were averaged and plotted using MATLAB (Mathworks) and fitted with a 4-parameter logistic regression of the form

$$y = D + \frac{A - D}{1 + \left(\frac{x}{C}\right)^B} \tag{12}$$

where *A* and *D* are the maximum and minimum asymptote, respectively, *B* is the Hill slope, and *C* is the inflection point. The curve-fitting program was written by G. Cardillo[182]. Changes in the dynamic range were evaluated based on the dissociation constant, K_D. This value was assumed to be equivalent to the inflection point, *C*, which is true when the overall amount of the target in solution is not significantly depleted by binding to the probe[43].

In some cases, the binding data demonstrated high heteroscedasticity, with standard deviation values at high concentrations 100-fold larger than those at low concentrations. The 4PL curves fitted to these datasets were found to have a poor fit of the lower end of the dynamic range, as assessed by visual inspection. In these cases, a weighting function of 1/Y or 1/Y^2 was applied following the protocol devised by Xiang et al[183].

3.5 Modified Colocalized Bead Assays

3.5.1 Colocalized Bead Assay with Stiffened Linker

To test the effects of stiffening the flexible linker, CLAMP beads were assembled as described in section 3.2. Oligos complementary to the hook oligo were incubated with the fully assembled CLAMP beads, and then the rest of the assay followed the method described in section 3.3. The stiffening oligo addition method is described in detail below.

Oligos measuring from 10 to 45-nt were purchased from IDT (Coralville, Iowa). These stiffening oligos were diluted to 2 μM in a high-salt buffer (PBS 1X + 0.05% tween-20 + 450 mM NaCl). Meanwhile, the beads were retrieved from storage and the required amount of each was pooled in a single tube. The combined beads were then split into pools and resuspended in the high-salt buffer. A different stiffening oligo was added to each pool, and the contents pipette mixed at least 10 times, for a final oligo concentration of 1 μM and bead concentration of 1000 beads/μL. The beads were then incubated for 1 hour at room temperature, during which they were rotated end-over-end and protected from light. After incubation, the beads were washed three times (PBS 1X + 0.1% tween-20) and then either used immediately or stored overnight in the wash buffer at 4°C.

In the preliminary experiment, 4 antigen concentrations were tested to limit the number of wells to be measured. Our group had previously found that excessively long experiments produced variations between the first and last wells measured. The concentration conditions were selected based on standard curves generated for these targets in a previous experiment using the same batch of beads. The conditions represented points of "low", "middle", and "high" signal on the standard curve, plus a blank buffer condition.

3.5.2 Colocalized Bead Assays using DIG Molecules as Affinity Binders

3.5.2.1 Fabrication

Digoxigenin (DIG) molecules were used as the capture and detection affinity binders for a new CBA. An anti-DIG antibody was used as the target.

DIG-conjugated oligos were acquired from IDT. The DIG-hook strand was identical to the original hook oligo, but with a DIG molecule in place of the thiol group. The DIG-surface strand had the same sequence as the barcoding oligos, but at the 5' end a five-nucleotide spacer was added followed by a DIG molecule. The barcoding protocol described in section 3.2.2 was followed, with the following modifications. During the annealing step, the DIG-surface strand was annealed with the spacer oligo using the same method as for the barcoding oligos. However, unlike the barcoding oligos, the DIG-surface strand was not also annealed with the capture oligo. After annealing, the capture/dye and spacer/dye duplexes and the spacer/DIG-surface duplex were mixed at a pre-determined ratio. In total, 90 pmol of DNA were combined in 25 μL of

buffer. For example, a barcoding mixture might contain 30 pmol of capture/coder duplex, 30 pmol of spacer/coder duplex, and 30 pmol of spacer/DIG-surface duplex. Only the duplexes including the barcoding oligos would determine the spectral barcode; of the 60 pmol including barcoding oligos, 54 pmol might contain the blank coder strand and 6 pmol contain the Cy3-conjugated strand. The full set of surface ratios and associated barcodes is shown in Table 1. The rest of the barcoding protocol was as described in section 3.2.2, excluding the addition of biotinylated antibodies.

Table 1: Barcoding mixture for DIG CBA. All units in pmol. No other barcoding strands were used, and are omitted from the table for space

CO/DIG-hook content	**SO/DIG-surface content**	**SO/coder content**	**Sub-total of CO+SO**	**Blank coder**	**Cy3 coder**
10	70	10	20	20	0
10	40	40	50	47	3
30	30	30	60	54	6
40	10	40	80	71	9
70	10	10	80	68	12

The method for pull-down of the DIG-hook strand was identical to that described previously for the antibody hook.

3.5.2.2 Preliminary Assay and QC

Anti-digoxigenin antibodies conjugated to Alexa Fluor 488 were acquired from R&D systems (IC7520G).

The required amount of each DIG CBA was pooled in a single tube. The beads were blocked as detailed in section 3.3.1. After blocking the beads were buffer exchanged to washing buffer then split into three clean tubes. For two of the tubes, the buffer was then exchanged for assay buffer containing anti-DIG-AF488 antibodies. To limit the time required for this preliminary experiment, only two concentrations of anti-DIG were used, 800 ng/mL and 800 fg/mL (approx. 5 nM and 5 fM). These concentrations represented a “high” and “low” condition based on previous assays using CLAMP beads. The beads were mixed at least 10 times with a pipette,

then both tubes rotated end-over-end at room temperature for 3 hours. The tubes were protected from light during the incubation. After incubation, the beads were washed 4 times using a manual pipette and then buffer exchanged to displacing buffer containing 10 nM of displacer oligo. The beads were mixed at least 10 times with a pipette, then rotated end-over-end at room temperature for 30 minutes. The beads were washed 4 times then immediately stored in an icebox for transportation to the cytometer.

At the same time, two quality control tests were prepared. After the blocked CBA beads were distributed to new tubes, and two were mixed with the assay target, the third tube was stored at 4°C in the dark for 3 hours. The buffer was then exchanged for a QC buffer (PBS 1X + 0.05% tween-20 + 300 mM NaCl) containing a labelling oligo at 1 μM. The labelling oligo was a 16-nt strand, entirely complementary to the hook oligo, with a Cy5 fluorophore conjugated to the 5' end (IDT). This set of beads, referred to as hook QC beads, were incubated and washed per the standard displacement protocol (section 3.3.2), then stored on ice for transportation to the cytometer (see section 3.3.3 for cytometry)

The second quality control set was referred to as antibody QC beads. During the fabrication of DIG CBA beads detailed in section 3.5.2.1, a portion were withheld and did not have the DIG-hook strand pulled down. For the antibody QC, the required amount of each bead was pooled in a single tube. The beads were blocked using the same method as the assay condition. Following blocking, the beads were buffer exchanged to the wash buffer and then stored at 4°C in the dark for 3 hours. The buffer was then exchanged for QC buffer containing 1 μg/mL of anti-DIG-AF488 antibodies. The beads were incubated and washed per the standard displacement protocol (section 3.3.2), then stored on ice for transportation to the cytometer.

At the cytometer, each tube was resuspended using a vortex mixer and then the contents were distributed to 4 cytometry tubes. The cytometry tubes were held on ice until it was their turn to be measured, and each was vortexed for at least 2 seconds immediately before being introduced to the SIP.

3.5.2.3 Standard Curve Assay

DIG CBA beads were fabricated as described in section 3.5.2.1, using much lower surface- and hook-DIG content (Table 2). In addition, no barcoding dyes were used. The beads of the first bead set, having no capture oligo on their surface, did not undergo pull-down of the DIG-hook.

Table 2: Barcoding mixture for DIG CBA. All units in pmol. No barcoding strands were used, and are omitted from the table for space

CO/DIG-hook content	**surface DIG content**	**SO content**	**Sub-total of CO+SO**	**Blank coder**
0	5	85	85	85
5	5	80	85	85
10	5	75	85	85

The beads could not be pooled, since they did not have barcoding oligos, so instead the required amount of each type was added to a separate tube. The beads were blocked following the standard method in section 3.3.1. After blocking, the buffer was exchanged to the assay buffer. Meanwhile, an aliquot of anti-DIG-AF488 was defrosted and serially diluted in assay buffer. The beads were distributed to a 96-well plate, along with the diluted target, following the standard assay protocol. The well plate was then incubated on a covered orbital shaker at 950 rpm for 3 hours at room temperature. The beads of the second and third bead sets, which contained DIG-hook, were washed 4 times using an automated liquid handler. The standard displacement protocol was then followed for these beads. The beads of the first bead set did not undergo washing or displacement. However, because they were on the same plate, they experienced magnetic collection along with the other bead sets. These beads were not manually resuspended with a pipette after magnetic collection, which may have led to insufficient mixing. The well plate was incubated on a covered orbital shaker at 950 rpm for 30 minutes at room temperature. After incubation, all the beads were washed four times using the automated liquid handler. The well plate was stored on ice for transportation to the cytometer and measured as detailed in section 3.3.3.

Two quality control assays were performed as described in section 3.5.2.2.

3.5.3 DIG Colocalized Bead Assay with Two Flexible Linkers

Fabrication

A set of capture oligos of increasing length, biotinylated at the 5' end, were acquired from IDT. Two types of DIG-hook strand were also acquired from IDT. One had 21-nt complementary to the capture oligo, plus a 9-nt toehold region, and was conjugated to a DIG molecule at the 5' end. This strand was denoted as the "releasable hook". The other DIG-hooks had increasing lengths of complementarity to the capture oligo, from 20 to 50-nt. They were each conjugated to a DIG molecule at the 3' end and were identified as the "fixed hook".

The spacer oligo and each of the capture oligos were diluted in barcoding buffer to 10 μM. The blank coder strand was added to each tube at 10% excess. These stock solutions were then annealed by incubating them on a 70°C heat block for 5 minutes, and then cooling to room temperature for at least 15 minutes. The spacer oligo was mixed with each of the capture oligos at the ratios shown in Table 3. Very low amounts of the capture oligo were used to increase the average distance between probe complexes. 90 pmol of DNA from each set was diluted with barcoding buffer to make 25 μL of barcoding solution. The remainder of the barcoding protocol was the same as in section 3.2.2, excluding the addition of biotinylated antibodies.

Table 3: Barcoding mixture for DIG CBA with two hook oligos. All units in pmol unless otherwise indicated.

CO complementary length (nt)	**CO/DIG-hook content**	**SO content**	**Sub-total of CO+SO**	**Blank coder**
20	5	85	90	90
30	5	85	90	90
40	5	85	90	90
50	5	85	90	90

The pull-down step was performed as described in section 3.2.3, except that the pull-down mixture contained both the releasable DIG-hook and the fixed DIG-hook that matched the capture oligo used.

Standard Curve Assay

Unlabelled anti-DIG antibodies were acquired from R&D Systems (MAB75201).

The required amount of each DIG CBA bead type was blocked in a separate tube, following the standard protocol (section 3.3.1). Meanwhile, an aliquot of anti-DIG was defrosted and serially diluted. The rest of the assay followed the standard protocol of section 3.3.2, except that the beads were incubated with the target for four hours at room temperature. Washing was performed using an automated liquid handler. The well plate was stored on ice for transportation to the cytometer and measured as detailed in section 3.3.3.

3.5.4 Measurement of anti-DIG Affinity

The DIG CBA beads fabricated in section 3.5.2.1 that had no capture oligo on their surface were used. These beads were blocked following the protocol in section 3.3.1. Meanwhile, the anti-DIG antibodies were defrosted and serially diluted in assay buffer. The beads and the antibody targets were plated as described in section 3.3.2. The well plate was then incubated on a covered orbital shaker at 950 rpm for 3 hours at room temperature.

After incubation, the beads were washed four times using an automated liquid handler. In the case of the anti-DIG-AF488 antibodies, the beads were resuspended in the wash buffer and stored on ice for transportation to the cytometer.

In the case of the unlabelled anti-DIG antibodies, the beads were resuspended in 100uL of assay buffer. A goat anti-mouse secondary antibody conjugated to Cy5 was diluted in assay buffer and added to each well for a final antibody concentration of 1 ug/mL. The plate was incubated for 1.5 hours at room temperature on a covered orbital shaker at 950 rpm. The beads were washed four times and resuspended in the wash buffer. The plate was stored on ice for transportation to the cytometer.

3.5.5 Calculation of Average Separation Between DNA Strands

According to the manufacturer, 1 mg of M-270 streptavidin-coated Dynabeads (Invitrogen) can bind 200 pmol of single-stranded DNA. Double-stranded DNA is wider and more negatively charged, so we estimated that the same mass of beads would bind about 120 pmol of dsDNA. 1

mg corresponds to 6-7 x 10^7 individual beads; we used the midpoint for our calculations. In our current barcoding procedure, we incubate 3.25 x 10^6 beads with 90 pmol of biotinylated dsDNA. The surface of the beads should be fully saturated, at 1.11 x 10^6 dsDNA strands per bead. The beads have a nominal diameter of 2.8 μm; assuming them to be smooth spheres, each has a surface area of 24.6 μm^2. Therefore, the surface density of dsDNA is 4.5 x 10^4 strands/μm^2. If the strands are randomly distributed on the surface then the average nearest neighbour distance can be derived from the Poisson distribution function as $\langle d \rangle = {}^{1}/_{2\sqrt{\sigma}}$ [184], where σ is the density in 2 dimensions. Since DNA is self-avoiding, the strands will be slightly more ordered than a true Poisson distribution. For a fully uniform distribution the nearest neighbour distance is doubled, $\langle d \rangle = {}^{1}/_{\sqrt{\sigma}}$. The actual distribution is likely somewhere between perfectly ordered and perfectly random, though this has not been characterized for DNA immobilized through biotin/streptavidin binding. A characterization of the nanoscale distribution of thiolated DNA bound to a gold surface found that the distribution was only slightly more uniform than a true random surface[185]. Using the Poisson-derived equation and the density derived above, the average nearest neighbour distance between DNA strands on the bead is 2.4 nm. However, not all the strands on the bead are identical. In section 3.5.2 we tested a range of capture oligo to spacer oligo ratios. Assuming that the CO/SO ratio on the bead surface is the same as in the barcoding mixture, the average distance between neighbouring capture strands varies from 2.7 nm to 7 nm. In section 3.5.3 the capture oligo made up just 5 out of 90 pmol of DNA in the barcoding mixture. The average distance between neighbouring capture oligos is expected to be 10 nm.

3.6 Liquid-Phase Colocalized Assays

3.6.1 Colocalized Assay

Fabrication

Linear probe strands were designed that were similar in form to a padlock probe. They consisted of two target-recognition sequences, 7 nucleotides in length, separated by an AT-rich linker region measuring 15 to 63 nucleotides. The probe strands were conjugated to a fluorophore (Cy5) at the 5' end and a quencher (Iowa Black RQ) at the 3' end. Target strands were designed that were complementary to both recognition sites, such that the target-probe complex was in the

form of a ring with the fluorophore and quencher held in proximity. All DNA strands were acquired from IDT.

Standard Curve Assay

The probe strands were diluted to 20 nM with in-solution assay buffer (PBS 1X + 0.005% tween-20 + 450 mM NaCl). 3 replicates were prepared for each probe. 25uL of the probe solution was distributed to each well of a solid black polystyrene 96-well plate (Nunclon) using a multi-channel manual pipette. The target strands were serially diluted with in-solution assay buffer, then 25uL was distributed each well such that the final concentration of probe strands was 10 nM. The contents of each well were pipette mixed at least 10 times. The well plate was then incubated on a covered orbital shaker at 950 rpm for 30 minutes at room temperature. After incubation, the plates were protected from light and maintained at room temperature for transportation to the plate reader.

3.6.2 Plate Reader Measurement

The fluorescence intensity of each well was measured using a plate reader (SpectraMax i3). For the first experiment the "height optimization" function was run; thereafter the optimized height value (0.73 mm from plate) was used for all experiments. The excitation filter was set as a 9nm band centred at 640nm and the emission was collected as a 15nm band centred at 670nm. These values were determined following the optimization procedure detailed in the SpectraMax user manual. By default, 6 readings were made per well, with the average intensity value being reported.

3.6.3 Analysis of Plate Reader Data

The plate reader data were imported to GraphPad Prism (GraphPad Software) and analyzed by nonlinear regression. Two different equations were used for fitting: the 4-parameter logistic model described in section 3.4 and the quadratic binding equation[43].

$$[P \cdot T] = \frac{([P]_0 + [T]_0 + K_D) - \sqrt{([P]_0 + [T]_0 + K_D)^2 - 4[P]_0[T]_0}}{2} \tag{13}$$

Where P is the probe, T is the target, and nought indicates the initial condition.

The quadratic binding equation can be used in a 3-parameter logistic model, which assumes no cooperativity (Hill coefficient = 1). This model is most appropriate when the probe concentration is on the same order of magnitude as the K_D value, as it accounts for both the free and bound target[43].

The 4PL model does not account for the target depletion; thus, its inflection point is more accurately defined as the EC_{50}, the target concentration that produces 50% occupation of the probe. The K_D value can be approximated from the EC_{50} as

$$K_D = EC_{50} - \frac{[probe]}{2} \tag{14}$$

However, this approximation is most accurate when the target depletion is less than 10%, meaning the probe concentration is at most one-tenth of the calculated K_D value[40].

3.6.4 Monovalent Affinity Measurement

Fabrication

The affinity measurement system consisted of two matched strands. The first, called the KD-probe strand, was identical to one of the two target recognition sequences of the probes described in section 3.6.1. The KD-probe strands were conjugated to a fluorophore (Cy5) on the 5' end. The second strand was called the KD-target strand and was identical to one half of the target strand described in section 3.6.1. The KD-target strands were conjugated to a quencher (Iowa Black RQ) on the 3' end. A control strand was also designed, which had the same sequence as one of the KD-probe strands but was conjugated to a quencher (Iowa Black RQ) on the 3' end. All DNA strands were acquired from IDT.

Affinity Assay

The assay steps were identical to those described in section 3.6.1, with the KD-probe and KD-target strands used in place of the standard probe and target strands, respectively. 4 replicates were prepared. Measurement steps followed the plate reader protocol described in section 3.6.2, and the analysis followed section 3.6.3.

3.7 DNA Oligo Design and Handling

All oligonucleotides were purified by IDT prior to shipment. Oligos measuring less than 30 nt and without modification underwent standard desalting, while oligos longer than 30 nt or with modification (thiol, fluorophore, etc.) underwent HPLC purification. All oligonucleotides were received pre-dissolved in IDT's LabReady format (100 μM concentration in IDTE buffer, pH 8.0). Oligos were stored at -20°C immediately upon reception. In cases where concentrations of 50 nM or lower were required for experiments, 1 μM aliquots diluted in PBS 1X + 0.1% tween-20 were prepared, quantified, and stored at -20°C.

Before each use, oligo tubes or aliquots were defrosted by leaving them on the benchtop for several minutes, protected from light with foil. The oligos were then mixed vigorously for 10 seconds using a vortex mixer then spun down for 10 seconds using a benchtop centrifuge to homogenize the contents.

3.7.1 Nanodrop Quantification of Oligonucleotides

Before use in experiments, oligo strands were quantified using a spectrophotometer (Nanodrop 1000, ThermoFisher Scientific). An oligonucleotide calculator[186] was used to determine the molecular weight of each strand and predict the concentration; if it was above the measurement limit specified by the manufacturer (2400 ng/μL) then 10 μL was diluted 1:1 with PBS 1X + 0.1% tween-20. Otherwise, measurements were made directly from the stock tube. Three droplets were measured from each sample, following the manufacturer's protocol. In the case of rare and expensive samples, the same droplet was measured three times. The average of the measurements was used as the stock concentration for all subsequent calculations for experiments.

3.7.2 Design of Orthogonal DNA Strands

New DNA sequences were designed according to the following method:

First, a random string generator was used to create a series of 30 strings of the desired length containing the characters A, T, C or A, T, G. C and G bases were never placed in the same strand unless it was required for complementarity to pre-existing sequences. The randomly generated strings were assessed visually, and strings containing (i) 4 or more A or T in a row or (ii) 3 or

more C or G in a row were eliminated. The retained strings were assessed for secondary structures using the Mfold server's Quikfold tool[187]. The cut-off depended on the application – strands intended to hybridize to others were accepted if they had no secondary structures with T_m > 40°C, while those that would remain single-stranded in solution (ex. hook oligo) were accepted in they had no secondary structures with T_m > 40°C or ΔG < 0 kcal/mol. Next, the candidate strings and all existing DNA sequences that they would encounter were assessed for unintended dimers using Primer Pooler[188]. Dimerization with strands that would be annealed in an earlier step, and therefore would not be available for hybridization, was not of concern. Strings that formed dimers with ΔG < -7 kcal/mol were eliminated. Pairs of strings that formed dimers with ΔG < 0 kcal/mol were reassessed with Mfold[187] – those with T_m < 10°C were retained. If multiple candidate strands remained, the one(s) with the lowest dimer T_m was selected. The final set of DNA sequences was analyzed with NUPACK to verify that populations of unintended dimers were expected to be minimal[189].

3.7.3 Design of DNA Affinity Binders

DNA probe and target pairs were designed according to the method described above. The Van't Hoff equation was used to calculate a first approximation of K_D[190]:

$$\Delta G = RT \ln K_D \tag{15}$$

Where R is the gas constant, T is the assay temperature, and ΔG is the Gibbs' free energy of binding. K_D values on the order of 100 nM were targeted such that the lower end of the dynamic range would be above the limit of detection of the plate reader.

4. Results and Discussion

The dynamic range is the interval of analyte concentrations where an assay can provide quantitative information. There is a need to adjust an assay's dynamic range to allow measurement of biomarkers with large clinical ranges or to detect several analytes simultaneously in a multiplexed assay. The methods for modifying the dynamic range can be divided into three categories: modification of the sample, the affinity binder, or the apparent affinity. When two affinity binders are joined together by a flexible linker to form a single bivalent molecule, the apparent affinity or avidity of the new molecule is greater than the affinity of either molecule on its own. The linker increases the probability of bivalent binding, thereby enhancing the apparent affinity. Modulation of the linker's entropy has been shown to alter the dynamic range of simple assays and may also be applicable to more complex sandwich assays.

We selected colocalized bead assays (CBA) as a focus, given the widespread use of bead-based sandwich assays. We defined colocalized bead assays as system having a matched pair of sandwich affinity binders pre-assembled to a micron-sized bead via one or more flexible linkers. We used the colocalization-by-linkage assay on microparticles (CLAMP), represented in Figure 22B, as a starting point because it is a real-world system with the potential for robust and sensitive analyte measurement. According to our literature analysis, modification of the length and rigidity of the flexible linker should alter the number of states permitting formation of a sandwich complex. We hypothesize that altering the linker's entropy will allow tuning of the apparent affinity, and therefore the dynamic range, of a CBA.

However, in a CBA there are several factors that also influence sandwich complex formation. These are: reagent density and stochasticity, linker length and flexibility, location of linker/affinity binder cross-link, affinity binder flexibility, and each binder's monovalent affinity (Figure 22A).

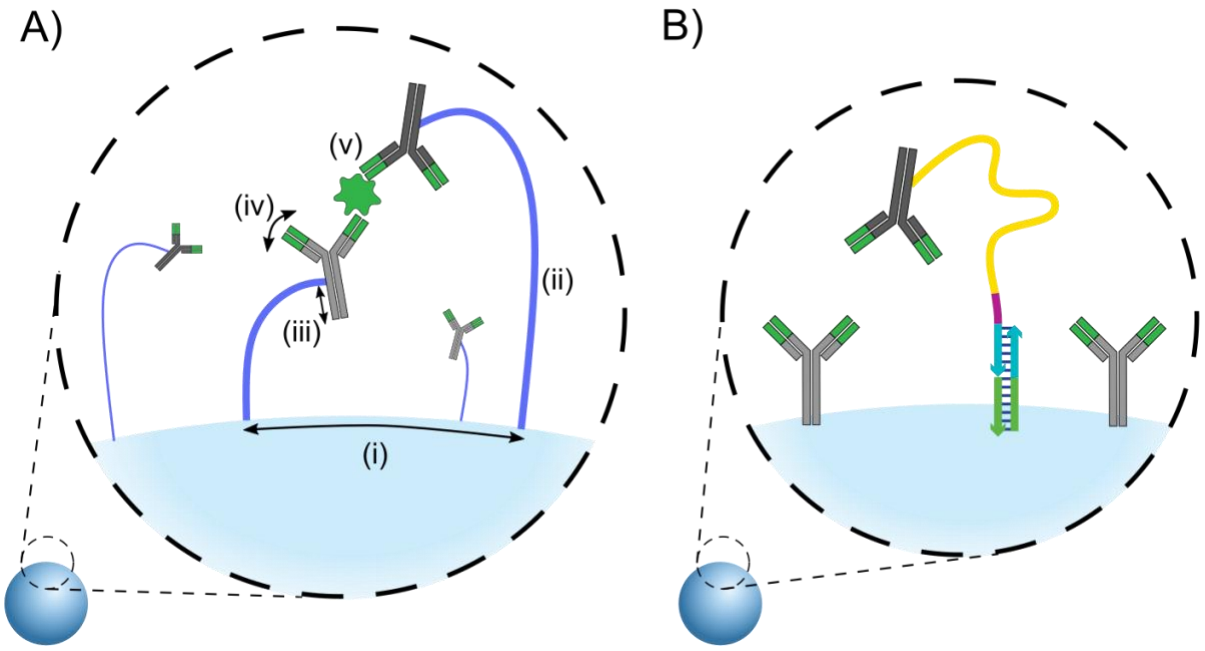

Figure 22: A) Simplified representation of a colocalized bead assay, wherein a matched detection and capture affinity binder are pre-assembled on the surface of a bead. One affinity binder may be conjugated directly to the bead, or both may be tethered to the surface by a linker molecule. Whereas antibodies are shown here, they are representative of any affinity binder. The blue linkers could be any flexible molecule, such as a PEG, polypeptide, or oligonucleotide chain. The factors that influence the formation of a sandwich complex are: (i) reagent density and stochasticity, (ii) linker length and flexibility, (iii) location of linker/affinity binder cross-link, (iv) affinity binder flexibility, and (v) monovalent affinity of each affinity binder. B) Representation of the CLAMP assay, used as a starting point in this thesis. The capture antibody is conjugated directly to the bead, while the detection antibody is tethered by a flexible DNA oligonucleotide. The hook oligo can be released by a displacer strand, which binds to a toehold region (pink).

In this thesis, we investigated the effect of these factors on the apparent affinity and the dynamic range. We also evaluated the assay's signal window, defined as the difference in signal magnitude between the lowest and highest detectable concentrations[191]. Several examples of assays in literature with modified dynamic range also had severely narrowed signal windows[47,138,141,142]. Consideration of this value allowed us to assess the utility of an assay; a modified dynamic range is useless if the assay's signal window is too small to measure samples with precision.

We began by stiffening the flexible linker in the CLAMP assay, as it was the simplest change to implement. We sought to determine if linker flexibility could overcome the other factors listed

above. Second, we limited the role of the affinity binder flexibility by using small molecules in place of capture and detection antibodies. We kept the linker length constant and increased the average separation between affinity binders to reduce the number of states permitting binding. Third, we sought to reduce the effect of surface stochasticity by limiting the separation of affinity binders to a linear distance. We examined the impact of increasing the absolute distance between affinity binders on a system with short flexible linkers. Fourth, we employed a reductionist approach, developing a liquid-phase colocalized assay to investigate the role of the linker length in isolation from the other factors. Finally, we compared two published mathematical models of apparent affinity modification of liquid-phase colocalized assays to our results and literature results. We also evaluated the factors that should be included in a more complex system such as a colocalized bead assay.

4.1 Exploring the Effect of Linker Flexibility on the Apparent Affinity of a Colocalized Bead Assay

Here we first sought to examine whether stiffening of the flexible linker could be used to modify the apparent affinity and dynamic range of a CBA. We used the CLAMP as a starting point, given the points discussed previously. We hypothesized that the flexibility of the linker was the dominating factor determining binding dynamics, and therefore progressively stiffening the linker would progressively shift the apparent affinity.

To modify the flexibility of the hook oligo, we incubated fully assembled CLAMP beads with oligos of different lengths complementary to a portion of the hook oligo (Figure 23). The stiffening oligos were 10, 20, 30, or 45 nt in length. A strand of each length located towards either the 3’ or 5’ end of the hook oligo was tested, except for the 45 nt stiffener which covered the entire tested length, for a total of 7 conditions. The full sequences can be found in the appendix (section 7.2). We diluted the stiffening oligos in a high salt buffer (PBS 1X, 0.05% tween-20, 450 mM NaCl) to overcome electrostatic repulsion between the free DNA and beads. As a control, we incubated one set of CLAMP beads with the same buffer without stiffening oligos and used them for a parallel assay.

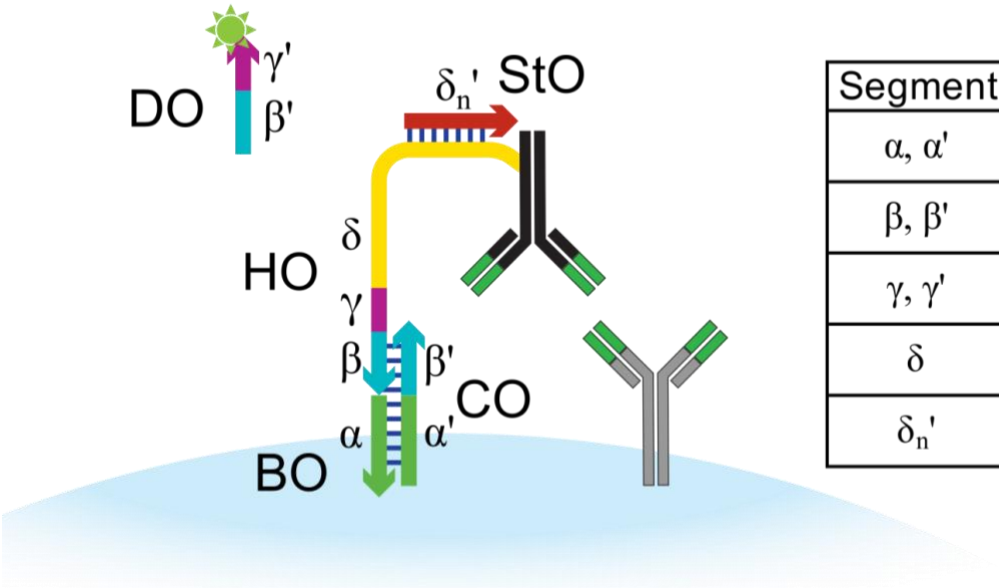

Segment	Length (nt)
α, α'	21
β, β'	21
γ, γ'	9
δ	51
δ_n'	10-45

Figure 23: Simplified representation of the surface complex in the CLAMP with stiffened hook oligo. The capture antibody and CO strand are biotinylated, providing a strong connection to the streptavidin-coated bead. The StO strands used were 10, 20, 30, and 45 nt in length and were located either towards the 3' or 5' end of the hook oligo. The CO strand was conjugated to the bead via streptavidin-biotin complex. HO: hook oligo, BO: barcoding oligo, CO: capture oligo, DO: displacer oligo, StO: stiffener oligo.

Double-stranded DNA is shorter than single-stranded due to the formation of the helix, so increasing the portion of the hook oligo that was double-stranded also decreased the length of the linker. We considered that reducing the linker length would also limit the probability of bivalent binding, though we did not assess this effect independently of the change in stiffness.

The primary factors that might confound the effects of stiffening the linker were the flexibility of the affinity binder and the reagent stochasticity. As was discussed in section 2.2.3, IgG antibodies have numerous points of flexibility. In the CLAMP, the antibodies are also about 25% the length of the hook oligo in the CLAMP (10 nm [192] vs 60 nt (approx. 40 nm)). Due to the stochasticity of oligo conjugation to the bead surface, it is likely that some tethered detection antibodies have access to multiple surface-bound capture antibodies. It would be more difficult to alter the probability that these antibodies bind, since they experience a high density of available binding sites. The relative densities of capture antibodies and capture oligos have not been characterized, so we cannot estimate what portion of detection antibodies might be in this situation.

Batch-to-batch inconsistencies in the CLAMP bead fabrication and variations in the assay method might also influence the effect of stiffening the linker. The CLAMP assay was regularly performed with an antigen incubation of either 3 hours at RT or 15 hours at 4°C, as these conditions had previously been shown to produce equivalent binding curves[181].

Effect of Incubation Time on Stiffened CLAMP

We tested whether this equivalency applied to the stiffened CLAMP as well by performing an experiment using CLAMP beads prepared against three different targets. Interferon gamma (IFN-γ), interleukin 12 (IL-12), and interleukin 1 beta (IL-1β) were selected as targets from the existing CLAMP library because they demonstrated significant fluorescence change over the dynamic range. We expected this would make changes in the signal window more noticeable in binding curve experiments. The CLAMP beads were incubated with several stiffener oligos, then used in a multiplexed assay. In place of an antigen incubation, the beads were incubated with blank buffer for 3 hours at RT or 15 hours at 4°C, then displaced as normal. Only the blank condition was measured to ensure that any differences observed could not be a result of changes in binding dynamics. We observed some differences between the two conditions for the stiffened CLAMP, as well as for the control (Figure 24). However, the changes were not consistent between targets, and were small compared to the variation (SD). Therefore, we cannot conclude that the two incubation times are more different for the stiffened CLAMP than they are for the control.

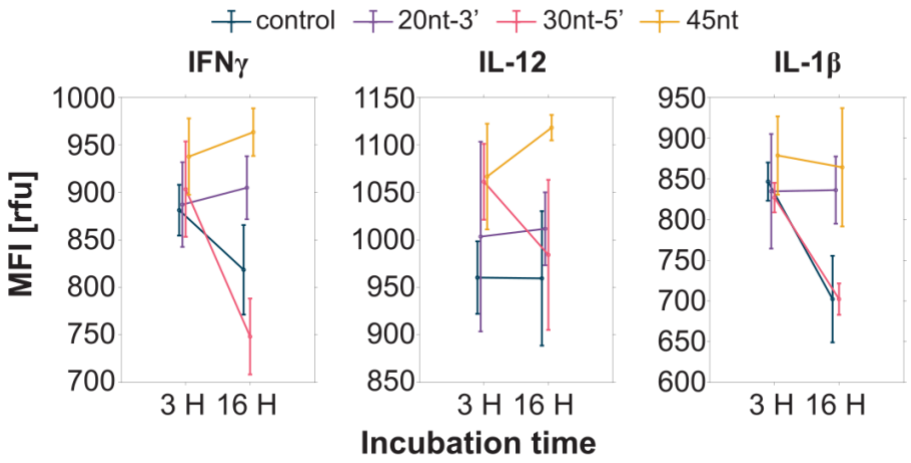

Figure 24: Effect of incubation time on background signal for stiffened CLAMP beads. The beads were incubated with blank buffer for 3 hours at RT or 15 hours at 4°C. We observed small differences between the two incubations for the stiffened

CLAMP, though they were not significantly different from the control. The names of the stiffeners correspond to their length and approximate location on the hook oligo. The control set was incubated with buffer while the other sets were incubated with stiffener oligos. The full sequences can be found in the appendix (section 7.2). Error bars represent one standard deviation. n=4.

Effect of Stiffening on CLAMP Binding Curve – Limited Binding Curve

We evaluated the effect of stiffening the hook oligo on the apparent affinity by generating binding curves for CLAMP beads from the same batch as in Figure 24. To test all the stiffeners in a single assay, allowing direct comparison of the results, we selected a limited set of concentrations. The concentrations represented low, medium, and high points from a standard curve generated using the same CLAMP batch, plus a blank. The stiffened beads were incubated with the antigen for three hours at RT.

Our results revealed that stiffening the hook oligo influenced the median fluorescence intensity measured (Figure 25A). However, since the concentrations represented only a subset of the standard curve, it was unclear whether the decrease in fluorescence represented a shift or stretch of the dynamic range, or a reduction of the signal window. We selected several stiffening strands to test in a full 12-point standard curve. The 30-nt strand at the 5' end of the hook (30nt-5') and the 20-nt strand at the 3' end (20nt-3') were chosen because they had the greatest effect on the maximum fluorescence (Figure 25B). The 45-nt stiffening strand was also selected as the most extreme modification.

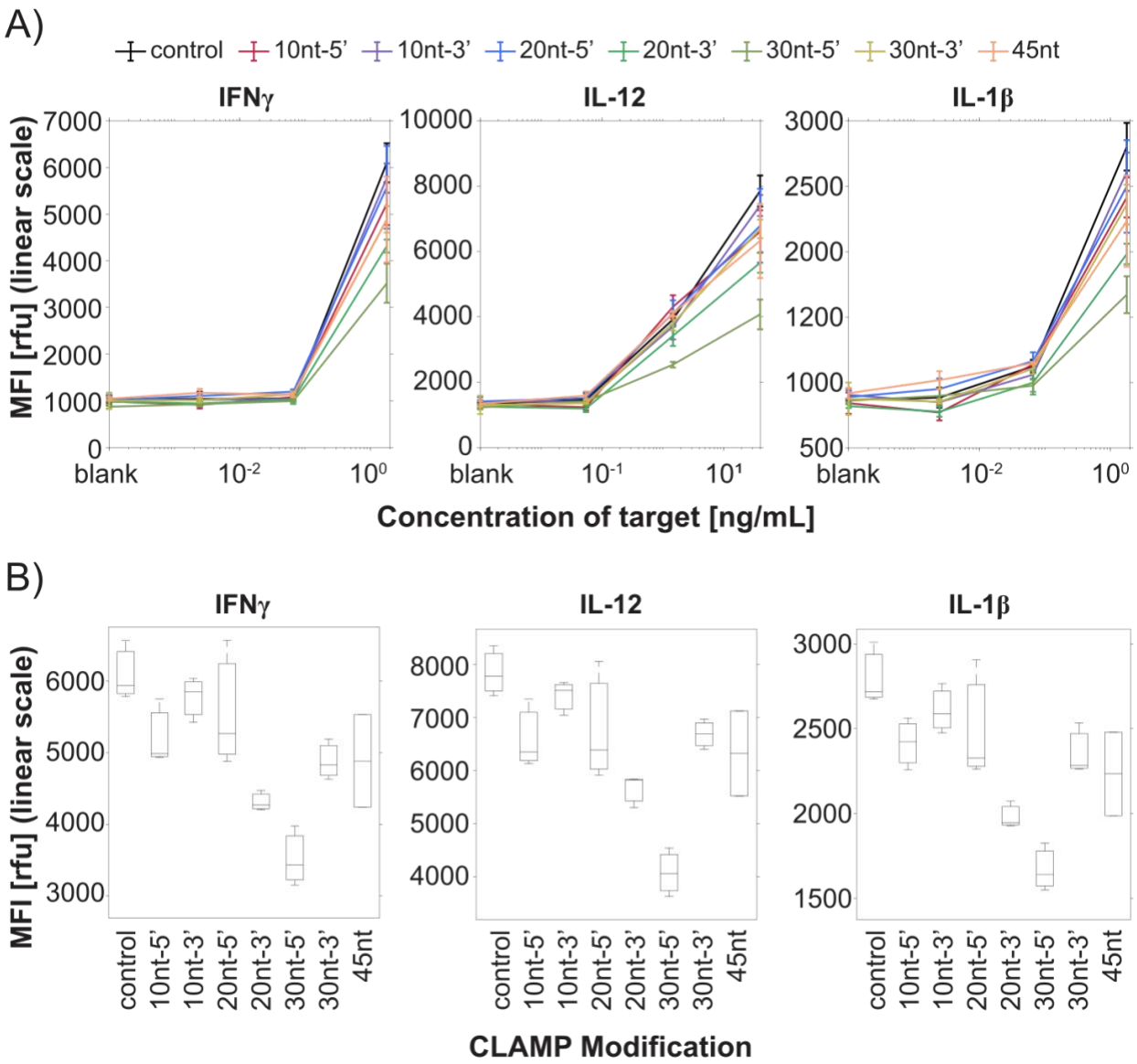

Figure 25: Impact of stiffening the hook oligo on the binding curves of CLAMP against three targets. A) Binding curves generated using a limited set of concentrations. IFNγ and IL-1β: 0.00244, 0.0658, 1.78 ng/mL. IL-12: 0.0061, 1.48, 40 ng/mL. Stiffening the hook oligo had an effect on the fluorescence at the high concentration, and this effect was consistent across targets. Without a full binding curve, it cannot be determined whether this change represents narrowing of the signal window or a shift of the dynamic range. Error bars represent one standard deviation. n=3. B) Box-and-whisker plot of the median fluorescence intensity measurements at the high concentration. All the stiffeners reduced the MFI to some extent, as compared to the control. The stiffeners with the greatest impact on MFI (20nt-3' and 30nt-5') and the most extreme modification (45nt) were selected for further analysis. The central mark indicates the median, and the bottom and top of the box represent the 25th and 75th percentiles, respectively. The whiskers indicate the most extreme data points. n=3.

Effect of Stiffening on CLAMP Binding Curve – Full Binding Curve

CLAMP beads from the same batch as in Figure 24 and Figure 25 were incubated with the selected stiffeners, then used in a multiplex assay. The beads were incubated with the antigen mixture overnight at 4°C to test whether a longer incubation time would change the effect of stiffening the hook oligo.

The results of our 12-point standard curve indicated that stiffening the hook did not lead to a shift in the dynamic range. Instead, it produced a lowering of the maximum signal intensity in some cases, and an increase in background in all cases (Figure 26). This did produce changes in the measured apparent affinity, but by visual examination this is due to changes in the signal window, and not a shift of the dynamic range.

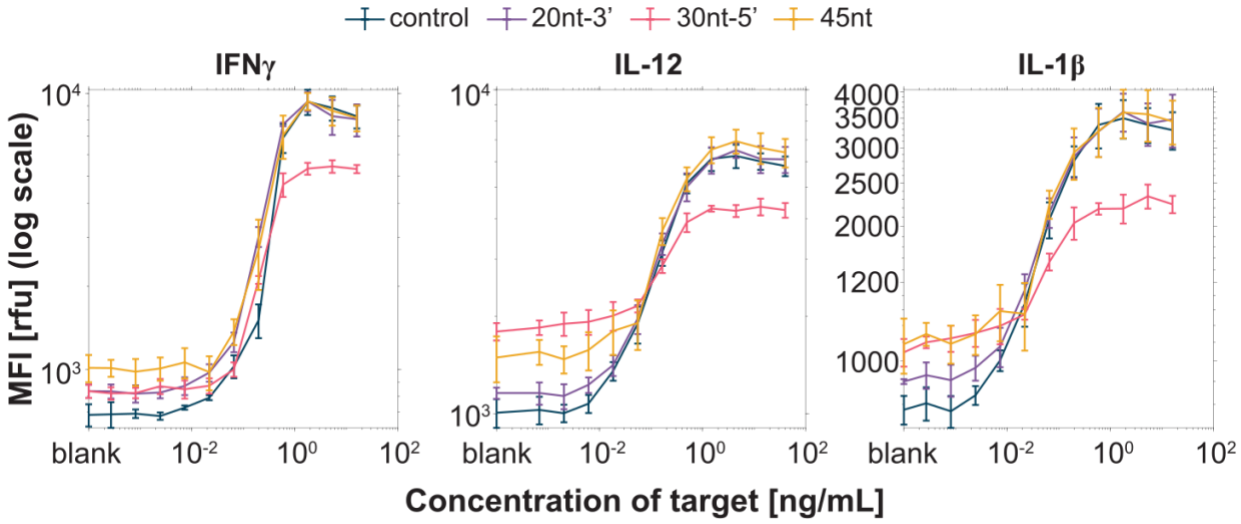

Figure 26: Effect of stiffening the hook oligo on the binding curves of CLAMP using an overnight incubation at 4°C. Compared to the control, all the stiffened CLAMP sets have a narrowed signal window and no significant change in apparent affinity. The K_D values for each target of the control and 20nt-3', 30nt-5', and 45nt stiffened CLAMP were calculated by fitting with a 4PL curve. IFNγ: 0.290, 0.181, 0.214, 0.239 ng/mL. IL-12: 0.121, 0.117, 0.200, 0.197 ng/mL. IL-1β: 0.0452, 0.0417, 0.0821, 0.0830 ng/mL. Error bars represent one standard deviation. n=4.

We observed that the results of the full binding curve (Figure 26) are inconsistent with those of the limited binding curve experiment (Figure 25). In the limited binding curve experiment, CLAMP beads stiffened with the selected stiffeners had a lower MFI than the control at the high concentration, whereas for the full binding curve only the stiffener 30nt-5' had significantly

lower MFI at saturation. Considering the blank, in the limited binding curve experiment the stiffened CLAMP beads did not vary significantly from the control, while for the full binding curve the blank signals are 15-80% greater than the control. The IL-1β results for both binding curve experiments and the background experiment (Figure 24) are tabulated in Table 4. The lack of reproducibility between experiments suggests that the CLAMP beads were not affected consistently by stiffening.

Table 4: background and saturation MFI signal of CLAMP beads with stiffened hook oligos against IL-1β relative to unstiffened (control) condition

	Experiment (incubation time)	**Difference in MFI signal from control**		
		20nt-3'	**30nt-5'**	**45nt**
Blank	Background (3 H)	-1.4%	-2.3%	+3.8%
	Background (15 H)	+19%	0%	+23%
	Limited binding curve (3H)	-5.7%	-0.92%	+5.7%
	Full binding curve (15 H)	+16%	+34%	+40%
Saturation/High concentration	Limited binding curve (3 H)	-29%	-40%	-20%
	Full binding curve (15 H)	+5.7%	-31%	+4.6%

We observed that stiffening the hook oligo, even as far as making it entirely rigid double-stranded DNA, is insufficient to overcome the primary factors influencing apparent affinity. These factors likely contributed to the varied effects of stiffening on the signal window. In the CLAMP, we hypothesize that the dominating factors are the antibody flexibility and the stochastic distribution of reagents on the surface.

4.2 Exploring the Effect of Average Reagent Separation on the Apparent Affinity of a CBA

Here we sought to examine the effect of changing the average distance between the capture and detection affinity binders on a colocalized bead assay. We hypothesized that increasing the average separation between capture and detection affinity binders while keeping the linker the same would decrease the number of states permitting binding, thereby decreasing the apparent affinity. To reduce the role of the affinity binder flexibility, we designed a new CBA using small molecules as the capture and detection moieties and an antibody as the analyte. Digoxigenin

(DIG) is a hapten molecule measuring 0.4 kDa, against which several high-affinity antibodies have been raised. One DIG molecule was conjugated to the end of a long, flexible hook oligo. A second DIG was conjugated to a short DNA strand that hybridized to an oligo conjugated to the bead surface (Figure 27).

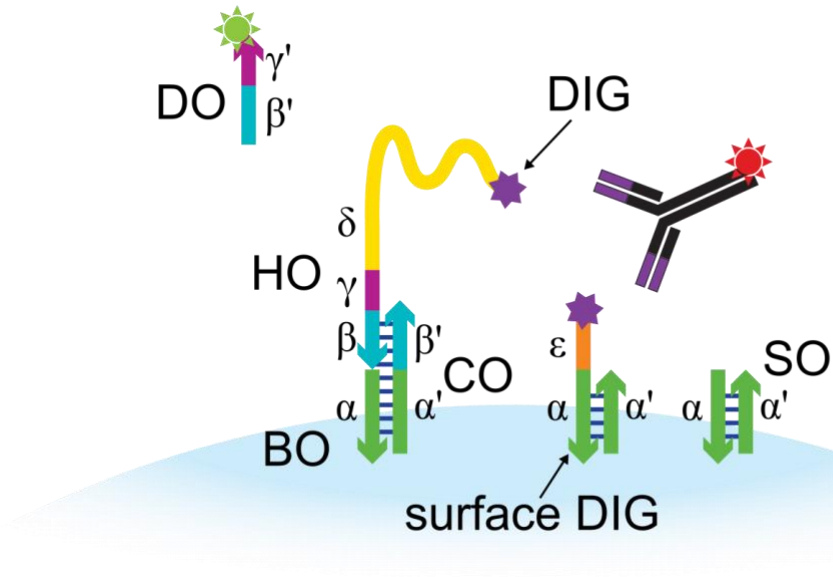

Segment	Length (nt)
α, α'	21
β, β'	21
γ, γ'	9
δ	51
ε	5

Figure 27: Simplified representation of digoxigenin colocalized bead assay. The CO and SO strands are biotinylated, providing connection to the bead. DIG: digoxigenin, CO: capture oligo, HO: hook oligo, BO: barcoding oligo, SO: spacer oligo, DO: displacer oligo

Whereas in section 4.1 the capture and detection affinity binders were non-identical antibodies, the colocalized bead assay in Figure 27 uses the same molecule as both the capture and detection moiety. This format creates the potential for the analyte molecule (the anti-DIG antibody) to bind to two hook-conjugated DIG molecules or two surface DIG molecules, instead of one hook DIG and one surface DIG (Figure 28). In the first and second cases, no assay signal (DO-conjugated fluorophore) would be detectable after displacement. We considered using a hetero-specific antibody to avoid this outcome. However, we expected that some antibodies would bind in the ideal orientation, such that we could characterize the role of average separation. We elected to use a fluorophore-conjugated anti-DIG antibody as the analyte so that we could evaluate how many antibodies bound to two surface DIG molecules vs. one hook DIG and one surface DIG. The anti-DIG antibody we acquired was pre-conjugated to AF488, which forms a FRET pair with the DO fluorophore (Cy5). However, their Förster radius was found to be 5.2 nm, with the donor-acceptor intensity ratio decreasing rapidly beyond this distance[193]. Since the Cy5 would be

located at the end of the hook oligo, and the AF488 close to the surface (Figure 28ii, bottom), we expected the FRET between them would be very low.

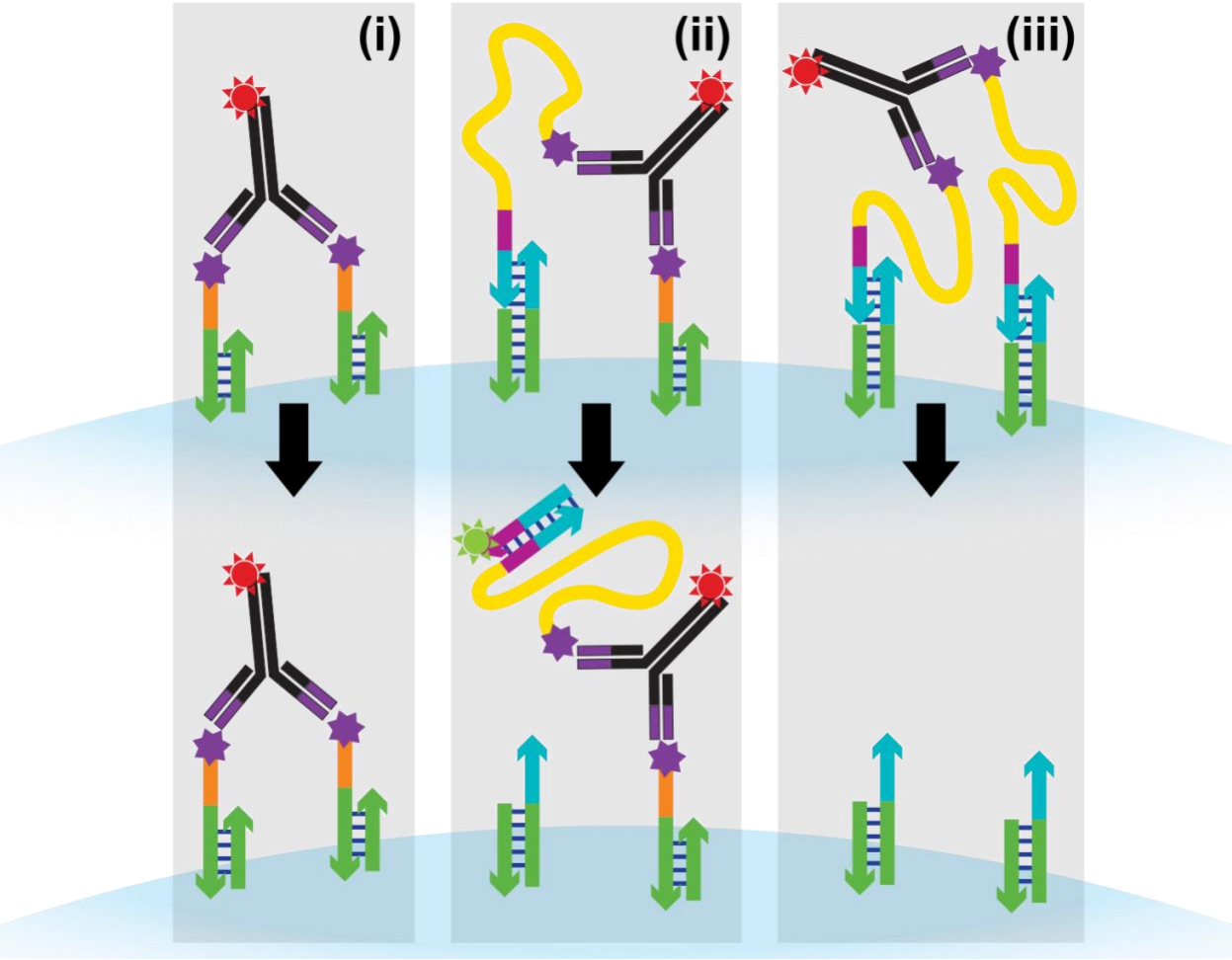

Figure 28: Possible sandwich binding formations for a colocalized bead assay using identical capture and detection affinity binders, before (top) and after (bottom) incubation with the displacement oligo. Note that the antibody is the analyte in this assay. (i) The anti-DIG antibody binds to two surface DIG molecules. After displacement the antibody signal is retained, but the assay signal (DO-Cy5) is not present. (ii) Anti-DIG binds to one surface DIG and one hook DIG molecule. After displacement the antibody signal is retained, and a detectable assay signal is also measured. (iii) Anti-DIG binds to two hook DIG molecules. Both hooks are displaced, releasing the antibody. Neither the antibody signal nor the assay signal is measured.

DIG molecules have been used as labels since the 1990's[194], and have minimal impact on the binding or behaviour of the molecule they are conjugated to[194,195]. Therefore, we expected that the surface DIG duplexes would compete equivalently with the other duplexes for streptavidin

sites on the bead surface. We hypothesized that changing the amount of each duplex in the barcoding mixture would allow us to control the density, and therefore the average separation, of each affinity binder.

Effect of Changing Barcoding Mixture on Reagent Density

To test our hypothesis that the DIG-conjugated oligos would compete equivalently with the other oligos in the barcoding mixture, we fabricated colocalized bead assays using a range of capture oligo/surface DIG ratios. Each set of beads was incubated with a total 90 pmol of DNA, containing a combination of the three surface-bound DNA duplexes shown in Figure 27. For instance, bead set 1 was incubated with 70 pmol of surface DIG duplex, 10 pmol of capture oligo duplex, and 10 pmol of spacer duplex. If the duplexes compete equivalently to bind to the bead surface, then the ratio of capture oligo to surface DIG on the bead should be 1:7. Assuming a Poisson distribution, the average distance between capture oligos will be ~7 nm (see section 3.5.5 for estimation). The barcoding mixtures for the bead sets tested are shown in Table 5.

Table 5: Barcoding mixtures tested in the surface density experiment. The total of the capture oligo (CO), surface DIG, and spacer oligo (SO) duplexes is always 90 pmol. The capture and spacer oligos are hybridized to barcoding oligos (BO), some of which are conjugated to a Cy3 fluorophore. The remaining barcoding oligos are not conjugated to a dye.

Bead set	**BO-Cy3 content [pmol]**	**CO/BO duplex [pmol]**	**Surface DIG/SO duplex [pmol]**	**BO/SO duplex [pmol]**	**Theoretical average CO-CO separation [nm]**
1	0	10	70	10	7.06
2	3	10	40	40	7.06
3	6	30	30	30	4.06
4	9	40	10	40	3.53
5	12	70	10	10	2.67

To differentiate the bead sets, some of the capture and spacer oligos were hybridized to barcoding oligos labeled with a Cy3 fluorophore. The excitation spectrum of Cy3 has substantial overlap with the emission spectrum of AF488, and the two fluorophores may have been close enough together to experience FRET.

We performed two fabrication quality control (QC) experiments to measure the relative amounts of each affinity binder. In the surface DIG QC experiment, represented in Figure 29A, CBA beads that had not had the hook oligo pulled down were incubated with anti-DIG-AF488. Due to the size of an antibody, we considered that steric hindrance might result in underestimation of surface DIG at higher concentrations. In the hook DIG QC experiment, represented in Figure 29B, full CBA beads from the same batch were incubated with a short Cy5-conjugated oligo that was complementary to a portion of the hook oligo. To approximate the background fluorescence of the surface DIG QC beads, we measured the MFI of the hook DIG QC beads in the AF488 channel. To approximate the background fluorescence of the hook DIG QC beads, we measured the MFI of the surface DIG QC beads in the Cy5 channel. Since only one fluorophore was added to each QC experiment, we expected that any signal measured in the opposite channel was due to autofluorescence of the bead and surface components, which were the same in both QC experiments. Previous testing demonstrated minimal non-specific binding of antibodies or DNA strands to blocked beads[196], so we did not include a control for either the anti-DIG antibody or the labelling oligo sticking to beads without surface DIG or DIG hook. We hypothesized that the relative AF488 signal would decrease from bead set 1 to 5 proportionate to the amount of surface DIG in the barcoding mixture. Similarly, the relative Cy5 signal would increase from bead set 1 to 5 proportionate to the amount of capture oligo in the barcoding mixture.

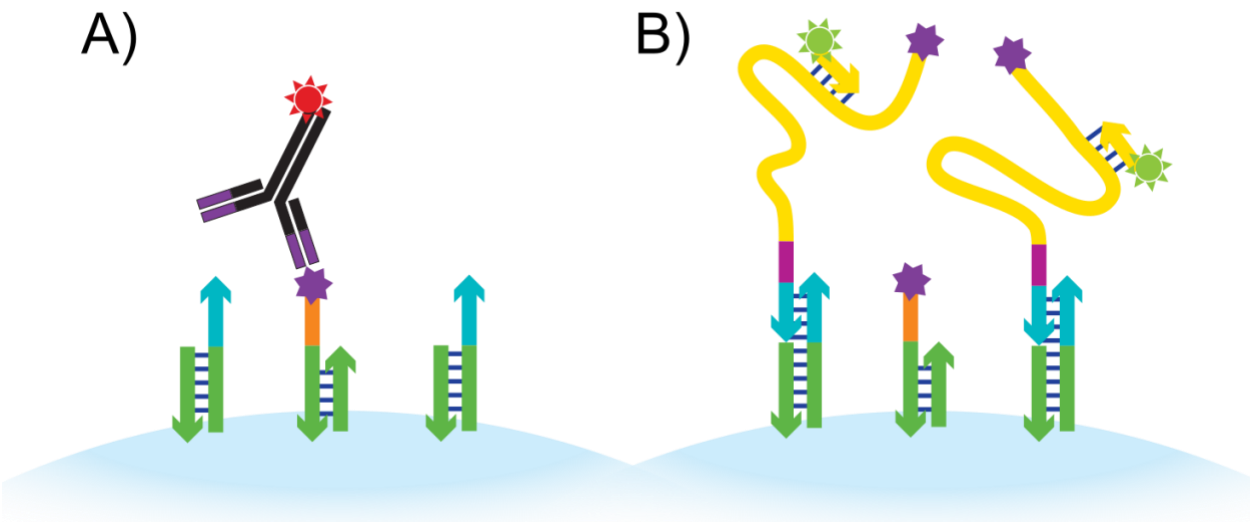

Figure 29: Quality control setups for measure reagent density. A) Surface DIG QC: CBA beads without hook oligos were incubated with anti-DIG-AF488. B) DIG Hook QC: after pulling down hook oligos to the same CBA batch, the beads were incubated with a short Cy5-conjugated oligo that was complementary to a portion

of the hook oligo.

For the surface DIG QC signal and DIG Hook QC background, the populations of the fourth and fifth bead sets (4:1 and 7:1) could not be differentiated by spectral barcode. However, the bead-to-bead CV of the data signal from the combined population was very low. We interpreted this result to mean that the two bead populations had near-identical MFI values. The same value was used for each bead set and is displayed in Figure 30 and Table 6.

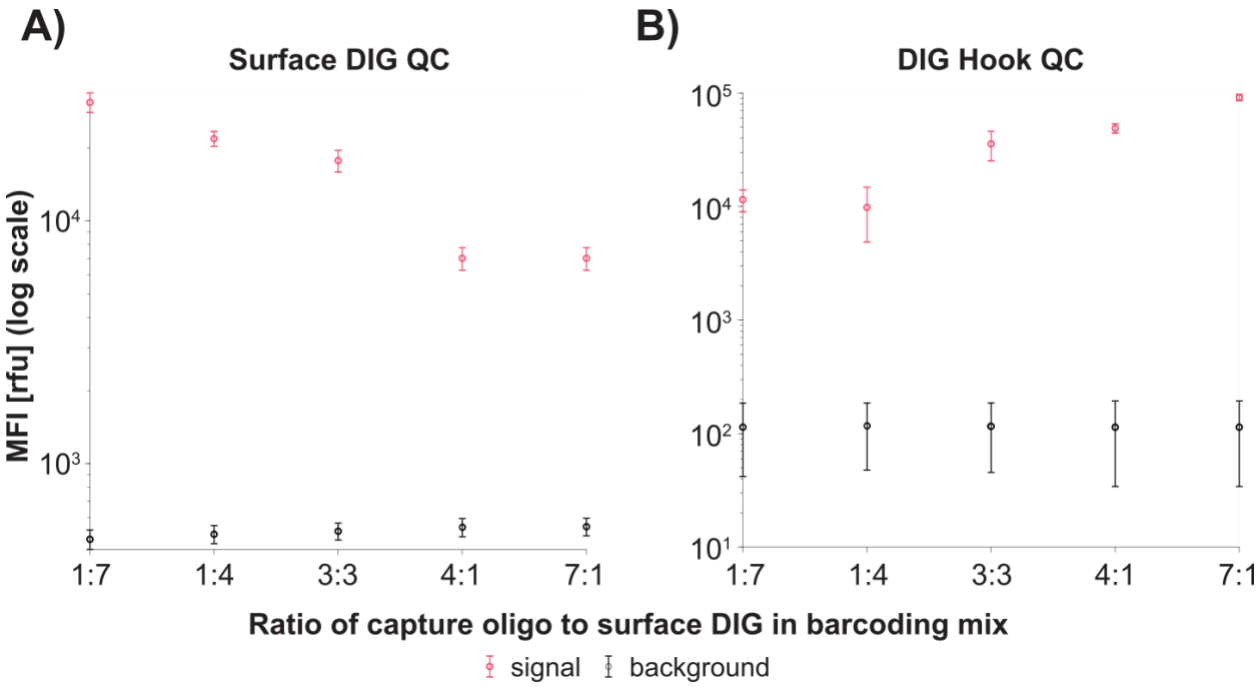

Figure 30: Quality control (QC) results for DIG CBA beads with varied surface densities of DNA strands. The background signal the surface DIG QC experiment was approximated by measuring the DIG hook QC beads in the AF488 channel, and vice versa. For the surface DIG QC signal and DIG Hook QC background, the populations of the bead sets 4 and 5 (4:1 and 7:1) could not be differentiated by barcode. The variation of the data signal from the combined populations was very low. The same value is plotted for both bead sets. A) The surface DIG was detected by anti-DIG-AF488 antibodies. The amount of antibody bound decreases as the portion of surface DIG in the barcoding mixture decreases. The relative fluorescence values are presented in Table 6. B) The DIG hook was detected by short fluorescent oligos complementary to the hook oligo. The amount of HO detected increases as the incubation ratio of CO increases. Error bars represent the standard deviation of the entire bead population for that bead set (500 to 2000 beads)

Table 6: Comparison of relative fluorescence from QC experiments (background subtracted). The population of bead sets 4 and 5 could not be differentiated by barcode when anti-DIG-AF488 was present. The variation of the data signal from the combined populations was very low. The same value is used for both bead sets.

Bead set	**CO portion (out of 9)**	**Cy5 (Hook) signal relative to bead set 1**		**Surface DIG portion (out of 9)**	**AF488 (anti-DIG) signal relative to bead set 4/5**
1	1	1		7	4.66
2	1	0.856		4	3.28
3	3	3.12		3	2.65
4	4	4.28		1	1
5	7	8.03		1	1

The results of the quality control experiments indicated that increasing the portion of surface DIG in the barcoding mixture led to an increase in the amount of surface DIG on the bead (Figure 30A). Meanwhile, increasing the portion of capture oligo led to an increase in the amount of DIG hook present (Figure 30B). The change in relative fluorescence between bead sets is not the same as the change in relative proportions of the components in the barcoding mixture (Table 6). However, this may be the result of FRET or steric hindrance, as discussed previously. The overlap in the spectral barcodes of bead sets 4 and 5 only when anti-DIG-AF488 was present confirms that some FRET occurred.

Based on these results, we concluded that we could control the portion of each strand on the surface by changing its respective portion in the barcoding mixture. Although, we could not determine whether we had accurate control of the surface proportion of each component due to the aforementioned confounding factors. Nonetheless, we concluded that we could change the average reagent separation.

Effect of Changing the Average Reagent Separation on the CBA Binding Curve

We next conducted an experiment to test the effect on the apparent affinity of changing the average distance between the capture and detection affinity binder. Colocalized bead assays using DIG molecules as affinity binders were fabricated as represented in Figure 27. The amount of detection affinity binder (DIG hook) and capture affinity binder (surface DIG) were reduced

to much lower amounts to increase the role of the hook oligo's length and flexibility in binding (Table 7). We tested beads having only surface DIG as a control to determine the effect of colocalization on apparent affinity. We hypothesized that the apparent affinity of the colocalized bead assays would be higher than the single binder assay (surface DIG only), due to bivalent binding with the hook DIG. We also hypothesized that the bead assays with a smaller average distance between the capture and detection affinity binders (surface and hook DIG) would have higher apparent affinity due to the increased number of states permitting binding.

Table 7: Barcoding mixtures used to measure the effect of average reagent separation. The total of the capture oligo (CO), surface DIG, and spacer oligo (SO) duplexes is always 90 pmol. No fluorophore-labeled barcoding oligos were used in this experiment.

Bead set (BC)	**CO/BO duplex [pmol]**	**Surface DIG/SO duplex [pmol]**	**BO/SO duplex [pmol]**	**Theoretical average CO-CO separation [nm]**
3	0	5	85	--
4	5	5	80	9.98
5	10	5	75	7.06

To verify that the CBA beads had been fabricated correctly, we performed two quality control experiments. We incubated full CBA beads with either anti-DIG-AF488 or a short Cy5-labeled oligo complementary to a portion of the hook oligo. Bare beads that had not been incubated with the labeled antibody or oligo were measured as a control. Previous testing demonstrated minimal sticking of antibodies to blocked beads[196], so we did not include a control for this. Unexpectedly, the results of the experiment indicated that the amount of anti-DIG-AF488 bound to bead set 3 was greater than to bead set 4, despite bead set 4 having more total DIG (Figure 31). We hypothesized that the long hook oligo might reduce the number of antibodies reaching the surface. Nonetheless, the results of the QC confirmed that the DIG was available to bind.

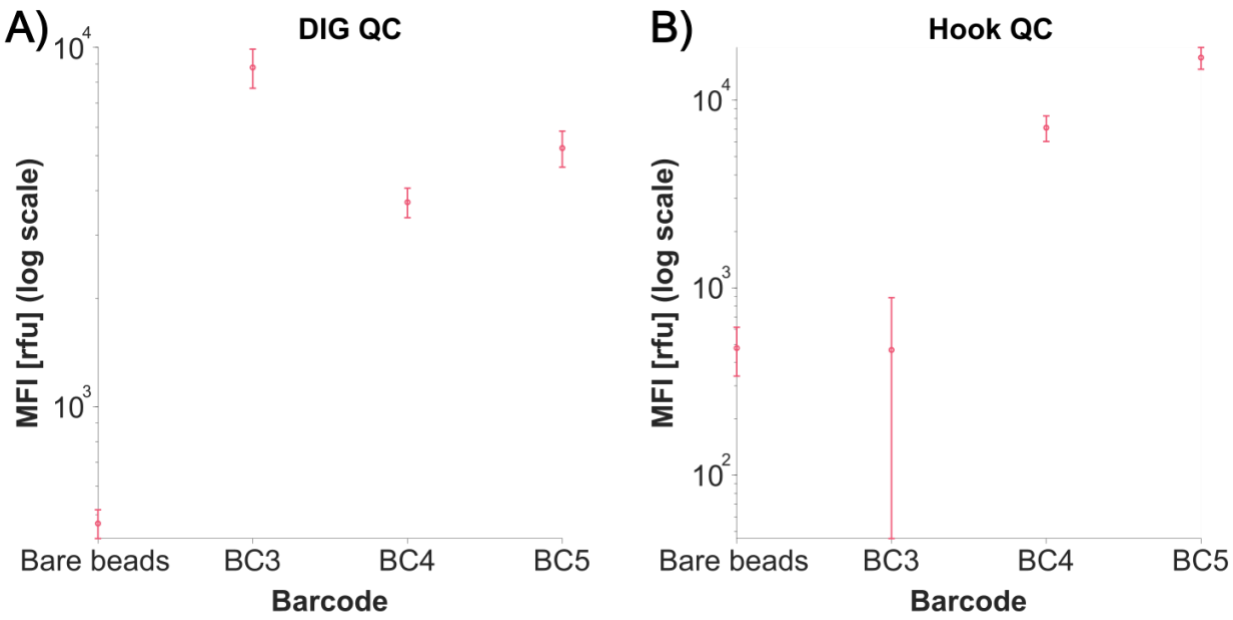

Figure 31: QC results for fully fabricated DIG CBA beads with varied surface densities. A) QC of surface DIG and DIG hook, via simultaneous detection with a labelled anti-DIG antibody. The results indicate that the DIG is available for binding. B) QC of hook oligo, using a short, labeled oligo complementary to a portion of the hook. The results demonstrate that the amount of hook pulled down increases with increasing CO content in the barcoding mixture. The bare bead signal from each channel is provided for qualitative comparison. Error bars represent the standard deviation of the entire bead population for that bead set (1000 to 2500 beads)

The CBA beads were incubated with a serial dilution of anti-DIG-AF488, then incubated with a Cy5-labeled displacement oligo. The results of this experiment indicated that the apparent affinities of the colocalized assays were not significantly different from each other or from the single-binder assay (Figure 32A). The K_D values were 47, 35.9, and 33.2 ng/mL for bead set 3, 4, 5 respectively. Further, the amount of antibody present at the end of the assay decreased with increasing hook surface component, while the signal from the displacer strand did not increase substantially above background (Figure 32B). Since the QC experiment had indicated the DIG molecules were available to bind, we hypothesized that the anti-DIG antibodies bound preferentially to two hook DIGs and were lost after displacement (Figure 28iii). An alternative explanation would be that antibodies that properly formed a hook-surface complex dissociated before measurement. However, based on the single binder assay (bead set 3) the anti-DIG antibody has an affinity in the pico-molar range. Since the off-rate typically correlates with the dissociation constant[197], the rate of dissociation of bound antibody complexes is expected to be

on the order of hours to days[198,199]. Therefore, antibody dissociation is unlikely to have contributed significantly to the observed result.

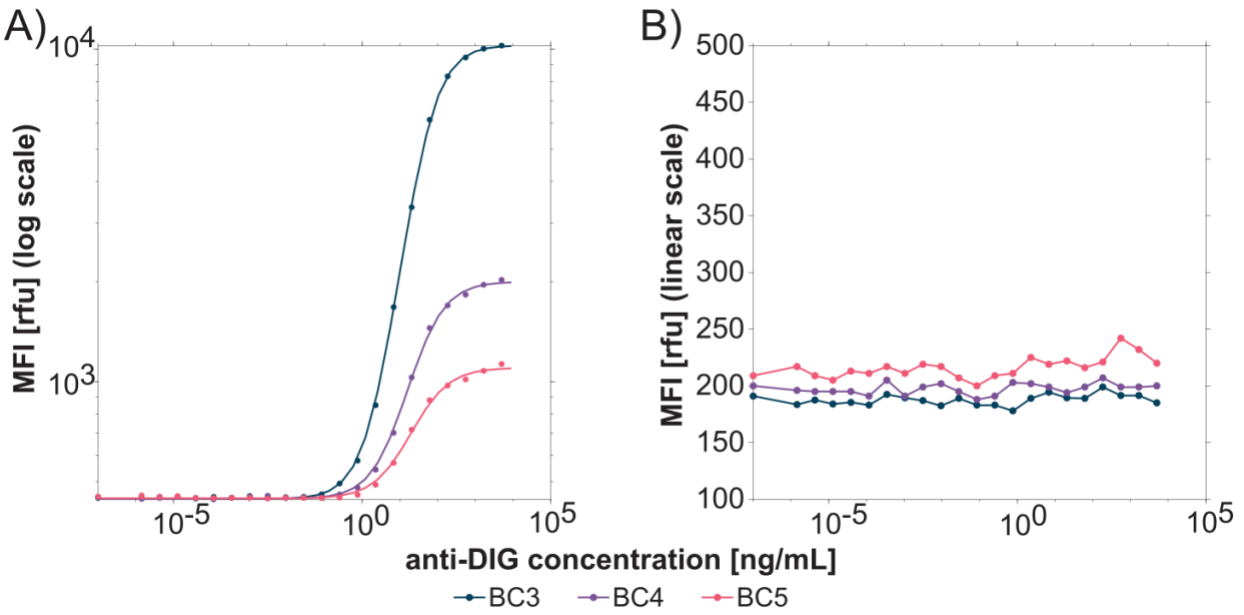

Figure 32: Assay signals measured in the anti-DIG colocalized bead assay, from the A) analyte (anti-DIG), B) displacement oligo. The amounts of capture oligo, surface DIG, and spacer oligo in the barcoding mixture (in pmol) were: 0, 5, 85 (BC3), 5, 5, 80 (BC4), 10, 5, 75 (BC5). BC3 was used as a control for a single DIG assay without colocalization. A) The antibody signals were fitted with a 4PL curve. The K_D values were measured as 47, 35.9, and 33.2 ng/mL for BC3, 4, 5 respectively. The amount of antibody present after displacement decreased with increasing capture oligo. B) The DO signal did not increase significantly above background. No error bars are shown. n=2 for BC3, n=1 for BC4 and BC5

Though our results did not offer insight into the role of average reagent separation on the apparent affinity, they highlighted an important factor influencing sandwich complex formation in a colocalized bead assay – the accessibility of the affinity binders. This factor is especially important when identical affinity binders are used. When non-identical affinity binders are used, once a hook-conjugated detection affinity binder has bound to an analyte, other detection affinity binders are prevented from binding (assuming the molecule has just one of each epitope). This provides an opportunity for the analyte to encounter the microparticle surface and interact with the capture affinity binder. Alternatively, when identical affinity binders are used, the capture and detection affinity binders compete for the same epitopes. If the capture affinity binder is much less accessible, then the formation of capture/detection sandwiches is rare.

4.3 Exploring the Effect of Absolute Reagent Separation on the Apparent Affinity of a CBA

We next sought to investigate the role of the absolute separation between capture and detection affinity binders, while reducing the impact of surface stochasticity. We designed a new colocalized bead assay wherein the capture and detection affinity binder (two DIG molecules) were affixed to a single DNA support (Figure 33). Short flexible linkers allowed the affinity binders to occupy multiple positions. An anti-DIG antibody was used as the analyte. This system more closely resembled the models for colocalized assays found in literature, where binding is intramolecular[153]. We hypothesized that increasing the separation of the DIG molecules beyond the maximum width of an antibody (~15 nm[192]) would decrease the number linker positions that permitted bivalent binding, thus decreasing the apparent affinity.

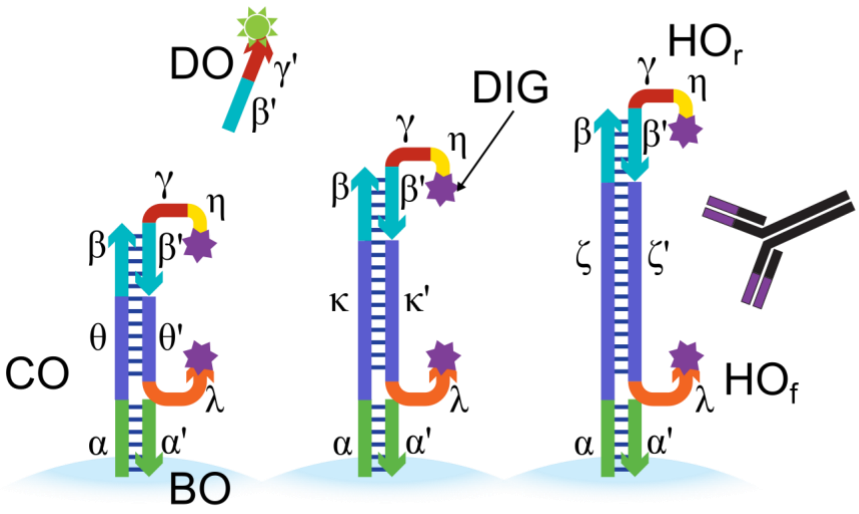

Segment	Length (nt)
α, α'	21
β, β'	21
γ, γ'	9
η	1
λ	10
θ, θ'	20
κ, κ'	30
ζ, ζ'	40

Figure 33: Simplified representation of double-hook digoxigenin CBA, with increasing separation between the DIG molecules. (Left) CO-20, (middle) CO-30, (right) CO-40. The fourth condition tested, CO-50, is omitted for space. The anti-DIG antibody used in this assay was unlabelled. DIG: digoxigenin, CO: capture oligo, BO: barcoding oligo, DO: displacer oligo, HO$_f$: fixed hook oligo, HO$_r$: releasable hook oligo

A DIG molecule was conjugated to each of two hook oligos. One hook included a toehold sequence that was recognized by a fluorescently labelled displacer oligo. The other, fixed hook oligo was designed with an increasing length complementary to the capture oligo, such that the separation between the two DIG molecules was increased. The lengths of the capture oligos were

also increased – the shortest capture oligo, CO20, had 20nt complementary to each of the hooks (Figure 33, left). The next, CO30, had 30nt complementary to the fixed hook oligo and 20nt complementary to the releasable hook (Figure 33, middle), and so on for CO40 (Figure 33, right) and CO50 (not shown). A small amount of capture oligo was used in the barcoding mixture (5 pmol CO, 85 pmol of spacer oligo) to increase the average distance between capture strands (est. 10 nm). This was expected to reduce the incidence of the anti-DIG antibodies binding bivalently to two different capture complexes.

We considered that the nick in the DNA helix between the ends of the hooks (Figure 33, β' and either θ', κ', or ζ') might affect the separation between affinity binders. Based on published literature, we expected that the capture oligo/hook oligo complex would spontaneously shift between linear and bent states but would predominantly exist in a linear form[200–208]. In the linear form, the distance between flexible hook domains was 13.9, 17.3, 20.7, 24.1 nm.

Due to the large number of samples, it took more than 2 hours to complete the cytometry measurements. However, the high affinity anti-DIG antibody would have a slow off-rate, so substantial loss of positive complexes is not expected from the first to last sample measured. Indeed, the data do not demonstrate a decrease in the fluorescence measured in later samples.

No negative control set was measured, as previous testing had shown minimal sticking of antibodies to blocked beads[196]. A positive control was not included due to the large number of samples.

Our results indicated that increasing the absolute distance between affinity binders did not produce a significant shift in the apparent affinity (Figure 34). We measured variations in the hill coefficients and K_D values for the different conditions, though the confidence is low due to the low replicate number (Table 8). There was a substantial increase in the overall fluorescence as the separation increased, but the magnitude of the signal window was not significantly different between the four conditions. We proposed that the longer oligos used to increase the affinity binder separation also provided more opportunity for the fluorescent displacer strand to bind non-specifically. This would increase the non-specific binding rate without having a substantial effect on the relative signal window. Inclusion of an additional negative control set, having a double stranded capture oligo and no hook oligos (segments β, θ, κ, ζ and complements in Figure

33), would be required to confirm this. Moreover, the magnitude of the signal window in this experiment was very low compared to previous assays. Previous colocalized bead assays have shown a fluorescence range of about one order of magnitude. This low maximum fluorescence may be a result of formation of inter-probe complexes, wherein both releasable hooks are displaced.

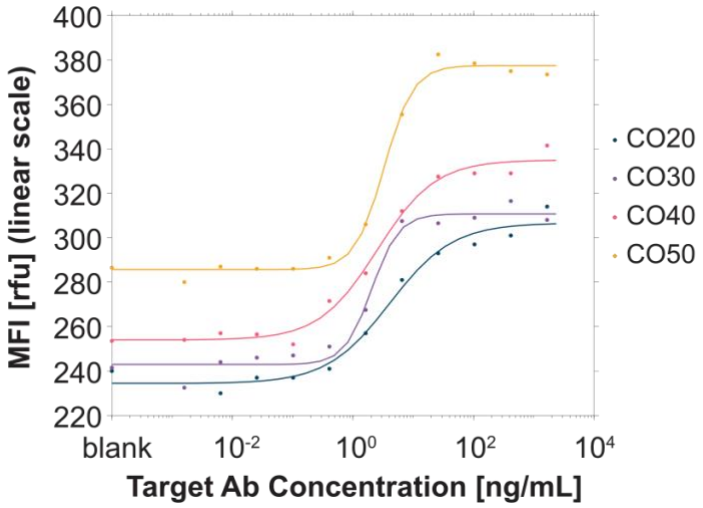

Figure 34: Binding curves for anti-DIG double-hook CBA with increasing separation between affinity binders (20-50 nucleotides complementarity between CO and HOf). The data were fitted with 4PL curves. The K_D values were calculated as 4.09 ng/mL, 2.05 ng/mL, 2.54 ng/mL, and 3.29 ng/mL for CO20, CO30, CO40, and CO50, respectively. Increasing the distance between the affinity binders (DIG molecules) did not significantly alter the dynamic range. Increasing the length led to an increase in background signal, but no change in the magnitude of the signal window. No error bars are shown. n=2

Table 8: Parameters determined from fitting the anti-DIG binding curves with a 4PL equation. 95% confidence intervals are reported

Bead set	**Affinity binder separation [nm]**	**K_D [ng/mL]**	**Hill slope**	**R^2**
CO20	13.9	4.09 [1.09, 7.08]	0.835 [0.373, 1.30]	0.98
CO30	17.3	2.05 [1.18, 2.92]	1.92 [0.362, 3.48]	0.98
CO40	20.7	2.54 [1.26, 3.83]	0.905 [0.538, 1.27]	0.99
CO50	24.1	3.29 [2.47, 4.10]	1.81 [1.22, 2.40]	0.99

Based on our results, we inferred that the absolute separation between affinity binders in a colocalized bead assay has some effect on the apparent affinity. However, there may exist other factors that have greater influence on the apparent affinity.

4.4 Exploring the Effect of Linker Length in Isolation

We next sought to further characterize the role of the linker by minimizing interference due to surface density and stochasticity on the bead. We designed a liquid-phase colocalized assay using a linear DNA probe similar in form to a padlock probe (Figure 35, left). The probe oligo consisted of two binding site regions and a linker region and was conjugated to a quencher at the 5' end and a fluorophore at the 3' end. The linker region consisted predominantly of A and T bases, and measured 15, 25, 35, 43, or 53 nt. The probe was combined with a dilution series of a target strand complementary to both binding sites. When the target strand was bound bivalently by the probe then the quencher and fluorophore were held in proximity (Figure 35, right).

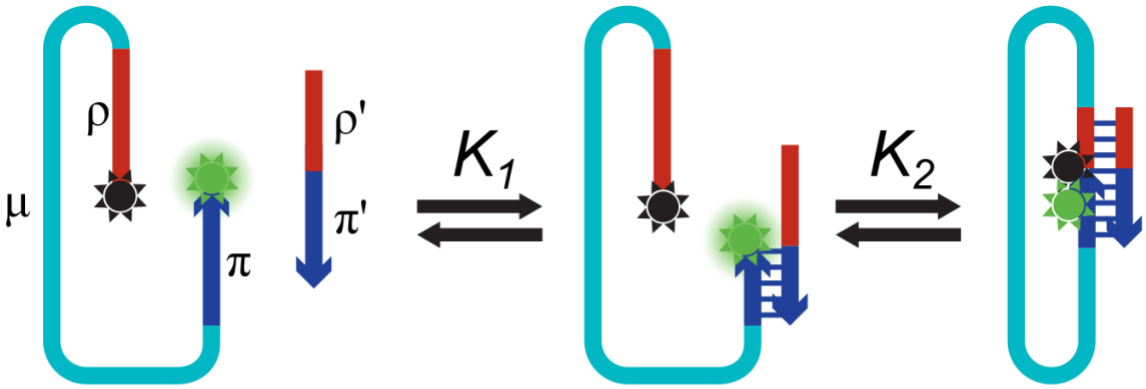

Segment	Length (nt)
μ	15-53
ρ, ρ'	7
π, π'	7

Segment	Sequence (5' to 3')
ρ	TTCTACA
π	ACATCTT

Figure 35: Simple representation of the liquid-phase colocalized probe and target. (left) The probe strand consists of two binding site regions (ρ, π) and a linker region (μ). The strand is conjugated to a quencher at the 5' end (black sun) and a fluorophore at the 3' end (green sun). The target strand is complementary to both binding sites (ρ', π'). The first binding domain hybridizes with the complementary epitope region on the target with an affinity of K_1 (left to middle). This interaction may dissociate, or the second binding domain may interact with its respective epitope region with an affinity of K_2 (middle to right). It is equally probable that

the target would first bind to the blue or red binding domain first. When both binding domains have bound the target, the quencher and fluorophore are held in proximity, resulting in a decrease in the measured fluorescence. Note that the segments π, π', ρ, ρ' are shown shorter after binding to represent the decrease in per-base length between single- and double-stranded DNA.

Monovalent Affinity Measurement

To quantify the apparent affinity enhancement resulting from colocalization, we first sought to determine the monovalent affinity of the binding domains. We measured the hybridization of a strand representing one binding domain with a strand representing half of the target to generate a binding curve (Figure 36). Wells containing only buffer were measured as a positive control (no fluorescence). A negative control, measuring quenching between non-complementary strands, was not included in this experiment. An earlier experiment measuring the monovalent affinity of a longer probe that included the same sequence tested here indicated that quenching did not occur when a non-complementary strand conjugated with a quencher was titrated with a fluorescent probe strand (appendix, section 7.1).

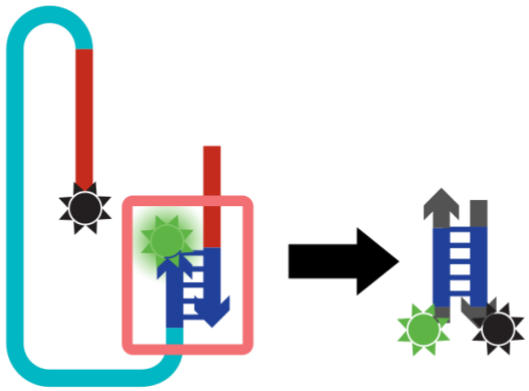

Figure 36: Monovalent affinity probe (fluorophore) and target (quencher) strands, derived from the colocalized probe shown in Figure 35. T bases were added to either end of the sequence to reach the minimum manufacturable length.

The results indicated that the monovalent affinity of the binding domain is approximately 649 or 658 nM (Table 9). Both fitting equations found similar results and achieved good quality of fit (Figure 37, Table 9). The first and last concentrations were excluded from the regression analysis due to the discrepancy with neighbouring points. Inclusion of the first point (blank) resulted in a Hill slope value of -1.3. No cooperativity is expected for monovalent probe/target interactions, so a Hill slope value other than -1 or 1 does not have a physical explanation. We were unable to

find a satisfactory explanation for the discrepancy, though we considered that it may be due to systemic error such as spatial bias[75]. Randomization of the well plate layout was not feasible for human preparation, so all the blank samples were in the left-most column of wells on the plate. Future work should implement a fully automated liquid-handling system, such that samples can be randomized across the plate without risk of human error.

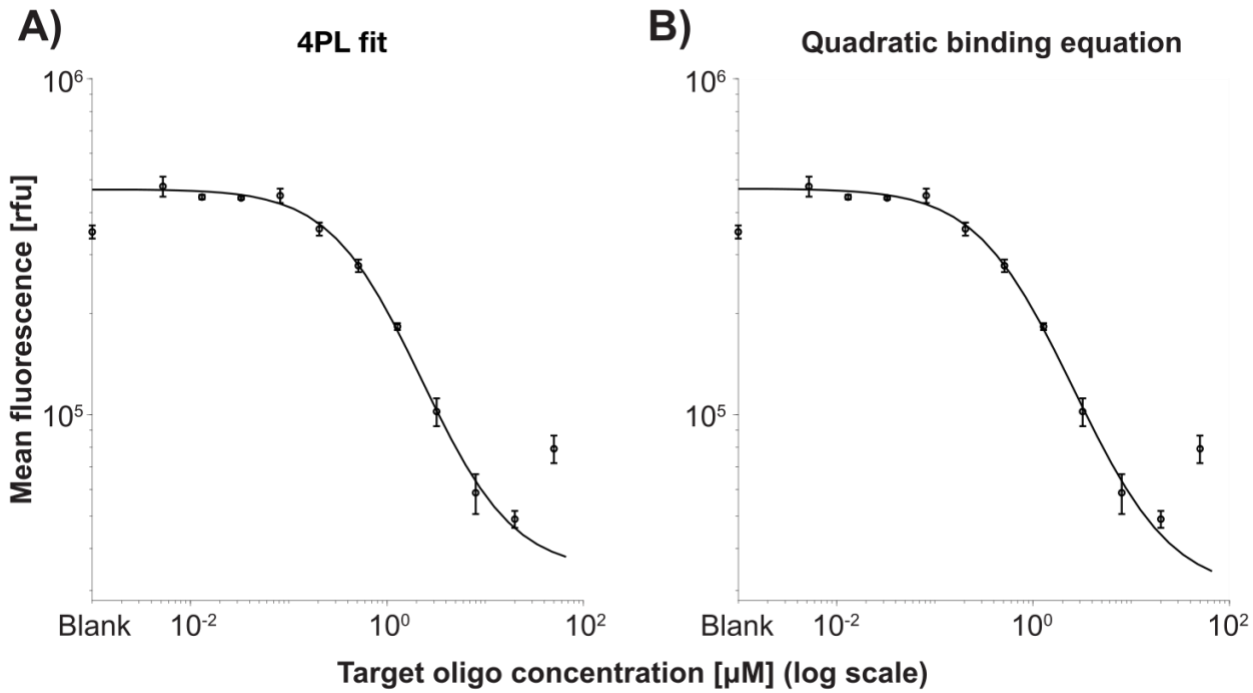

Figure 37: Binding curve data of monovalent probes fitted using A) 4PL equation, B) quadratic binding equation. The first and last concentration were excluded from analysis and are shown for discussion purposes. The K_D values were calculated as 649 nM and 658 nM, respectively. Wells containing only buffer were measured as a positive control (data not shown, mean fluorescence 6045±2800 rfu). Error bars represent one standard deviation. n=4

Table 9: Parameters determined from nonlinear regression analysis of binding curves. Asymmetric 95% confidence intervals are reported.

Fitting equation	**K_D [nM]**	**Hill slope**	**R^2**
Four parameter logistic	649 [552, 769]	-1.06 [-1.24, -0.895]	0.99
Quadratic Binding	658 [559, 774]	N/A	0.99

The last concentration of 50 µM resulted in an increase in fluorescence at high concentrations, characteristic of the hook effect. Neither of the binding curve models used account for the hook effect, so the last point was excluded from analysis. The hook effect indicates that at levels of the

quencher-linked target strand beyond saturation, fewer target/probe complexes are forming. Although the target strands had low affinity for each other ($\Delta G = -0.3$), it is possible that at sufficiently high concentrations the brief interactions between target strands occurred frequently enough to sequester some of the strands. This would result in the probe strands experiencing a lower concentration of available target strands, thus increasing the fluorescence measured. The presence of the hook effect reduces the confidence with which we can determine the target concentration beyond which the probes are saturated. While redesigning the target sequence might reduce the incidence of self-hybridization of the target strand, it would also reduce the on-target affinity (due to the removal of G/C pairs), shifting the binding curve towards higher concentrations. We also considered increasing the reaction temperature or reducing the salt content of the buffer, which would reduce the stability of target self-dimers. However, this would also decrease the stability of the probe/target complex, possibly by the same magnitude. Therefore, we concluded that the calculated monovalent affinity values of 649 or 658 nM might be underestimations.

Effect of Increasing Linker Length on Apparent Affinity

We next explored changing the length of the linker region as a means to modify the apparent affinity of our colocalized probe. We hypothesized that increasing the length of the linker region would increase the number of states permitting bivalent binding and therefore increase the apparent affinity. To test this hypothesis, we generated binding curves for probes with identical binding site regions and linkers of 15, 25, 35, 43, and 53 nucleotides (Figure 35A, segment μ). The binding curves were fitted with a 4PL equation (Figure 38A) and the quadratic binding equation (Figure 38B). Wells containing only buffer were measured as a positive control.

We observed that increasing the linker length decreased the dissociation constant, thereby increasing the apparent affinity (Figure 38C). However, the maximum K_D shift achieved was less than 5-fold and appeared to be reaching an asymptote at a linker length of 53-nt. This result indicated that increasing the length of the linker further would not offer significant improvements. At the same time, the fluorescence change from maximum to minimum was substantially decreased for the 15-nt linker. The confidence intervals of the determined K_D for this probe were either undefined or spanned more than one order of magnitude (Table 10). This result indicated that the 15-nt linker probe would have very little utility in an actual bioassay, as

an unknown concentration could not be determined with any accuracy. This phenomenon may be due to the reduced separation between the quencher and fluorophore in the "open" state, leading to significant quenching in the absence of a target. Meanwhile, the increased fluorescence at higher concentrations may indicate that the linker is too short to accommodate binding, hindering formation of the "closed" state.

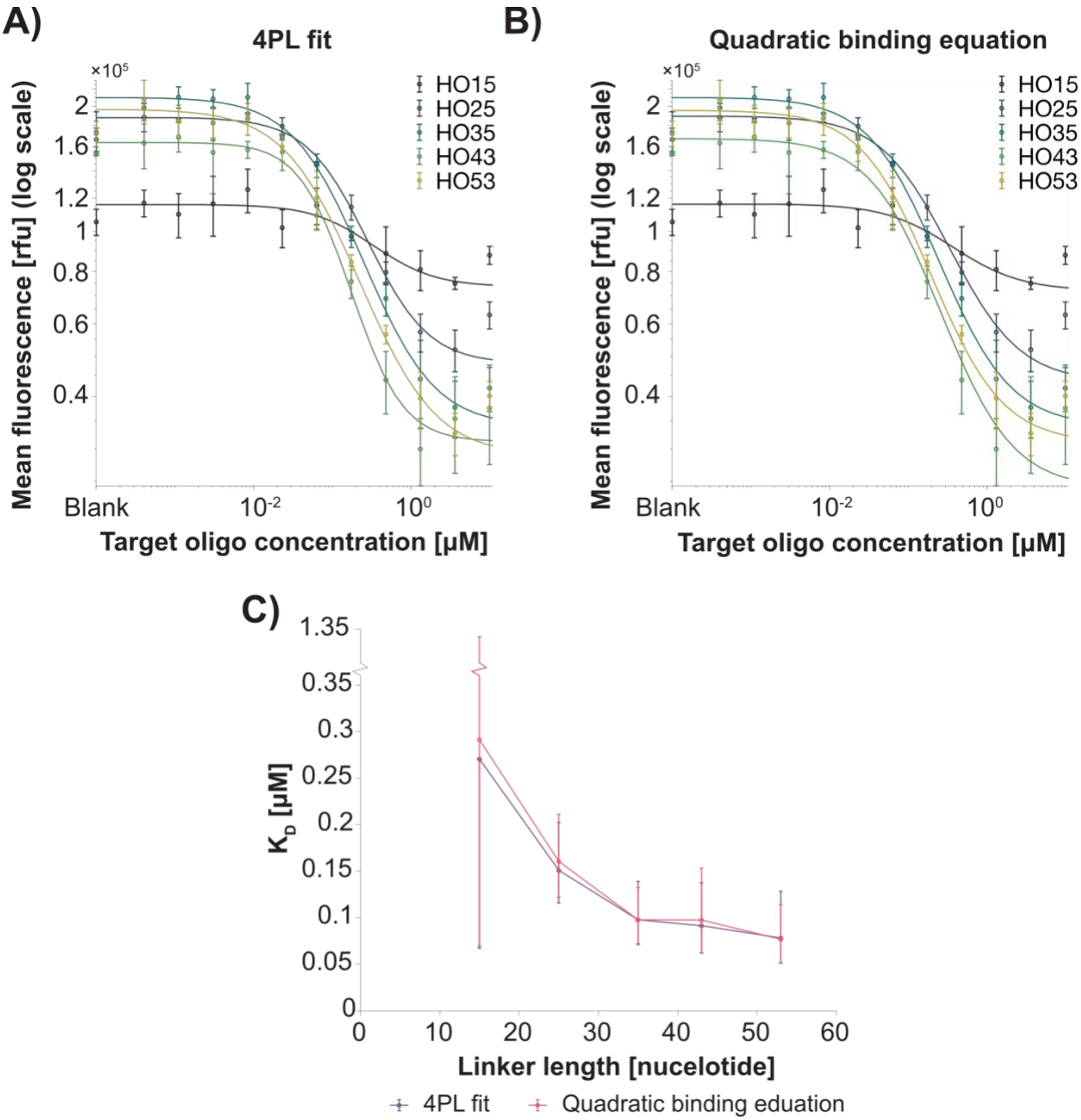

Figure 38: Binding curves of probes with increasing linker length (15-53 nt) fitted with the A) 4PL equation, B) quadratic binding equation. The signal window for the 15 nt linker is too narrow to be practically used for calibration. Wells containing

only buffer were measured as a positive control (data not shown, mean fluorescence 6398±1700 rfu). Error bars represent one standard deviation. n=3. C) Dissociation constants for different linker lengths. The total change in apparent affinity achieved is about 3.5-fold. However, the confidence interval for the 15 nt linker is so large, the calculated K_D value is meaningless. The change in K_D values appears to be reaching a plateau for the 53 nt linker, suggesting further increasing the linker length would not offer significant apparent affinity shift. Error bars represent the asymmetric 95% confidence intervals. Where error bars are not shown, the confidence interval could not be determined.

Table 10: Parameters determined from nonlinear regression analysis of binding curves. Asymmetric 95% confidence intervals are reported. und = undefined.

Probe linker length [nt]	**Fitting equation**	**K_D [nM]**	**Hill slope**	**R^2**
15	Four PL	271 [67.2, und]	-1.11 [und, 0.103]	0.64
	Quadratic Binding	291 [69.5, 1340]	N/A	0.64
25	Four PL	151 [116, 202]	-1.16 [-1.49, -0.897]	0.98
	Quadratic Binding	160 [122, 211]	N/A	0.98
35	Four PL	97.6 [71.1, 139]	-1.02 [-1.32, -0.776]	0.98
	Quadratic Binding	97.6 [72.0, 132]	N/A	0.98
43	Four PL	91.2 [62.0, 137]	-1.38 [-2.14, -0.896]	0.94
	Quadratic Binding	97.5 [61.7, 153]	N/A	0.94
53	Four PL	78.1 [51.1, 128]	-0.961 [-1.41, -0.625]	0.96
	Quadratic Binding	76.7 [51.4, 114]	N/A	0.96

As in the assay to determine the monovalent affinity, we observed a hook effect at higher target concentrations. This may be due to the same cause as proposed for the monovalent affinity experiment. Alternatively, it may be due to the increased incidence of target/probe/target triplexes. As the concentration of target strands increases, there is an increased probability that a binding site will bind to a free target before binding to a target bound by the colocalized site on the same probe. This probability is expected to increase as the linker length increases, until the two binding sites are effectively independent of each other. While increasing the probe affinity would lower the saturating target concentration, thereby decreasing the magnitude of the hook effect, we have shown that this would require decreasing the probe concentration to obtain accurate estimations of K_D. Lowering the probe concentration would put the fluorescence values

below the plate reader's limit of detection, so we kept the same target sequence and excluded the last point from our binding curve analysis.

Effect of Increasing Binding Site Separation on Sensitivity to Changes in Linker Length

Based on published literature, we hypothesized that increasing the separation between the binding sites in the "closed" state would make the probe's K_D, and by extension its dynamic range, more sensitive to changes in linker length. The binding site separation is defined as the distance between the ends of the linker that permits bivalent binding[151]. Since the length of DNA changes upon hybridization, due to the adoption of the helix structure, we defined the binding site separation as being equal to the length of the target strand when it is monovalently bound. For the unmodified target strand, with seven base pairs and seven single-stranded bases, we estimated the separation to be approximately 7 nm. We fabricated new target strands having spacer nucleotides between the two epitope sequences. The addition of each spacer nucleotide would theoretically increase the separation by ~0.7 nm. However, since ssDNA is flexible, we considered that the effective binding site separation may be less. Wells containing only buffer were measured as a positive control.

Results for the unmodified target strand and a target with a two-nucleotide spacer, measured in the same assay, are shown in Figure 39. For simplicity, only the 4PL fitted data is shown; the quadratic binding equation fitted data can be found in the appendix (section 7.1).

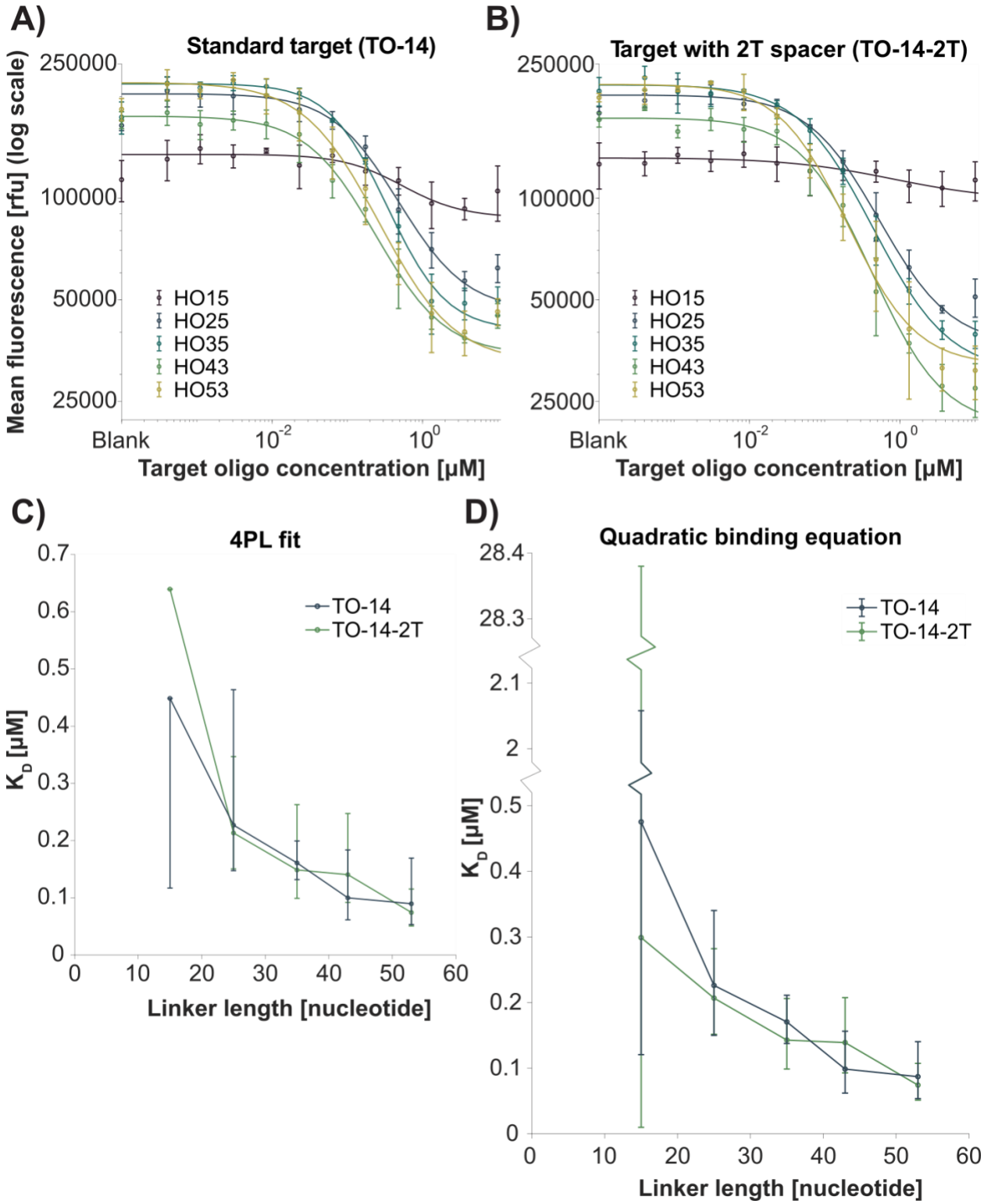

Figure 39: Binding curves of probes with increasing linker length (15-53 nt), fitted with a 4PL equation. A) unmodified target strand (TO-14), B) target strand with 2 nt spacer (TO-14-2T). For both targets, the signal window for the 15 nt linker is too narrow to be useful as a calibration curve. The target with 2 nt spacer has a larger signal window for all probes except HO15. Wells containing only buffer were

measured as a positive control (data not shown, mean fluorescence 6621±1600 rfu). Error bars represent one standard deviation. n=3. (C and D) Change of dissociation constants with increasing linker length, for two different target lengths, fitted with C) 4PL equation or D) quadratic binding equation. The total change in apparent affinity is about 5-fold, and appears to be reaching a plateau for the 53 nt linker. However, the confidence intervals for the 15 nt linker are either uncalculable or very large, such that the calculated K_D value is meaningless. Error bars represent the asymmetric 95% confidence interval. Where error bars are not shown, the confidence interval could not be determined.

Our results indicated that there was no significant change in the apparent affinity's sensitivity to linker length when the binding site separation was increased by 1.3 nm (Figure 39, C and D, Table 11). However, the change in binding site separation may not have been enough to produce an observable change in the dynamics. In particular, the flexibility of the DNA target may have masked the effects. Future work will test larger spacer lengths and rigid spacers to determine if a more substantial change will influence the apparent affinity's sensitivity to entropic modulation.

Table 11: Parameters determined from nonlinear regression analysis of the binding curves with a four-parameter logistic model for the unmodified target strand (TO-14) and the target strand with 2-nt spacer (TO-14-2T). 95% confidence intervals are reported. und=undefined

Probe linker length [nt]	**Target strand**	**K_D [µM]**	**Hill slope**	**R^2**
15	TO-14	0.429 [0.117, und]	-1.08 [-3.80, 0.143]	0.67
	TO-14-2T	0.639 [und, und]	-0.604 [und, 0.905]	0.4
25	TO-14	0.227 [0.147, 0.464]	-1.02 [-1.55, -0.625]	0.96
	TO-14-2T	0.213 [0.151, 0.347]	-0.961 [-1.30, -0.697]	0.97
35	TO-14	0.161 [0.132, 0.199]	-1.16 [-1.41, -0.958]	0.99
	TO-14-2T	0.149 [0.0990, 0.263]	-0.926 [-1.33, -0.613]	0.97
43	TO-14	0.100 [0.0615, 0.184]	-0.986 [-1.49, -0.616]	0.95
	TO-14-2T	0.140 [0.0919, 0.247]	-0.983 [-1.46, -0.636]	0.96
53	TO-14	0.0896 [0.0532, 0.169]	-0.928 [-1.39, -0.585]	0.95
	TO-14-2T	0.0743 [0.0506, 0.115]	-1.02 [-1.43, -0.725]	0.97

4.5 Comparing Models for Simple Colocalized Assays & Extension to a Model for the Apparent Affinity of a CBA

Finally, we sought to compare our liquid-phase colocalized assays to published models of the conformational entropy of intrinsically disordered linkers. Our goal was to validate our findings that the apparent affinity of the liquid-phase assay we tested is only somewhat sensitive to linker modification. If the models adequately represented our system, then we could use them to estimate the changes needed to make the system more sensitive to linker length. Otherwise, if the models did not represent our system, they could offer insight into the parameters necessary for a more appropriate model.

Since the liquid-phase colocalized assay is a simplified representation of the colocalized bead assay, we sought to build upon the published models of entropic linkers to propose a model for the apparent affinity of a colocalized bead assay.

The apparent affinity of a colocalized assay is defined as

$$K_{D,apparent} = \frac{K_{D,1} \times K_{D,2}}{C_{eff}} \tag{16}$$

Where $K_{D,1}$ and $K_{D,2}$ are the monovalent affinities of the binding domains. C_{eff} can be understood as the effective concentration of the second binding domain once the first has bound. The equation for C_{eff} is derived from a statistical mechanical model of the flexible linker.

Wormlike Chain Model

The effective concentration produced by a wormlike chain is derived from the following probability density function[151]:

$$p(r) = \left(\frac{3}{4\pi l_p l_c}\right)^{\frac{3}{2}} \exp\left(-\frac{3r^2}{4l_p l_c}\right)\left(1 - \frac{5l_p}{4l_c} + \frac{2r^2}{{l_c}^2} - \frac{33r^4}{80l_p{l_c}^3} - \frac{79{l_p}^2}{160{l_c}^2} - \frac{329r^2 l_p}{120{l_c}^3} + \frac{6799r^4}{1600{l_c}^4} - \frac{3441r^6}{2800l_p{l_c}^5} + \frac{1089r^8}{12800{l_p}^2{l_c}^6}\right) \tag{17}$$

$$C_{eff} = p(r = d_0) \tag{18}$$

Where l_p and l_c are the persistence length and contour length of the chain, respectively, and r is the end-to-end vector of the linker. The effective concentration is then the probability that $r=d_0$, where d_0 is the separation between the binding domains that permits bivalent binding. We used the above function to calculate the theoretical apparent affinity for our measured monovalent affinity, using the physical parameters of single-stranded DNA (l_p=1.5 nm[160–163]) and a range of linker lengths (Figure 40).

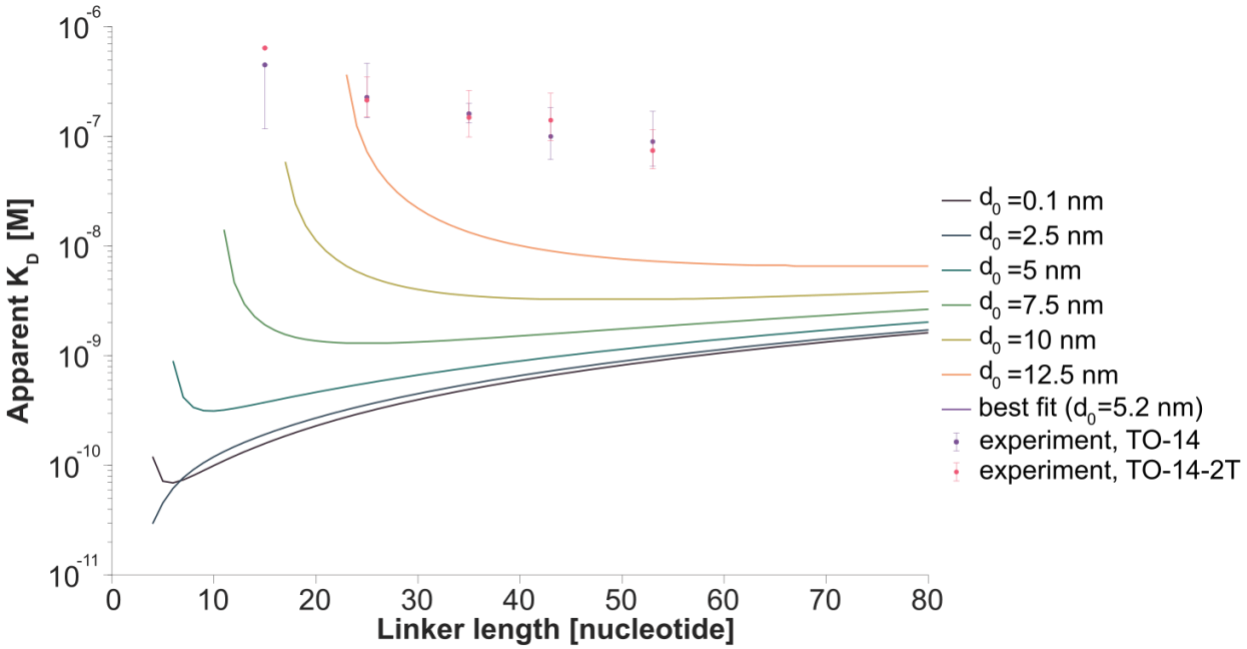

Figure 40: Dissociation constant vs. linker length curves generated using the wormlike chain model, with a monovalent affinity of 650 nM, and physical parameters for single-stranded DNA (l_p=1.5 nm). The curves were truncated below linker values that produced a negative K_D, which does not have physical meaning. Experimental values are K_D values measured in section 4.4, based on fitting with a 4PL equation. The experimental affinities are significantly lower than those predicted by the model for any d_0 value. d_0: separation between the binding domains that permits bivalent binding, TO-14: unmodified target strand, TO-14-2T: target strand with 2-nt spacer

Our measured apparent affinity values were significantly lower (higher K_D value) than those predicted by the wormlike chain model (Figure 40). The model's creator reported that it was in good agreement with published measurements of the apparent affinity of bivalent affinity binders[151]. Subsequent studies using peptide linkers found the model described their systems[209,210] However, some studies that tested bivalent thrombin aptamers, using ethylene glycol or nucleic acid linkers, found that the wormlike chain model over-predicted the affinity

enhancement[154,211,212]. The wormlike chain model may not be appropriate for linkers with longer persistence lengths.

Freely jointed Chain Model

The effective concentration produced by a freely-jointed chain, or random coil, is commonly expressed as follows[132,152]:

$$C_{eff}(d) = \frac{p}{N_A\left(L\sqrt{N}\right)^3}\left(\frac{3}{2\pi}\right)^{\frac{3}{2}} e^{-\frac{3d^2}{2\left(L\sqrt{N}\right)^2}} \quad (19)$$

Where L is the length of each chain element, N is the number of links in the chain, and d is the separation between the binding sites that permits bivalent binding. p is a correction factor that accounts for volume exclusion[132]. The model above was originally conceived for a bivalent ligand binding to a bivalent receptor. The linker cannot occupy the volume of the receptor, so its search space is reduced, and its effective concentration is increased. Gargano et al. assumed that the receptor was sufficiently large to reduce the volume to a hemisphere, and thus proposed a value of p=2 [159]. This factor should not be lower than unity, which represents a full sphere.

We used the above function to calculate the theoretical apparent affinity for our measured monovalent affinity, using the physical parameters of single-stranded DNA (L=0.67 nm[160–162]) and a range of linker lengths (Figure 41).

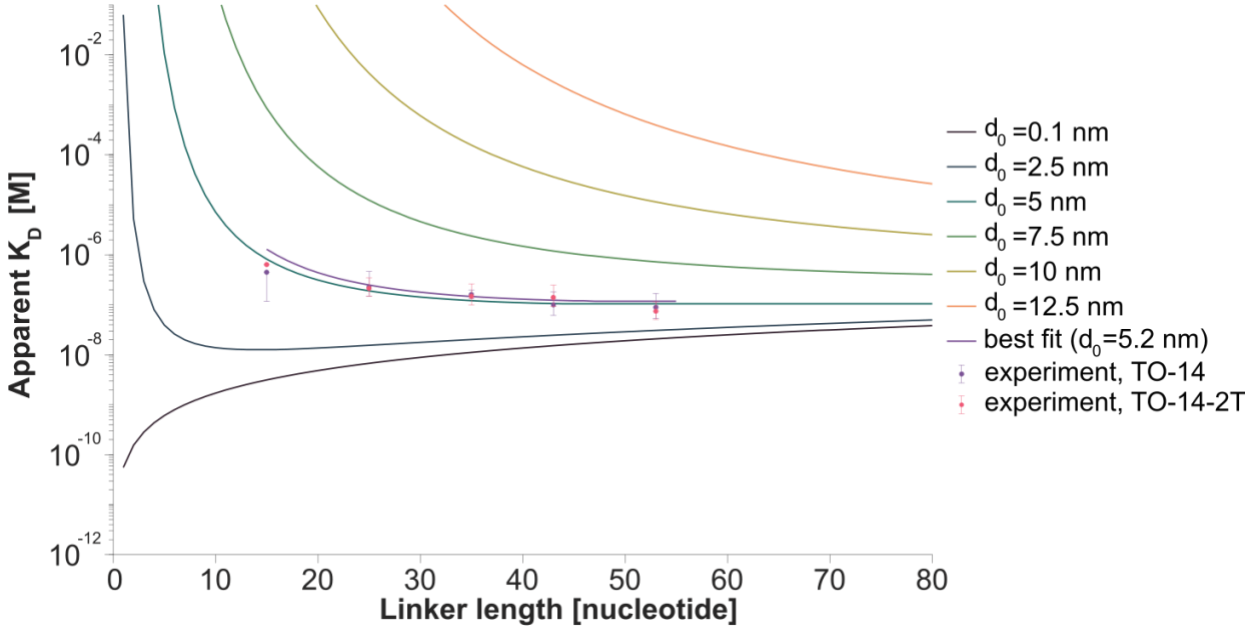

Figure 41: Dissociation constant vs. linker length curves, generated using the freely jointed chain model, a monovalent affinity of 650 nM, physical parameters for single-stranded DNA (L=0.67 nm), and a volume exclusion factor of p=0.0043. The curves were truncated below linker values that produced K_D greater than 0.1 M. Experimental values are K_D values measured in section 4.4, based on fitting with a 4PL equation. The model was found to have good agreement with the experimental data for a d_0 value of 5.2 nm, using least-square regression. The shortest linker was excluded from the analysis due to its large or undefined confidence interval. d_0: separation between the binding domains that permits bivalent binding, TO-14: unmodified target strand, TO-14-2T: target strand with 2 nt spacer

The model is in good agreement with our data for a binding site separation of 5.2 nm (Figure 41). We had previously estimated that our d_0 value was approximately 7 nm, but since our target is flexible while it is unbound, 5 nm is a reasonable result. According to the model, continuing to increase the linker length will not result in a further reduction of K_D. We found that for our system, when the linker length is very short (15 nt, 10 nm), the probe is unable to accommodate binding (see section 4.4). We assume that the model must have a limit of applicability where the linker becomes too short to bind bivalently, and inter-probe binding dominates ($K_{D,model} > K_{D,monovalent}$). More experiments are needed for us to evaluate this limit.

This result provides an important guideline for designing colocalized assays: the apparent affinity of an assay with a binding site separation of ~5 nm cannot be shifted more than five-fold using entropic methods. This substantially limits the dynamic range expansion possible. If an

adjustable dynamic range is desired, affinity binders should be chosen that bind to epitopes very close together – ideally less than 1 nm. More research is required to determine whether larger binding site separations (> 10 nm) would also permit dynamic range expansion; this will depend on the limit of applicability mentioned previously.

An important caveat of this result is that the volume exclusion factor we found to provide the best fit to the data, p=0.0043, is much lower than the minimum value of one defined by the model's authors[159]. This parameter has been similarly misapplied by others: Krishnamurthy et al. calculated p=0.12 ± 0.009[152] while Mariottini et al. found a value of p=0.016 ± 0.009[132]. This indicates that p is correcting for unknown factors which result in a lower apparent affinity than predicted, instead of the physical parameter it was intended to represent. For instance, Krishnamurthy and colleagues proposed that steric hindrance might inhibit the linker from accessing the narrow binding cleft in their system[152]. In the case of a nucleic acid linker, the negatively charged backbone may cause it to preferentially adopt less-compact forms[213], reducing the probability that the unbound domain occupies the space close to its binding site. Further research is needed to determine a better definition of p.

Alternate Models of Intrinsically Disordered Linkers

Self-avoiding wormlike chain models have been shown to better describe double-stranded DNA loop-formation than random chains[214], and may also be appropriate for single-stranded DNA linkers[213]. Self-avoiding models of entropic linkers have been explored through polymer physics. In this paradigm, the effective concentration produced by the linker varies with linker length according to a power law[149,150].

$$C_{eff} = p \times N^{-3v} \tag{20}$$

Where N is the number of elements in the linker and v is a scaling factor determined by the linker expansion. v varies from 0.33 for a globular molecule to 1 for a rigid rod. Increasing the inherent charge of the linker causes it to self-repulse and preferentially adopt elongated forms, which decreases the effective concentration[149]. However, the coefficient p has not been associated with a physical meaning and was observed to vary by more than an order of magnitude when the length or composition of the linker was modified[149]. A similar power law has been derived for the radius of gyration of a polymer, wherein the coefficient is defined by the self-avoiding chain

theory. In this case, the coefficient is dependent on the persistence length and segment length of the linker[215]. The coefficient for the effective concentration power law is likely defined by the same physical parameters, though the equation cannot be assumed to be the same. However, the derivation of new models for entropic linkers is beyond the scope of this thesis.

Extension to Colocalized Bead Assays

Based on the existing models for simple colocalized assays, the parameters of a model for the apparent affinity of a colocalized bead assay should include the affinity of the affinity binders used, the separation between binding sites, and the length and flexibility of the linker. However, based on our research, these are not the sole determining factors, and possibly not the most important factors. Therefore, the model should also consider the affinity binder size and flexibility, and the density and stochasticity of reagents on the surface.

5. Conclusion

5.1 Summary

We presented an exploration of the parameters that make the dynamic range of a sandwich assay with pre-assembled, linked affinity binders sensitive to entropic modulation. For colocalized bead assays we determined that (i) modifying the length and stiffness of the linker and (ii) altering the density and distribution of reagents on the surface had no measurable effect on the dynamic range of our representative system. However, for liquid-phase colocalized assays we found that increasing the length of the linker from 15 to 53 nucleotides produced a five-fold decrease in the apparent affinity. That the apparent affinity could be modified in the absence of the bead confirms that the linker has a role in determining the affinity of colocalized assays. However, in the case of the CBA, even making the linker entirely rigid double-stranded DNA— thereby also decreasing its length by 50%— was insufficient to alter the apparent affinity. Hence for the CBA, and within the range of linker length and rigidity we explored, the flexibility of the affinity binders, and their density and distribution, masked possible effects on the apparent affinity. These results suggest that for practical applications, changing linker length and rigidity is not a useful strategy for modifying the dynamic range of a CBA.

For liquid-phase colocalized assays, the magnitude of the apparent affinity modification resulting from changes in linker length is dependent on the distance between the binding sites on the target. We determined that for DNA probes with a binding site separation of approximately 5 nm, the apparent affinity can be modified by at most five-fold by increasing the linker length from 15 to 53 nucleotides. Increasing the linker beyond this length is unlikely to provide significant affinity change. Based on other results in literature, using affinity binder pairs that bind to epitopes in proximity (~1 nm) should allow the apparent affinity to be modified by more than ten-fold. Further, in our system we determined that when the linker length is reduced to 15 nucleotides (~10 nm), the signal window narrows to less than a two-fold fluorescence change from blank to saturation, such that the binding curve is not practically usable. The decreased change in fluorescence is likely due in part to reduced separation between the quencher and fluorophore in the “open” state, leading to quenching in the absence of a target. However, this phenomenon of inherent quenching cannot entirely explain the decreased signal window. The

narrow signal window may also indicate that the linker becomes too short to accommodate bivalent binding without strain. We had expected that there would be a lower limit to apparent affinity modification where the apparent affinity is equal to the monovalent affinity of a binding domain. In this case a target strand would be more likely to be bound by the binding domains of two different probes than by the binding domains of the same probe. However, we had not expected that this would lead to narrowing of the signal window.

Further, we observed that models currently used to predict the apparent affinity enhancement of colocalized assays do not conform to our results or other published examples. The wormlike chain model has been validated for peptide linkers but may not be appropriate for linkers with long persistence lengths like single-stranded DNA. Meanwhile the freely jointed chain model has limited utility, with one physical parameter being used as a correction factor to achieve agreement with data. Although this model can be made to fit experimental data, it cannot be used to make predictions of how a change will affect an existing system. Some authors have found that ssDNA is better represented by the self-avoiding chain model. We propose that this more complex model should be explored to describe apparent affinity enhancement.

While modelling of the linker may be adequate for a simple colocalized assay, a model for a colocalized bead assay must account for multiple configurations that permit binding. The factors of the proposed model should include the affinity binder size and flexibility, and the density and distribution (e.g., stochastic, deterministic, phase separated) of reagents on the surface.

5.2 Future Work

Exploring Parameters to Make Colocalized Bead Assays Sensitive to Entropic Modulation

To further investigate entropic modulation of the dynamic range of colocalized bead assays, future work will include (i) designing a new bead assay with deterministic reagent positioning and (ii) selecting affinity binders that bind to epitopes within close proximity (~1 nm) on the target. To reduce stochasticity, a nano-patterning technique should be implemented, such as covering the bead surface with nanoscale tetrahedrons or a self-assembling DNA mesh. Alternatively, a flat substrate could be used, allowing nano-patterning using lithography techniques. By precisely controlling the points of functionalization, the absolute distance between the surface affinity binder and the hook affinity binder could be adjusted. Therefore, a

change to the hook length or flexibility would affect all complexes uniformly. Smaller affinity binders, such as aptamers or nanobodies, could be used to reduce the uncertainty stemming from the large size and flexibility of antibodies. However, the selected affinity binder pair should recognize non-identical epitopes in proximity to provide the best opportunity for a measurable dynamic range shift.

Further Characterization of the Effect of Linker Length and Flexibility in the Liquid-phase

In this work, we demonstrated that liquid-phase colocalized assays with binding site separations of approximately 5 nm are relatively insensitive to linker length. Systems with much smaller binding site separations have previously been characterized, though to date very few assays with binding site separations greater than 5 nm have been investigated. We attempted to characterize larger binding site separations for liquid-phase colocalized assays, though the inherent flexibility of the DNA strands used as affinity binders and targets limited the range of conditions we could confidently assess. To investigate the role of binding site separation, a more rigid system should be designed. We suggest a DNA tetrahedron with a long, single-stranded linker extending from one vertex and a short binding site sequence attached to another. This system is equivalent to a colocalized probe that has already bound to its target with one binding domain. The proposed assay could be used to determine whether colocalized assays become sensitive to entropic modulations beyond a binding site separation of 5 nm.

We determined that at a linker length of 15 nucleotides (~10 nm), the signal window of our assay was significantly diminished to less than two-fold. Though this may be due in part to reduced separation between the quencher and fluorophore in the "open" state, leading to inherent quenching, we expect it also indicates that the linker is too short to accommodate bivalent binding without strain. This would make bivalent binding unfavourable, leading to the increase in the minimum fluorescence that we observed. The narrowing of the signal window defines a practical limit for apparent affinity adjustment. Characterization of this limit would require further testing using an alternate signal transduction method that is not affected by inherent quenching. The simultaneous addition of a ligase and an exonuclease followed by rolling circle amplification, as in the proximity ligation assay reviewed in section 2.2.6, could allow sensitive quantification of the characteristics of colocalized assays with short linker lengths.

6. Abbreviations

4PL: Four parameter logistic

a.u.: arbitrary units

Ab: Antibody

AF: Alexa Fluor™

AFM: Atomic force microscopy

BSA: Bovine serum albumin

CBA: Colocalized bead assay

CLAMP: Colocalization-by-linkage assay on microparticles

Cy: Cyanine

DIG: Digoxigenin

DNA: Deoxyribonucleic acid

ELISA: Enzyme-linked immunosorbent assay

FRET: Fluorescence resonance energy transfer

HPLC: High performance liquid chromatography

IgG: Immunoglobin G

LOD: Limit of detection

LOQ: Limit of quantification

MFI: Median fluorescence intensity

PAGE: Polyacrylamide gel electrophoresis

PBS: Phosphate-buffered saline

PCR: Polymerase chain reaction

QC: Quality control

RCA: Rolling circle amplification

rfu: Raw fluorescence units

RNA: Ribonucleic acid

RT: Room temperature

SELEX: Systematic Evolution of Ligands by EXponential enrichment

SIP: Sample injection port

7. Appendix

7.1 Supplementary Figures

7.1.1 Monovalent Affinity Measurement

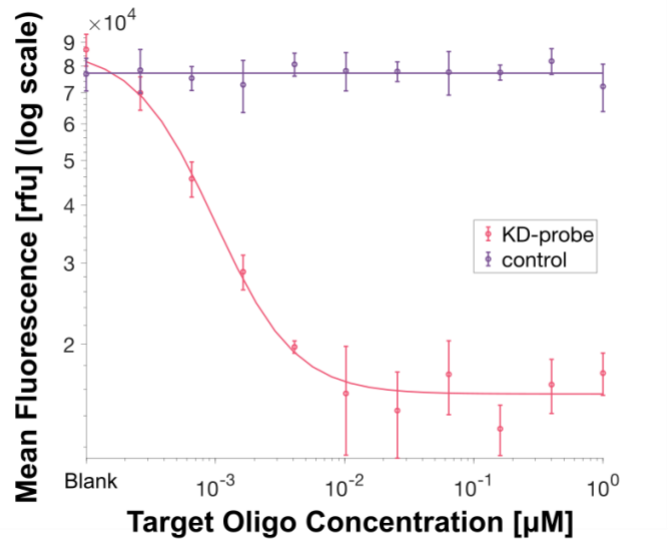

Figure 42: Binding curve data for a monovalent affinity probe fitted using a 4PL curve. A horizontal line is superimposed on the control data to guide the reader's eye. 1 nM of an 11 nt probe strand labelled with Cy5 was mixed with titrations of an 11 nt complementary target strand or a non-complementary control strand, each labelled with a quencher. The sequences used can be found in section 7.2. Based on the results of the control condition, we concluded that fluorescence quenching was not due to increased fluorophore/quencher proximity in solution. The KD-probe results indicated that the 11 nt binding site's affinity was too high to be accurately measured using the plate reader ($K_D \leq$ [probe]). The binding site length was subsequently reduced to the 7 nt sequence used throughout the body of the thesis.

7.1.2 Liquid-Phase Colocalized Assays

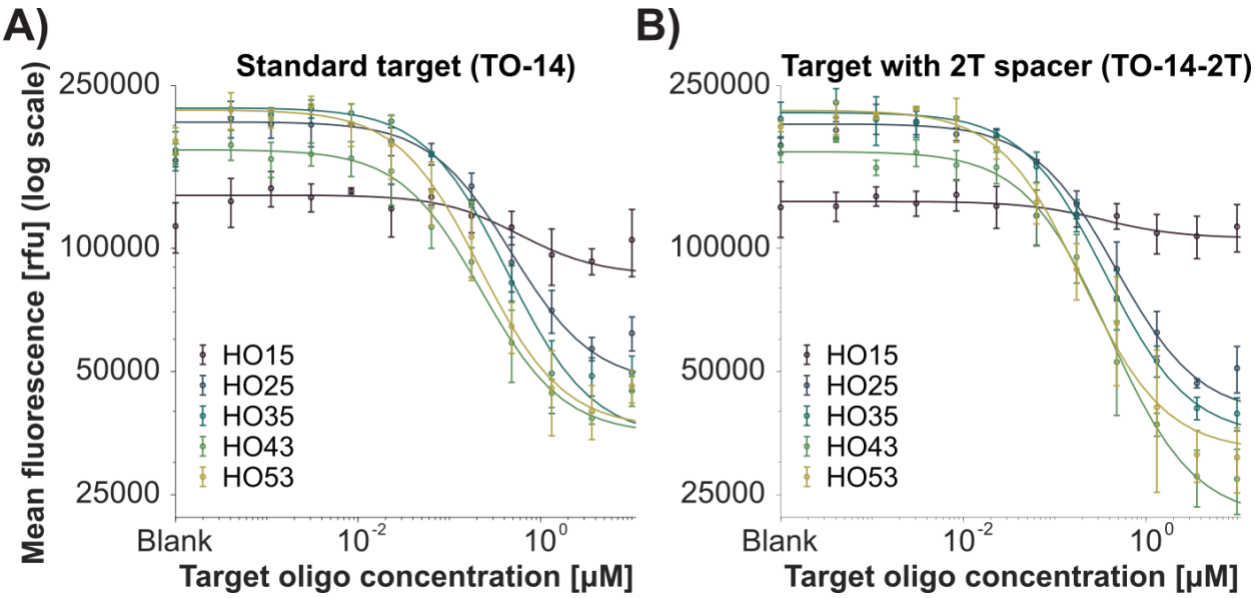

Figure 43: Binding curves of probes with increasing linker length (15-53 nt), fitted with the quadratic binding equation. A) unmodified target strand (TO-14), B) target strand with 2 nt spacer (TO-14-2T). For both targets, the signal window for the 15 nt linker is too narrow to be useful as a calibration curve. The target with 2 nt spacer has a larger signal window for all probes except HO15. Error bars represent one standard deviation. n=3.

Table 12: Parameters determined from nonlinear regression analysis of the binding curves with the quadratic binding equation for the unmodified target strand (TO-14) and the target strand with 2-nt spacer (TO-14-2T). 95% confidence intervals are reported.

Linker length [nt]	**Target strand**	**K_D [µM]**	**R^2**
15	TO-14	0.475 [0.121, 2.06]	0.67
	TO-14-2T	0.299 [0.00983, 28.4]	0.39
25	TO-14	0.226 [0.150, 0.340]	0.96
	TO-14-2T	0.207 [0.152, 0.282]	0.97
35	TO-14	0.171 [0.138, 0.211]	0.99
	TO-14-2T	0.143 [0.0987, 0.206]	0.97
43	TO-14	0.0986 [0.0620, 0.156]	0.95
	TO-14-2T	0.139 [0.0928, 0.208]	0.96
53	TO-14	0.0870 [0.0535, 0.140]	0.95
	TO-14-2T	0.0742 [0.0512, 0.107]	0.97

7.2 DNA Sequences Used

Table 13: DNA oligonucleotides used in this thesis, ordered by corresponding results sub-section. Intra-sequence gaps and colours are provided to delineate functional sub-sections and indicate complementarity

Section	Strand name	Sequence (5' to 3')
4.1	Capture oligo	(biotin) TTTTTTTTTGTGGCGGCGGTG ATTGGTTATTGAGAGTTTATG
	Spacer oligo	(biotin) TTTTTTTTTGTGGCGGCGGTG
	Barcoding oligo	CACCGCCGCCACAAAAAAAAA (Atto488/Cy3/Cy5/Cy5.5/none)
	Hook oligo	(Thiol) TTTTTTACTTTTCAACCACCACTCAACCATATTCAAAGCTTA CGATGCCGA CTCATTCGC CATAAACTCTCAATAACCAAT
	Displacer oligo	ATTGGTTATTGAGAGTTTATG GCGAATGAG (Cy5)
	Stiffener 10nt-5'	TCGGCATCGT
	Stiffener 10nt-3'	GTTGAAAAGT
	Stiffener 20nt-5'	TCGGCATCGTAAGCTTTGAA
	Stiffener 20nt-3'	TTGAGTGGTGGTTGAAAAGT
	Stiffener 30nt-5'	TCGGCATCGTAAGCTTTGAATATGGTTGAG
	Stiffener 30nt-3'	TTGAATATGGTTGAGTGGTGGTTGAAAAGT
	Stiffener 45nt	TCGGCATCGTAAGCTTTGAATATGGTTGAGTGGTGGTTGAAAAGT
4.2	Surface DIG	(DIG) TTTTT CACCGCCGCCACAAAAAAAAA
	DIG hook	(DIG) TTTTTTACTTTTCAACCACCACTCAACCATATTCAAAGCTTA CGATGCCGA CTCATTCGC CATAAACTCTCAATAACCAAT
	Labelling oligo	(Cy5) GTTGAGTGGTGGTTGA
4.3	CO-20	(biotin) TTTTTTTTTGTGGCGGCGGTG GTTGAGTGGTGGTTGTTAAT ATTGGTTATTGAGAGTTTATG
	CO-30	(biotin) TTTTTTTTTGTGGCGGCGGTG GTGTAATATGGTTGAGTGGTGGTTGTTAAT ATTGGTTATTGAGAGTTTATG
	CO-40	(biotin) TTTTTTTTTGTGGCGGCGGTG GAATAGTTAAGTGTAATATGGTTGAGTGGTGGTTGTTAAT ATTGGTTATTGAGAGTTTATG
	CO-50	(biotin) TTTTTTTTTGTGGCGGCGGTG GATAGTAAAGGAATAGTTAAGTGTAATATGGTTGAGTGGTGGTT GTTAAT ATTGGTTATTGAGAGTTTATG

	HOr	(DIG) T CTCATTCGC CATAAACTCTCAATAACCAAT
	HOf-20	ATTAACAACCACCACTCAACTTACT TCATT (DIG)
	HOf-30	ATTAACAACCACCACTCAACCATATTACACTTACT TCATT (DIG)
	HOf-40	ATTAACAACCACCACTCAACCATATTACACTTAACTATTCTTACT TCATT (DIG)
	HOf-50	ATTAACAACCACCACTCAACCATATTACACTTAACTATTCCTTTA CTATCTTACT TCATT (DIG)
4.4	Probe (15)	(Cy5) TTCTACA TCAAAAAAAAAAACT ACATCTT (IAbRQ)
	Probe (25)	(Cy5) TTCTACA TCAAAAAAAAAAAAAAAAAAAACT ACATCTT (IAbRQ)
	Probe (35)	(Cy5) TTCTACA TCAAATAAAATAAAATAAAATAAAATAAAAT AACT ACATCTT (IAbRQ)
	Probe (43)	(Cy5) TTCTACA TCATTTTAACTCAATAACCAATATTAACAACCACT CATTTACT ACATCTT (IAbRQ)
	Probe (53)	(Cy5) TTCTACA TCATTATCTCTCTCAATAACCAATATTAACAACC ACCACTCAACTCATTTACT ACATCTT (IAbRQ)
	TO-14	TGTAGAA AAGATGT
	TO-14-2T	TGTAGAA TT AAGATGT
Mono-valent affinity	KD-probe 7 nt	(Cy5) T TTCTACA TT
	KD-target 7 nt	TT TGTAGAA T (IAbRQ)
	KD-probe 11 nt	(Cy5) T TTCTACATCAT
	KD-target 11 nt	ATGATGTAGAA T (IAbRQ)
	KD-control 11 nt	TACTACATCTT T (IAbRQ)

8. References

1. Wilson, B. D. & Soh, H. T. Re-Evaluating the Conventional Wisdom about Binding Assays. *Trends Biochem. Sci.* **45**, 639–649 (2020).
2. Dagher, M. Cross-reactivity-free multiplexed immunoassays on microparticles. in *Scalable Affinity-Proteomics on Microparticles* 117–135 (McGill University, Montreal, 2018).
3. Gullberg, M. *et al.* Cytokine detection by antibody-based proximity ligation. *Proc. Natl. Acad. Sci. U. S. A.* **101**, 8420–8424 (2004).
4. Lundberg, M., Eriksson, A., Tran, B., Assarsson, E. & Fredriksson, S. Homogeneous antibody-based proximity extension assays provide sensitive and specific detection of low-abundant proteins in human blood. *Nucleic Acids Res.* **39**, e102 (2011).
5. Hansen, C. H., Yang, D., Koussa, M. A. & Wong, W. P. Nanoswitch-linked immunosorbent assay (NLISA) for fast, sensitive, and specific protein detection. *Proc. Natl. Acad. Sci.* **114**, 10367–10372 (2017).
6. Kosaka, P. M., Calleja, M. & Tamayo, J. Optomechanical devices for deep plasma cancer proteomics. *Semin. Cancer Biol.* **52**, 26–38 (2018).
7. Hartmann, M. *et al.* Expanding assay dynamics: a combined competitive and direct assay system for the quantification of proteins in multiplexed immunoassays. *Clin Chem* **54**, 956–963 (2008).
8. Slaats, J., ten Oever, J., van de Veerdonk, F. L. & Netea, M. G. IL-1β/IL-6/CRP and IL-18/ferritin: Distinct Inflammatory Programs in Infections. *PLOS Pathog.* **12**, e1005973 (2016).
9. ter Horst, R. *et al.* Host and Environmental Factors Influencing Individual Human Cytokine Responses. *Cell* **167**, 1111-1124.e13 (2016).
10. Ridker, P. M., Rifai, N., Stampfer, M. J. & Hennekens, C. H. Plasma Concentration of Interleukin-6 and the Risk of Future Myocardial Infarction Among Apparently Healthy Men. *Circulation* **101**, 1767–1772 (2000).
11. Hagi, T. *et al.* The diagnostic and prognostic value of interleukin-6 in patients with soft tissue sarcomas. *Sci. Rep.* **7**, 9640 (2017).
12. Oberhoffer, M. *et al.* Sensitivity and specificity of various markers of inflammation for the prediction of tumor necrosis factor-α and interleukin-6 in patients with sepsis. *Crit. Care Med.* **27**, (1999).
13. Chang, C.-W., Yang, S.-Y., Yang, C.-C., Chang, C.-W. & Wu, Y.-R. Plasma and Serum Alpha-Synuclein as a Biomarker of Diagnosis in Patients With Parkinson's Disease. *Front. Neurol.* **10**, 1388 (2020).
14. Peterson, E. A. *et al.* Evaluation of serum Amphiregulin levels in breast cancer patients and cancer-free controls. *Exp. Hematol. Oncol.* **2**, 25 (2013).
15. Kiyama, K. *et al.* Serum BAFF and APRIL levels in patients with IgG4-related disease and their clinical significance. *Arthritis Res. Ther.* **14**, R86 (2012).

16. Ghermezi, M. *et al.* Serum B-cell maturation antigen: a novel biomarker to predict outcomes for multiple myeloma patients. *Haematologica* **102**, 785–795 (2017).

17. Gejl, A. K. *et al.* Associations between serum and plasma brain-derived neurotrophic factor and influence of storage time and centrifugation strategy. *Sci. Rep.* **9**, 9655 (2019).

18. Kercheva, M. *et al.* Serum Levels of Bone Morphogenetic Proteins 2 and 4 in Patients with Acute Myocardial Infarction. *Cells* **9**, 2179 (2020).

19. Demir, N. A. *et al.* Are bone morphogenetic protein-7 (BMP-7) serum levels correlated with development of hepatic fibrosis? *J. Infect. Dev. Ctries.* **8**, 605–610 (2014).

20. Van Dijck, A. *et al.* Reduced serum levels of pro-inflammatory chemokines in fragile X syndrome. *BMC Neurol.* **20**, 138 (2020).

21. Holub, M. *et al.* Cytokines and Chemokines as Biomarkers of Community-Acquired Bacterial Infection. *Mediators Inflamm.* **2013**, 190145 (2013).

22. Lannergård, A., Larsson, A., Kragsbjerg, P. & Friman, G. Correlations between serum amyloid A protein and C-reactive protein in infectious diseases. *Scand. J. Clin. Lab. Invest.* **63**, 267–272 (2003).

23. Michels, M. *et al.* Normal free interleukin-18 (IL-18) plasma levels in dengue virus infection and the need to measure both total IL-18 and IL-18 binding protein levels. *Clin. Vaccine Immunol.* **22**, 650–655 (2015).

24. Italiani, P. *et al.* Circulating levels of IL-1 family cytokines and receptors in Alzheimer's disease: new markers of disease progression? *J. Neuroinflammation* **15**, 342 (2018).

25. Di Iorio, A. *et al.* Serum IL-1beta levels in health and disease: a population-based study. 'The InCHIANTI study'. *Cytokine* **22**, 198–205 (2003).

26. Colafrancesco, S. *et al.* IL-18 Serum Level in Adult Onset Still's Disease: A Marker of Disease Activity. *Int. J. Inflam.* **2012**, 156890 (2012).

27. van de Veerdonk, F. L. *et al.* IL-18 Serum Concentration Is Markedly Elevated in Acute EBV Infection and Can Serve as a Marker for Disease Severity. *J. Infect. Dis.* **206**, 197–201 (2012).

28. Bernard Jr, J. R. *et al.* Salvage radiotherapy for rising prostate-specific antigen levels after radical prostatectomy for prostate cancer: dose–response analysis. *Int. J. Radiat. Oncol. Biol. Phys.* **76**, 735–740 (2010).

29. Malle, E. & De Beer, F. C. Human serum amyloid A (SAA) protein: a prominent acute-phase reactant for clinical practice. *Eur. J. Clin. Invest.* **26**, 427–435 (1996).

30. Ohmura, N., Tsukidate, Y., Shinozaki, H., Lackie, S. J. & Saiki, H. Combinational Use of Antibody Affinities in an Immunoassay for Extension of Dynamic Range and Detection of Multiple Analytes. *Anal. Chem.* **75**, 104–110 (2003).

31. Elshal, M. F. & McCoy, J. P. Multiplex bead array assays: performance evaluation and comparison of sensitivity to ELISA. *Methods* **38**, 317–323 (2006).

32. Rissin, D. M. *et al.* Multiplexed single molecule immunoassays. *Lab Chip* **13**, 2902–2911 (2013).

33. Ray, C. A. *et al.* Development, validation, and implementation of a multiplex immunoassay for the simultaneous determination of five cytokines in human serum. *J. Pharm. Biomed. Anal.* **36**, 1037–1044 (2005).

34. Fredriksson, S. *et al.* Multiplexed protein detection by proximity ligation for cancer biomarker validation. *Nat. Methods* **4**, 327–329 (2007).

35. Laforte, V., Lo, P.-S., Li, H. & Juncker, D. Antibody Colocalization Microarray for Cross-Reactivity-Free Multiplexed Protein Analysis. in *Serum/Plasma Proteomics: Methods and Protocols* (eds. Greening, D. W. & Simpson, R. J.) 239–261 (Springer New York, 2017).

36. Sittampalam, G. & Coussens, N. Preface. in *Assay Guidance Manual [Internet]* (eds. Sittampalam, G., Grossman, A., Brimacombe, K. & Arkin, M.) (Eli Lilly & Company and The National Center for Advancing Translational Sciences, 2012).

37. Schreiber, G., Haran, G. & Zhou, H.-X. Fundamental aspects of protein-protein association kinetics. *Chem. Rev.* **109**, 839–860 (2009).

38. Pollard, T. D. A Guide to Simple and Informative Binding Assays. *Mol. Biol. Cell* **21**, 4061–4067 (2010).

39. Pollard, T. D. & De La Cruz, E. M. Take advantage of time in your experiments: a guide to simple, informative kinetics assays. *Mol. Biol. Cell* **24**, 1103–1110 (2013).

40. Hulme, E. C. & Trevethick, M. A. Ligand binding assays at equilibrium: validation and interpretation. *Br. J. Pharmacol.* **161**, 1219–1237 (2010).

41. Gesztelyi, R. *et al.* The Hill equation and the origin of quantitative pharmacology. *Arch. Hist. Exact Sci.* **66**, 427–438 (2012).

42. Prinz, H. Hill coefficients, dose-response curves and allosteric mechanisms. *J. Chem. Biol.* **3**, 37–44 (2010).

43. Jarmoskaite, I., AlSadhan, I., Vaidyanathan, P. P. & Herschlag, D. How to measure and evaluate binding affinities. *Elife* **9**, e57264 (2020).

44. Azadeh, M. *et al.* Calibration Curves in Quantitative Ligand Binding Assays: Recommendations and Best Practices for Preparation, Design, and Editing of Calibration Curves. *AAPS J.* **20**, 22 (2017).

45. Findlay, J. W. A. & Dillard, R. F. Appropriate calibration curve fitting in ligand binding assays. *AAPS J.* **9**, E260–E267 (2007).

46. Hill, A. V. A new mathematical treatment of changes of ionic concentration in muscle and nerve under the action of electric currents, with a theory as to their mode of excitation. *J. Physiol.* **40**, 190–224 (1910).

47. Jeong, J.-E. *et al.* Principal factors that determine the extension of detection range in molecular beacon aptamer/conjugated polyelectrolyte bioassays. *Chem. Sci.* **6**, 1887–1894 (2015).

48. Ricci, F., Vallee-Belisle, A., Simon, A. J., Porchetta, A. & Plaxco, K. W. Using Nature's 'Tricks' To Rationally Tune the Binding Properties of Biomolecular Receptors. *Acc Chem Res* **49**, 1884–1892 (2016).

49. Glass, T. R., Ohmura, N. & Saiki, H. Least Detectable Concentration and Dynamic Range of Three Immunoassay Systems Using the Same Antibody. *Anal. Chem.* **79**, 1954–1960 (2007).

50. Armbruster, D. A. & Pry, T. Limit of blank, limit of detection and limit of quantitation. *Clin. Biochem. Rev.* **29 Suppl 1**, S49–S52 (2008).

51. Rozet, E., Marini, R. D., Ziemons, E., Boulanger, B. & Hubert, P. Advances in validation, risk and uncertainty assessment of bioanalytical methods. *J. Pharm. Biomed. Anal.* **55**, 848–858 (2011).

52. Rozet, E. *et al.* Analysis of recent pharmaceutical regulatory documents on analytical method validation. *J. Chromatogr. A* **1158**, 111–125 (2007).

53. Food and Drug Administration, U. S. *Bioanalytical method validation guidance for industry*. (2018).

54. Miyai, K. Classification of immunoassay. in *Principles and Practice of Immunoassay* (eds. Price, C. P. & Newman, D. J.) 246–264 (Palgrave Macmillan, London, 1991).

55. Gosling, J. P. A Decade of Development in Immunoassay Methodology. *Clin. Chem.* **36**, 1408–1427 (1990).

56. Deshpande, S. S. Separation and Solid-Phase Systems. in *Enzyme Immunoassays* 193–228 (Springer, Boston, 1996).

57. Stevens, F. J., Jwo, J., Carperos, W., Köhler, H. & Schiffer, M. Relationships between liquid- and solid-phase antibody association characteristics: implications for the use of competitive ELISA techniques to map the spatial location of idiotopes. *J. Immunol.* **137**, 1937–1944 (1986).

58. del Rosario Stumpo, R., Llera, A. S., Cardoso, A. I. & Poskus, E. Solid versus liquid phase assays in detection of insulin antibodies influence of iodination site on labelled insulin binding. *J. Immunol. Methods* **169**, 241–249 (1994).

59. Yao, Z. *et al.* A homogeneous split-luciferase assay for rapid and sensitive detection of anti-SARS CoV-2 antibodies. *Nat. Commun.* **12**, 1806 (2021).

60. Wang, T.-T. *et al.* A feasible image-based colorimetric assay using a smartphone RGB camera for point-of-care monitoring of diabetes. *Talanta* **206**, 120211 (2020).

61. Lynes, M. A. Solid-Phase Immunoassays. *Curr. Protoc. Toxicol.* **23**, 18.7.1-18.7.19 (2005).

62. Peterson, A. W., Heaton, R. J. & Georgiadis, R. M. The effect of surface probe density on DNA hybridization. *Nucleic Acids Res.* **29**, 5163–5168 (2001).

63. Sekar, M. M. A., Bloch, W. & St John, P. M. Comparative study of sequence-dependent hybridization kinetics in solution and on microspheres. *Nucleic Acids Res.* **33**, 366–375 (2005).

64. Held, G. A., Grinstein, G. & Tu, Y. Modeling of DNA microarray data by using physical properties of hybridization. *Proc. Natl. Acad. Sci.* **100**, 7575–7580 (2003).

65. Levicky, R. & Horgan, A. Physicochemical perspectives on DNA microarray and biosensor technologies. *Trends Biotechnol.* **23**, 143–149 (2005).

66. Li, J., Zrazhevskiy, P. & Gao, X. Eliminating Size-Associated Diffusion Constraints for Rapid On-Surface Bioassays with Nanoparticle Probes. *Small* **12**, 1035–1043 (2016).

67. Esteban Fernandez de Avila, B. *et al.* Determinants of the detection limit and specificity of surface-based biosensors. *Anal Chem* **85**, 6593–6597 (2013).

68. Ranallo, S., Rossetti, M., Plaxco, K. W., Vallée-Bélisle, A. & Ricci, F. A modular, DNA-based beacon for single-step fluorescence detection of antibodies and other proteins. *Angew. Chem. Int. Ed. Engl.* **127**, 13412–13416 (2015).

69. McNeely, P. M., Naranjo, A. N., Forsten-Williams, K. & Robinson, A. S. A(2A)R Binding Kinetics in the Ligand Depletion Regime. *SLAS Discov.* **22**, 166–175 (2017).

70. Vignali, D. A. A. Multiplexed particle-based flow cytometric assays. *J. Immunol. Methods* **243**, 243–255 (2000).

71. Nolan, J. P. & Mandy, F. Multiplexed and microparticle-based analyses: Quantitative tools for the large-scale analysis of biological systems. *Cytom. Part A* **69A**, 318–325 (2006).

72. Carson, R. T. & Vignali, D. A. A. Simultaneous quantitation of 15 cytokines using a multiplexed flow cytometric assay. *J. Immunol. Methods* **227**, 41–52 (1999).

73. de Jager, W., te Velthuis, H., Prakken, B. J., Kuis, W. & Rijkers, G. T. Simultaneous detection of 15 human cytokines in a single sample of stimulated peripheral blood mononuclear cells. *Clin. Diagn. Lab. Immunol.* **10**, 133–139 (2003).

74. Wang, L. & Cheng, Z. An enzyme-linked immunosorbent assay with a new way to control the edge effect and its application for bevacizumab pharmacokinetic studies in beagle dogs by fitting with a new pharmacokinetic model. *Anal. Methods* **7**, 8936–8941 (2015).

75. Normandeau, F., Ng, A., Beaugrand, M. & Juncker, D. Spatial Bias in Antibody Microarrays May Be an Underappreciated Source of Variability. *ACS Sensors* **6**, 1796–1806 (2021).

76. van Reenen, A., de Jong, A. M. & Prins, M. W. J. How Actuated Particles Effectively Capture Biomolecular Targets. *Anal. Chem.* **89**, 3402–3410 (2017).

77. Kellar, K. L. & Iannone, M. A. Multiplexed microsphere-based flow cytometric assays. *Exp. Hematol.* **30**, 1227–1237 (2002).

78. Edwards, B. S., Oprea, T., Prossnitz, E. R. & Sklar, L. A. Flow cytometry for high-throughput, high-content screening. *Curr. Opin. Chem. Biol.* **8**, 392–398 (2004).

79. Thiviyanathan, V. & Gorenstein, D. G. Aptamers and the next generation of diagnostic reagents. *Proteomics Clin. Appl.* **6**, 563–573 (2012).

80. Janeway Jr, C. A., Travers, P., Walport, M. & Shlomchik, M. J. The interaction of the antibody molecule with specific antigen. in *Immunobiology: The Immune System in Health and Disease* 122–127 (Garland Science, New York, 2001).

81. Chiu, M. L., Goulet, D. R., Teplyakov, A. & Gilliland, G. L. Antibody Structure and Function: The Basis for Engineering Therapeutics. *Antibodies (Basel, Switzerland)* **8**, 55 (2019).

82. Hopkins, N. A. E. Antibody Engineering for Biosensor Applications. in *Recognition Receptors in Biosensors* (ed. Zourob, M.) 451–529 (Springer, New York, 2010).

83. Janeway, C. J., Travers, P., Walport, M. & Shlomchik, M. J. The structure of a typical antibody molecule. in *Immunobiology: The Immune System in Health and Disease* 116–122 (Garland Science, New York, 2001).

84. Adlersberg, J. B. The immunoglobulin hinge (Interdomain) region. *Ric. Clin. e Lab.* **6**, 191–205 (1976).

85. Wang, W., Singh, S., Zeng, D. L., King, K. & Nema, S. Antibody structure, instability, and formulation. *J. Pharm. Sci.* **96**, 1–26 (2007).

86. Saphire, E. O. *et al.* Contrasting IgG Structures Reveal Extreme Asymmetry and Flexibility. *J. Mol. Biol.* **319**, 9–18 (2002).

87. Adams, R. L. P., Knowler, J. T. & Leader, D. P. *The biochemistry of the nucleic acids*. (Chapman & Hall, London, 1992).

88. Zhu, Z. Design, Synthesis, Purification, and Characterization of Molecular Beacons. in *Molecular Beacons* (eds. Yang, C. J. & Tan, W.) 1–17 (Springer, Berlin, Heidelberg, 2013).

89. Carothers, J. M. & Szostak, J. W. In Vitro Selection of Functional Oligonucleotides and the Origins of Biochemical Activity. in *The Aptamer Handbook* (ed. Klussmann, S.) 1–28 (John Wiley & Sons, Hoboken, 2006).

90. Yang, X. *et al.* Characterization and application of a DNA aptamer binding to L-tryptophan. *Analyst* **136**, 577–585 (2011).

91. Hermann, T. & Patel, D. J. Adaptive Recognition by Nucleic Acid Aptamers. *Science* **287**, 820–825 (2000).

92. Rohloff, J. C. *et al.* Nucleic Acid Ligands With Protein-like Side Chains: Modified Aptamers and Their Use as Diagnostic and Therapeutic Agents. *Mol. Ther. Nucleic Acids* **3**, e201–e201 (2014).

93. Juncker, D., Bergeron, S., Laforte, V. & Li, H. Cross-reactivity in antibody microarrays and multiplexed sandwich assays: shedding light on the dark side of multiplexing. *Curr. Opin. Chem. Biol.* **18**, 29–37 (2014).

94. Cox, K. *et al.* Immunoassay Methods. in *Assay Guidance Manual [internet]* (eds. Sittampalam, G., Grossman, A., Brimacombe, K. & Arkin, M.) (Eli Lilly & Company and The National Center for Advancing Translational Sciences, Bethesda, 2012).

95. Kobayashi, N. & Goto, J. Noncompetitive immunoassays for small molecules with high sensitivity and specificity. *Adv. Clin. Chem.* **36**, 139–170 (2001).

96. Ishikawa, E. Introduction: classification of immunoassays. in *Laboratory techniques in biochemistry and molecular biology; Ultrasensitive and rapid enzyme immunoassay* (ed. van der Vliet, P. C.) 1–3 (Elsevier, Amsterdam, 1999).

97. Gorman, K. T., Roby, L. C., Giuffre, A., Huang, R. & Kay, B. K. Tandem phage-display for the identification of non-overlapping binding pairs of recombinant affinity reagents. *Nucleic Acids Res.* **45**, e158 (2017).

98. Park, J. Y. & Kricka, L. J. Interferences in Immunoassay. in *The Immunoassay Handbook* (ed. Wild, D.) 403–416 (Elsevier, Oxford, 2013).

99. James, L. C. & Tawfik, D. S. The specificity of cross-reactivity: promiscuous antibody binding involves specific hydrogen bonds rather than nonspecific hydrophobic stickiness. *Protein Sci.* **12**, 2183–2193 (2003).

100. Pla-Roca, M. *et al.* Antibody colocalization microarray: a scalable technology for multiplex protein analysis in complex samples. *Mol. Cell. Proteomics* **11**, M111.011460 (2012).

101. Bergeron, S., Laforte, V., Lo, P.-S., Li, H. & Juncker, D. Evaluating mixtures of 14 hygroscopic additives to improve antibody microarray performance. *Anal. Bioanal. Chem.* **407**, 8451–8462 (2015).

102. Li, H., Bergeron, S. & Juncker, D. Microarray-to-Microarray Transfer of Reagents by Snapping of Two Chips for Cross-Reactivity-Free Multiplex Immunoassays. *Anal. Chem.* **84**, 4776–4783 (2012).

103. Li, H., Munzar, J. D., Ng, A. & Juncker, D. A versatile snap chip for high-density sub-nanoliter chip-to-chip reagent transfer. *Sci. Rep.* **5**, 11688 (2015).

104. Frampton, J. P. *et al.* Aqueous two-phase system patterning of detection antibody solutions for cross-reaction-free multiplex ELISA. *Sci. Rep.* **4**, 4878 (2014).

105. Simon, A. B. *et al.* Aqueous two-phase systems enable multiplexing of homogeneous immunoassays. *Technology* **2**, 176 (2014).

106. Eiden, L., Yamanishi, C., Takayama, S. & Dishinger, J. F. Aqueous Two-Phase System Rehydration of Antibody–Polymer Microarrays Enables Convenient Compartmentalized Multiplex Immunoassays. *Anal. Chem.* **88**, 11328–11334 (2016).

107. Tongdee, M. *et al.* One-incubation one-hour multiplex ELISA enabled by aqueous two-phase systems. *Analyst* **145**, 3517–3527 (2020).

108. Koussa, M. A., Halvorsen, K., Ward, A. & Wong, W. P. DNA nanoswitches: a quantitative platform for gel-based biomolecular interaction analysis. *Nat. Methods* **12**, 123–126 (2015).

109. Chandrasekaran, A. R. *et al.* DNA Nanoswitch Barcodes for Multiplexed Biomarker Profiling. *Nano Lett.* **21**, 469–475 (2021).

110. Dagher, M. Assay architecture. in *Scalable Affinity-Proteomics on Microparticles* 119–120 (McGill University, Montreal, 2018).

111. Dagher, M. Multiplexed CLAMP. in *Scalable Affinity-Proteomics on Microparticles* 122–124 (McGill University, Montreal, 2018).

112. Fredriksson, S. *et al.* Protein detection using proximity-dependent DNA ligation assays. *Nat. Biotechnol.* **20**, 473–477 (2002).

113. Ke, R., Nong, R. Y., Fredriksson, S., Landegren, U. & Nilsson, M. Improving Precision of Proximity Ligation Assay by Amplified Single Molecule Detection. *PLoS One* **8**, e69813 (2013).

114. Söderberg, O. *et al.* Direct observation of individual endogenous protein complexes in situ by proximity ligation. *Nat. Methods* **3**, 995–1000 (2006).

115. Lundberg, M. *et al.* Multiplexed homogeneous proximity ligation assays for high-throughput protein biomarker research in serological material. *Mol. Cell. Proteomics* **10**, M110.004978 (2011).

116. Assarsson, E. *et al.* Homogenous 96-plex PEA immunoassay exhibiting high sensitivity, specificity, and excellent scalability. *PLoS One* **9**, e95192 (2014).

117. Gobet, N., Ketterer, S. & Meier, M. Design and validation of DNA libraries for multiplexing proximity ligation assays. *PLoS One* **9**, e112629 (2014).

118. Debski, P. R. & Garstecki, P. Designing and interpretation of digital assays: Concentration of target in the sample and in the source of sample. *Biomol. Detect. Quantif.* **10**, 24–30 (2016).

119. Rissin, D. M. *et al.* Single-molecule enzyme-linked immunosorbent assay detects serum proteins at subfemtomolar concentrations. *Nat. Biotechnol.* **28**, 595–599 (2010).

120. Rissin, D. M. *et al.* Simultaneous detection of single molecules and singulated ensembles of molecules enables immunoassays with broad dynamic range. *Anal. Chem.* **83**, 2279–2285 (2011).

121. Davies, C. Immunoassay Performance Measures. in *The Immunoassay Handbook* (ed. Wild, D.) 11–26 (Elsevier, Oxford, 2013).

122. Kang, D., Vallee-Belisle, A., Porchetta, A., Plaxco, K. W. & Ricci, F. Re-engineering electrochemical biosensors to narrow or extend their useful dynamic range. *Angew. Chem. Int. Ed. Engl.* **51**, 6717–6721 (2012).

123. Vallée-Bélisle, A., Ricci, F. & Plaxco, K. W. Engineering Biosensors with Extended, Narrowed, or Arbitrarily Edited Dynamic Range. *J. Am. Chem. Soc.* **134**, 2876–2879 (2012).

124. Hyytiä, H., Ristiniemi, N., Laitinen, P., Lövgren, T. & Pettersson, K. Extension of dynamic range of sensitive nanoparticle-based immunoassays. *Anal. Biochem.* **446**, 82–86 (2014).

125. Debski, P. R., Gewartowski, K., Sulima, M., Kaminski, T. S. & Garstecki, P. Rational design of digital assays. *Anal Chem* **87**, 8203–8209 (2015).

126. Krämer, P. M., Kremmer, E., Forster, S. & Goodrow, M. H. Extending the Working Range of Immunoanalysis by Exploitation of Two Monoclonal Antibodies. *J. Agric. Food Chem.* **52**, 6394–6401 (2004).

127. Kussie, P. H., Parhami-Seren, B., Wysocki, L. J. & Margolies, M. N. A single engineered amino acid substitution changes antibody fine specificity. *J. Immunol.* **152**, 146–152 (1994).

128. Xiang, J. I. M., Chen, Z., Delbaere, L. T. J. & Liu, E. Differences in antigen-binding affinity caused by single amino acid substitution in the variable region of the heavy chain. *Immunol. Cell Biol.* **71**, 239–247 (1993).

129. Wark, K. L. & Hudson, P. J. Latest technologies for the enhancement of antibody affinity. *Adv. Drug Deliv. Rev.* **58**, 657–670 (2006).

130. Yau, K. Y. F. *et al.* Affinity maturation of a VHH by mutational hotspot randomization. *J. Immunol. Methods* **297**, 213–224 (2005).

131. Demidov, V. V & Frank-Kamenetskii, M. D. Two sides of the coin: affinity and specificity of nucleic acid interactions. *Trends Biochem. Sci.* **29**, 62–71 (2004).

132. Mariottini, D., Idili, A., Nijenhuis, M. A. D., De Greef, T. F. A. & Ricci, F. DNA-Based Nanodevices Controlled by Purely Entropic Linker Domains. *J. Am. Chem. Soc.* **140**, 14725–14734 (2018).

133. Peng, L. & Tan, W. Thermodynamic and Kinetic Properties of Molecular Beacons. in *Molecular Beacons* (eds. Yang, C. J. & Tan, W.) 19–43 (Springer, Berlin, Heidelberg, 2013).

134. Hamula, C. L. A., Guthrie, J. W., Zhang, H., Li, X.-F. & Le, X. C. Selection and analytical applications of aptamers. *Trends Analyt. Chem.* **25**, 681–691 (2006).

135. Gold, L. *et al.* Aptamer-Based Multiplexed Proteomic Technology for Biomarker Discovery. *PLoS One* **5**, e15004 (2010).

136. Gelinas, A. D. *et al.* Crystal Structure of Interleukin-6 in Complex with a Modified Nucleic Acid Ligand. *J. Biol. Chem.* **289**, 8720–8734 (2014).

137. Vallée-Bélisle, A., Ricci, F. & Plaxco, K. W. Thermodynamic basis for the optimization of binding-induced biomolecular switches and structure-switching biosensors. *Proc. Natl. Acad. Sci.* **106**, 13802–13807 (2009).

138. Porchetta, A., Vallee-Belisle, A., Plaxco, K. W. & Ricci, F. Using distal-site mutations and allosteric inhibition to tune, extend, and narrow the useful dynamic range of aptamer-based sensors. *J. Am. Chem. Soc.* **134**, 20601–20604 (2012).

139. Ricci, F., Vallee-Belisle, A., Porchetta, A. & Plaxco, K. W. Rational design of allosteric inhibitors and activators using the population-shift model: in vitro validation and application to an artificial biosensor. *J. Am. Chem. Soc.* **134**, 15177–15180 (2012).

140. Armstrong, R. E. & Strouse, G. F. Rationally Manipulating Aptamer Binding Affinities in a Stem-Loop Molecular Beacon. *Bioconjug. Chem.* **25**, 1769–1776 (2014).

141. Jeong, J.-E. & Woo, H. Y. Control of electrostatic interaction between a molecular beacon aptamer and conjugated polyelectrolyte for detection range-tunable ATP assay. *Polym. Chem.* **8**, 6329–6334 (2017).

142. Wei, B. *et al.* Engineering Biosensors with Dual Programmable Dynamic Ranges. *Anal. Chem.* **90**, 1506–1510 (2018).

143. Munzar, J. D., Ng, A., Corrado, M. & Juncker, D. Complementary oligonucleotides regulate induced fit ligand binding in duplexed aptamers. *Chem. Sci.* **8**, 2251–2256 (2017).

144. Weikl, T. R. & von Deuster, C. Selected-fit versus induced-fit protein binding: Kinetic differences and mutational analysis. *Proteins Struct. Funct. Bioinforma.* **75**, 104–110 (2009).

145. Ouldridge, T. E., Sulc, P., Romano, F., Doye, J. P. K. & Louis, A. A. DNA hybridization kinetics: zippering, internal displacement and sequence dependence. *Nucleic Acids Res.* **41**, 8886–8895 (2013).

146. Srinivas, N. *et al.* On the biophysics and kinetics of toehold-mediated DNA strand displacement. *Nucleic Acids Res.* **41**, 10641–10658 (2013).

147. Huizenga, D. E. & Szostak, J. W. A DNA aptamer that binds adenosine and ATP. *Biochemistry* **34**, 656–665 (1995).

148. Pritišanac, I., Vernon, R. M., Moses, A. M. & Forman Kay, J. D. Entropy and Information within Intrinsically Disordered Protein Regions. *Entropy* **21**, (2019).

149. Sørensen, C. S. & Kjaergaard, M. Effective concentrations enforced by intrinsically disordered linkers are governed by polymer physics. *Proc. Natl. Acad. Sci.* **116**, 23124–23131 (2019).

150. Sørensen, C. S., Jendroszek, A. & Kjaergaard, M. Linker Dependence of Avidity in Multivalent Interactions Between Disordered Proteins. *J. Mol. Biol.* **431**, 4784–4795 (2019).

151. Zhou, H.-X. Quantitative account of the enhanced affinity of two linked scFvs specific for different epitopes on the same antigen. *J. Mol. Biol.* **329**, 1–8 (2003).

152. Krishnamurthy, V. M., Semetey, V., Bracher, P. J., Shen, N. & Whitesides, G. M. Dependence of effective molarity on linker length for an intramolecular protein-ligand system. *J. Am. Chem. Soc.* **129**, 1312–1320 (2007).

153. Einav, T., Yazdi, S., Coey, A., Bjorkman, P. J. & Phillips, R. Harnessing Avidity: Quantifying the Entropic and Energetic Effects of Linker Length and Rigidity for Multivalent Binding of Antibodies to HIV-1. *Cell Syst.* **9**, 466-474.e7 (2019).

154. Tian, L. & Heyduk, T. Bivalent ligands with long nanometer-scale flexible linkers. *Biochemistry* **48**, 264–275 (2008).

155. Rinker, S., Ke, Y., Liu, Y., Chhabra, R. & Yan, H. Self-assembled DNA nanostructures for distance-dependent multivalent ligand–protein binding. *Nat. Nanotechnol.* **3**, 418–422 (2008).

156. Anderson, B. R. & Granzier, H. Titin-based tension in the cardiac sarcomere: molecular origin and physiological adaptations. *Prog. Biophys. Mol. Biol.* **110**, 204–217 (2012).

157. Gobush, W., Yamakawa, H., Stockmayer, W. H. & Magee, W. S. Statistical Mechanics of Wormlike Chains. I. Asymptotic Behavior. *J. Chem. Phys.* **57**, 2839–2843 (1972).

158. Zhou, H.-X. Loops in Proteins Can Be Modeled as Worm-Like Chains. *J. Phys. Chem. B* **105**, 6763–6766 (2001).

159. Gargano, J. M., Ngo, T., Kim, J. Y., Acheson, D. W. K. & Lees, W. J. Multivalent Inhibition of AB5 Toxins. *J. Am. Chem. Soc.* **123**, 12909–12910 (2001).

160. Sim, A. Y. L., Lipfert, J., Herschlag, D. & Doniach, S. Salt dependence of the radius of gyration and flexibility of single-stranded DNA in solution probed by small-angle x-ray scattering. *Phys. Rev. E* **86**, 21901 (2012).

161. Chi, Q., Wang, G. & Jiang, J. The persistence length and length per base of single-stranded DNA obtained from fluorescence correlation spectroscopy measurements using mean field theory. *Phys. A* **392**, 1072–1079 (2013).

162. Murphy, M. C., Rasnik, I., Cheng, W., Lohman, T. M. & Ha, T. Probing single-stranded DNA conformational flexibility using fluorescence spectroscopy. *Biophys. J.* **86**, 2530–2537 (2004).

163. Roth, E., Glick Azaria, A., Girshevitz, O., Bitler, A. & Garini, Y. Measuring the Conformation and Persistence Length of Single-Stranded DNA Using a DNA Origami Structure. *Nano Lett.* **18**, 6703–6709 (2018).

164. Lu, Y., Weers, B. & Stellwagen, N. C. DNA persistence length revisited. *Biopolymers* **61**, 261–275 (2002).

165. Mazur, A. K. Wormlike Chain Theory and Bending of Short DNA. *Phys. Rev. Lett.* **98**, 218102 (2007).

166. Zhang, D. Y. & Winfree, E. Control of DNA Strand Displacement Kinetics Using Toehold Exchange. *J. Am. Chem. Soc.* **131**, 17303–17314 (2009).

167. von Hippel, P. H., Johnson, N. P. & Marcus, A. H. Fifty years of DNA "Breathing": Reflections on old and new approaches. *Biopolymers* **99**, 923–954 (2013).

168. Xie, N. *et al.* DNA tetrahedron nanostructures for biological applications: biosensors and drug delivery. *Analyst* **142**, 3322–3332 (2017).

169. Lo, P. K., Metera, K. L. & Sleiman, H. F. Self-assembly of three-dimensional DNA nanostructures and potential biological applications. *Curr. Opin. Chem. Biol.* **14**, 597–607 (2010).

170. Aldaye, F. A. & Sleiman, H. F. Modular Access to Structurally Switchable 3D Discrete DNA Assemblies. *J. Am. Chem. Soc.* **129**, 13376–13377 (2007).

171. Veneziano, R. *et al.* Role of nanoscale antigen organization on B-cell activation probed using DNA origami. *Nat. Nanotechnol.* **15**, 716–723 (2020).

172. Goodman, R. P. *et al.* Rapid Chiral Assembly of Rigid DNA Building Blocks for Molecular Nanofabrication. *Science* **310**, 1661–1665 (2005).

173. Goodman, R. P., Berry, R. M. & Turberfield, A. J. The single-step synthesis of a DNA tetrahedron. *Chem. Commun.* 1372–1373 (2004).

174. Li, Z. *et al.* A Replicable Tetrahedral Nanostructure Self-Assembled from a Single DNA Strand. *J. Am. Chem. Soc.* **131**, 13093–13098 (2009).

175. Sadowski, J. P., Calvert, C. R., Zhang, D. Y., Pierce, N. A. & Yin, P. Developmental Self-Assembly of a DNA Tetrahedron. *ACS Nano* **8**, 3251–3259 (2014).

176. Pei, H. *et al.* A DNA Nanostructure-based Biomolecular Probe Carrier Platform for Electrochemical Biosensing. *Adv. Mater.* **22**, 4754–4758 (2010).

177. Lin, M. *et al.* Programmable Engineering of a Biosensing Interface with Tetrahedral DNA Nanostructures for Ultrasensitive DNA Detection. *Angew. Chem. Int. Ed. Engl.* **54**, 2151–2155 (2015).

178. Goodman, R. P. *et al.* Reconfigurable, braced, three-dimensional DNA nanostructures. *Nat. Nanotechnol.* **3**, 93–96 (2008).

179. Schindelin, J. *et al.* Fiji: an open-source platform for biological-image analysis. *Nat. Methods* **9**, 676–682 (2012).

180. Dagher, M., Kleinman, M., Ng, A. & Juncker, D. Ensemble multicolour FRET model enables barcoding at extreme FRET levels. *Nat. Nanotechnol.* **13**, 925–932 (2018).

181. Rho, W. J. Assay Parameter Optimization. in *Optimization of a cross-reactivity-free proteomic platform toward neurological biomarker analysis* 74–77 (McGill University, Montreal, 2020).

182. Cardillo, G. Four parameters logistic regression - There and back again. (2012).

183. Xiang, Y. *et al.* A Simple Approach to Determine a Curve Fitting Model with a Correct Weighting Function for Calibration Curves in Quantitative Ligand Binding Assays. *AAPS J.* **20**, 45 (2018).

184. Clark, P. J. & Evans, F. C. Distance to Nearest Neighbor as a Measure of Spatial Relationships in Populations. *Ecology* **35**, 445–453 (1954).

185. Josephs, E. A. & Ye, T. Nanoscale Spatial Distribution of Thiolated DNA on Model Nucleic Acid Sensor Surfaces. *ACS Nano* **7**, 3653–3660 (2013).

186. Kibbe, W. A. OligoCalc: an online oligonucleotide properties calculator. *Nucleic Acids Res.* **35**, W43–W46 (2007).

187. Zuker, M. Mfold web server for nucleic acid folding and hybridization prediction. *Nucleic Acids Res.* **31**, 3406–3415 (2003).

188. Brown, S. S. *et al.* PrimerPooler: automated primer pooling to prepare library for targeted sequencing. *Biol. Methods Protoc.* **2**, bpx006 (2017).

189. Zadeh, J. N. *et al.* NUPACK: Analysis and design of nucleic acid systems. *J. Comput. Chem.* **32**, 170–173 (2011).

190. Schroeder, S. J. & Turner, D. H. Optical melting measurements of nucleic acid thermodynamics. *Methods Enzymol.* **468**, 371–387 (2009).

191. Iversen, P. W., Eastwood, B. J., Sittampalam, G. S. & Cox, K. L. A Comparison of Assay Performance Measures in Screening Assays: Signal Window, Z' Factor, and Assay Variability Ratio. *J. Biomol. Screen.* **11**, 247–252 (2006).

192. Tan, Y. H. *et al.* A nanoengineering approach for investigation and regulation of protein immobilization. *ACS Nano* **2**, 2374–2384 (2008).

193. Woźniak, A. K., Schröder, G. F., Grubmüller, H., Seidel, C. A. M. & Oesterhelt, F. Single-molecule FRET measures bends and kinks in DNA. *Proc. Natl. Acad. Sci.* **105**, 18337–18342 (2008).

194. Komminoth, P. Digoxigenin as an alternative probe labeling for in situ hybridization. *Diagn. Mol. Pathol.* **1**, 142–150 (1992).

195. Kessler, C. *et al.* The Digoxigenin: Anti-Digoxigenin (DIG) System. in *Nonradioactive labeling and detection of biomolecules* (ed. Kessler, C.) 35–69 (Springer, Berlin, Heidelberg, 1992).

196. Rho, W. J. DNA and Antibody Sticking. in *Optimization of a cross-reactivity-free proteomic platform toward neurological biomarker analysis* 66–72 (McGill University, Montreal, 2020).

197. Schwesinger, F. *et al.* Unbinding forces of single antibody-antigen complexes correlate with their thermal dissociation rates. *Proc. Natl. Acad. Sci.* **97**, 9972–9977 (2000).

198. Lad, L. *et al.* High-Throughput Kinetic Screening of Hybridomas to Identify High-Affinity Antibodies Using Bio-Layer Interferometry. *J. Biomol. Screen.* **20**, 498–507 (2014).

199. Landry, J. P., Ke, Y., Yu, G.-L. & Zhu, X. D. Measuring affinity constants of 1450 monoclonal antibodies to peptide targets with a microarray-based label-free assay platform. *J. Immunol. Methods* **417**, 86–96 (2015).

200. Roll, C., Ketterlé, C., Faibis, V., Fazakerley, G. V. & Boulard, Y. Conformations of Nicked and Gapped DNA Structures by NMR and Molecular Dynamic Simulations in Water. *Biochemistry* **37**, 4059–4070 (1998).

201. Yakovchuk, P., Protozanova, E. & Frank-Kamenetskii, M. D. Base-stacking and base-pairing contributions into thermal stability of the DNA double helix. *Nucleic Acids Res.* **34**, 564–574 (2006).

202. Kashida, H., Kurihara, A., Kawai, H. & Asanuma, H. Orientation-dependent FRET system reveals differences in structures and flexibilities of nicked and gapped DNA duplexes. *Nucleic Acids Res.* **45**, e105 (2017).

203. Le Cam, E. *et al.* Conformational Analysis of a 139 Base-pair DNA Fragment Containing a Single-stranded Break and Its Interaction with Human Poly(ADP-ribose) Polymerase. *J. Mol. Biol.* **235**, 1062–1071 (1994).

204. Hays, J. B. & Zimm, B. H. Flexibility and stiffness in nicked DNA. *J. Mol. Biol.* **48**, 297–317 (1970).

205. Lee, J. Y. *et al.* Investigating the sequence-dependent mechanical properties of DNA nicks for applications in twisted DNA nanostructure design. *Nucleic Acids Res.* **47**, 93–102 (2018).

206. Protozanova, E., Yakovchuk, P. & Frank-Kamenetskii, M. D. Stacked–Unstacked Equilibrium at the Nick Site of DNA. *J. Mol. Biol.* **342**, 775–785 (2004).

207. Furrer, P. *et al.* Opposite effect of counterions on the persistence length of nicked and non-nicked DNA. *J. Mol. Biol.* **266**, 711–721 (1997).

208. Häse, F. & Zacharias, M. Free energy analysis and mechanism of base pair stacking in nicked DNA. *Nucleic Acids Res.* **44**, 7100–7108 (2016).

209. van Dongen, E. M. W. M. *et al.* Variation of Linker Length in Ratiometric Fluorescent Sensor Proteins Allows Rational Tuning of Zn(II) Affinity in the Picomolar to Femtomolar Range. *J. Am. Chem. Soc.* **129**, 3494–3495 (2007).

210. Borcherds, W. *et al.* Optimal Affinity Enhancement by a Conserved Flexible Linker Controls p53 Mimicry in MdmX. *Biophys. J.* **112**, 2038–2042 (2017).

211. Hasegawa, H., Taira, K., Sode, K. & Ikebukuro, K. Improvement of Aptamer Affinity by Dimerization. *Sensors* **8**, 1090–1098 (2008).

212. Müller, J., Wulffen, B., Pötzsch, B. & Mayer, G. Multidomain Targeting Generates a High-Affinity Thrombin-Inhibiting Bivalent Aptamer. *ChemBioChem* **8**, 2223–2226 (2007).

213. McIntosh, D., Stevens, M. & Saleh, O. A. Single-Stranded DNA is not a Worm-Like Chain. *Biophys. J.* **104**, 28a (2013).

214. Pollak, Y., Goldberg, S. & Amit, R. Self-avoiding wormlike chain model for double-stranded-DNA loop formation. *Phys. Rev. E. Stat. Nonlin. Soft Matter Phys.* **90**, 52602 (2014).

215. Hofmann, H. *et al.* Polymer scaling laws of unfolded and intrinsically disordered proteins quantified with single-molecule spectroscopy. *Proc. Natl. Acad. Sci.* **109**, 16155–16160 (2012).